GA-Based Design of a Two-Degree-of-Freedom PID Controller for an Injera Cooking Machine

Ethel Cherotaw Cherenet

A Thesis Submitted to

The Department of Electrical Power and Control Engineering

School of Electrical Engineering and Computing

Presented in Partial Fulfillment of the Requirement for the Master of Science Degree in Electrical Power and Control Engineering (Control Engineering)

Office of Graduate Studies

Adama Science and Technology University

September 2021

Adama, Ethiopia

GA-Based Design of a Two-Degree-of-Freedom PID Controller for an Injera Cooking Machine

Ethel Cherotaw Cherenet

Advisor: Prof. Gang Gyoo Jin

A Thesis Submitted to

The Department of Electrical Power and Control Engineering School of Electrical Engineering and Computing

Presented in Partial Fulfillment of the Requirement for the Master of Science Degree in Electrical Power and Control Engineering (Control Engineering)

Office of Graduate Studies
Adama Science and Technology University

September 2021
Adama, Ethiopia

DECLARATION

I hereby declare that this Master Thesis entitled "GA-Based Design of a Two Degree of Freedom PID Controller for an Injera Cooking Machine" is my original work. That is, it has not been submitted for the award of any academic degree, diploma, or certificate in any other university. All sources of materials that are used for this thesis have been duly acknowledged through citation.

Ethel Cherotaw Cherenet		**September 09, 2021**
Name of the Student	Signature	Date

RECOMMENDATION

I, the advisor of this thesis, hereby certify that I have read the revised version of the thesis entitled "GA-Based Design of a Two-Degree-of-Freedom PID Controller for an Injera Cooking Machine." prepared under my guidance by Ethel Cherotaw Cherenet submitted in partial fulfillment of the requirements for the degree of Masters of Science in Control Engineering. Therefore, I recommend the submission of a revised version of the thesis to the department following the applicable procedures.

Prof. Gang Gyoo Jin		**September 09, 2021**
Major Advisor	Signature	Date

APPROVAL SHEET

I, the advisors of the thesis entitled "GA-Based Design of a Two-Degree-of-Freedom PID Controller for an Injera Cooking Machine" and developed by Ethel Cherotaw Cherenet, hereby certify that the recommendation and suggestions made by the board of examiners are appropriately incorporated into the final version of the thesis.

Prof. Gang Gyoo Jin ____________ **September 09, 2021**

Advisor Signature Date

We, the undersigned, members of the Board of Examiners of the thesis by Ethel Cherotaw Cherenet, have read and evaluate his thesis entitled "GA-Based Design of a Two-Degree-of-Freedom PID Controller for an Injera Cooking Machine" and examined the candidate during the open defense. This is, therefore, to certify that the thesis has been accepted in partial fulfillment of the requirement of the Degree of Masters in control engineering.

Chairperson Signature Date

Internal Examiner Signature Date

Muluneh Lemma (Phd) ____________ **September 9, 2021**

External Examiner Signature Date

Finally, approval and acceptance of the thesis is contingent upon submission of its final copy to the Office of Postgraduate Studies (OPGS) through the Department Graduate Council (DGC) and School Graduate Committee (SGC).

Department Head Signature Date

School Dean Signature Date

Office of Postgraduate Studies, Dean Signature Date

ACKNOWLEDGMENT

First, I would like to express my deepest gratitude and be delighted and grateful to my advisor **Professor. Doctor. Gang Gyoo Jin** for sharing his skillful expert advice, encouragement, enormous patience, and making himself available for guidance at various stages of this work.

I want to give my deepest gratitude and be grateful to **Mr. Feleke Fanta** for his suggestions, support, motivation, encouragement, and sharing of his work regarding the Injera Cooking Machine.

I want to express my deep appreciation and gratitude to the South Korean Professors, **Professor Gang Gyoo Jin, Professor. Seungnam Kim, Professor. MA Samsun and Professor. Dong Hwa Kim.**

I am also very grateful to **Dr. Tafesse Abera** and **Dr. Tefera T.yetayew** for their encouragement, motivation, and suggestion on my thesis work.

Furthermore, I would like to thank EPCE department head **Mr. Mesfien Megera** and Laboratory staff members, Especially **Mr.Shafi** and **Mr.Wassia**, for encouraging, making open Electrical Power Lab test the experimental setup and for making me feel very welcome during my thesis work.

Finally, I would like to thank my whole family and friends.

TABLE OF CONTENTS

LIST OF TABLES

LIST OF FIGURES

LIST OF ACRONYMS AND ABBREVIATIONS

AW	Anti-Windup
ARX	Auto-Regression Exogenous Input
CHR	The Chien, Hrones and Reswick Method
CVIJIN	Cevjin Method
DIS	Disturbance
ELPA	Electric Light Power Authority
EMIM	Electromagnetic Induction Injera Machine
FOPTD	First-Order Plus Time Delay
GA	Genetic Algorithm
GUI	Graphical-User-Interface
IAE	Integral Absolute Error
ICM	Injera Cooking Machine
NRMSE	Normalized Root Mean Square Error
PC	Personal Computer
PCPAAV-SSR	Proportional-Control-Phase-Angle-Analog-Voltage-SSR
PD	Proportional Derivative
PID	Proportional Integral Derivative Controller
SCR	Silicon Controlled Rectifiers
SOPTD	Second-Order Plus Time Delay
SP	Setpoint
SSR	Solid-State-Relay
TDOF PID	Two Degree of Freedom PID controller
TRIAC	Triode-For-Alternating-Current
1DOF PID	One Degree of Freedom PID Controller

LIST OF SYMBOLS

A	Effective heat transfer area
^{o}C	Degree Celsius
C_p	Thermal capacitance of the Injera Cooking plate
K_h	Internal gain of the Injera Cooking Plate
K_m	Process gain of temperature sensor and cooking plate
m(t)	Power Actuator input
N	Derivative factor
ℓ	Where the length of the cooking iron plate
L	Transport Delay
Q	Heat flow rate
R_p	Thermal Resistance of the cooking plate
T_s	Temperature sensor time constant
t_{st}	Steady-state time
T_t	Time tracking constant
t_{rt}	Transient time
U	Overall heat transfer coefficient
δ	Firing Angle
$\theta(t)$	Iron plate temperature
$\theta_r(t)$	Resistive coil temperature
σ	Thermal conductivity

ABSTRACT

Ethiopians eat Injera as their main meal, and many households use Injera Cooking Machine for baking Injera; maintaining the temperature of the Injera Cooking Machine (ICM) constant as the cooking temperature affects the taste and quality of cooked Injera. The two critical aspects in designing a temperature controller for Injera Cooking Machines are setpoint tracking and disturbance rejection. The setpoint tracking control tracks the setpoint when the ICM is raised to a cooking temperature at the start without giving excessive thermal stress. The disturbance rejection control keeps the cooking temperature constant. The adopted ON and OFF temperature control mechanism results in temperature fluctuation around the setpoint. Solving this problem with the existing one-degree-of-freedom (1DOF) PID controller cannot simultaneously enhance setpoint tracking and disturbance rejection performance. The thesis addresses the design of a two-degree-of-freedom PID (TDOF PID) controller incorporated with an Anti-Windup scheme and a Genetic Algorithm (GA) for simultaneous setpoint tracking and disturbance rejection response. The Anti-Windup technique reduced the error caused by Integral Windup, and GA estimates the system model parameters and tune controller parameters. An experimental setup incorporated with data acquisition obtains the system's actual response for subsequent use in model parameter estimation and model validation. The GA estimated model parameters has a +90% percentage fitting with the actual measured response, and the proposed controller simultaneously tracks the optimal cooking temperature and rejects the disturbance compared to 1DOF PID controllers with zero-percentage overshoot (M_p=0%), settling time(t_s=7.632-min), and recovery time (t_{rcy}=13.592-min). The Anti-Windup scheme eliminates the significant overshoot (M_p>20%) caused by the Integral Windup to zero percent (M_p=0%) with a faster settling time. The proposed controllers remove temperature fluctuation caused by the ON and OFF controllers and can replace the existing ON and OFF controller adopted in the current Injera Cooking Machine. Furthermore, the thesis supports the research gap on temperature controller design for ICM.

***Keywords**: AW, Disturbance Rejection, GA, ICM, Model Validation, Parameter Estimation Setpoint Tracking, TDOF PID, 1DOF PID.*

CHAPTER 1

INTRODUCTION

1.1 Background

Injera is a sour and tasty circular pancake with a soft and sponge-like texture. Injera Cooking plate used for baking Injera mainly consists of a cooking plate and a covering lid, and its local name is also called Injera Mitad, heater, and stove.

The prominent ingredient for producing Injera is teff, which is the world's tiniest grain. Baking Injera begins by mixing the teff flour with water and ferment by adding leftover batter from the previous baking session as a starter. When ready, the liquid dough is pitched and poured on a heated cooking plate that reaches a cooking temperature of $150^{\circ}C$ - $230^{\circ}C$. The cooking plate is covered with a lid, waits for 2-4 minutes, and ensures the cover holds the moisture inside the plate; otherwise, the result will be a cracked and deformed Injera [1]. Most Ethiopians cook Injera with traditional Three-Stone Mitad, Tigrian Mitad, and Mirt-Mitad (local name in Amharic), as depicted in Figure 1.1. The first conventional Mitad, as its name indicates, uses three separate stones for mounting. It consumes a massive biomass fuel to attain the required cooking temperature resulting in burns to the Injera maker.

(a) (b) (c)

Figure1. 1Traditional Mitad [1] [2] (a) Three-stone (b) Tigrian Mitad (c) Mirt-Mitad

The second Tigrian-Mitad uses an enclosed traditional Mitad designed using mud and is commonly used in the northern part of Ethiopia, mainly in Tigray. In contrast with the Three-

Stone Mitad, a well-built enclosed Tigrian Mitad is 12% efficient. It consumes less fuel and is easier to use, and protects the Injera maker from burns. The ministry of water and energy developed the third improved Mitad enclosed by cement called Mirt-Mitad [1] [2]. Comparing with the previous two traditional Mitad, Mirt-Mitad attains the cooking temperature faster. The biogas usage results in a highly polluted kitchen environment with soot and smoke affecting household inhabitant health. To solve this problem, Ethiopian Electric Light Authority (EELPA) developed in the early1960's the first electric Injera Cooking plate, as depicted in Figure 1.2 [1] [2].

Figure 1. 2 Electric Injera Cooking plate [1]

However, the main problem of the existing electric Injera Cooking plate is that it is energy inefficient. The causes of energy inefficiency are the high electrical energy needed to heat up to $150\,^{o}C$ to $230\,^{o}C$. This high energy requirement is due to high heat load (parts of the Injera Cooking plate to be heated up), poor heat insulation, and heat loss during overheating. An effort to improve the energy efficiency of the heater has been made by changing the existing structure and using alternative thermal and solar energy sources and a combination of solar thermal [2] [3] [4] [5]. However, there is a research gap in applying a temperature control system [6]. Injera bakers monitor the temperature through observations and using Injera Cooking Machine (ICM) equipped with an automatic ON and OFF temperature controller. The lack of a temperature control system results in temperature fluctuations.

The two significant aspects of temperature control design are setpoint tracking and disturbance rejection. The first aspect stands for an automatic adjustment to the required optimal cooking temperature. The disturbance rejection stands for keeping the Injera cooking temperature to the setpoint from the deviation mainly caused by liquid dough on the cooking plate. The ON and OFF controller is incapable of achieving those two objectives resulting in fluctuation. Solving this problem with the conventional or one-degree-of-freedom Proportional Integral Derivative

(1DOF PID) temperature controller does not enhance simultaneous setpoint tracking and disturbance rejection. The degree of freedom indicates the number of closed-loop transfer functions that can be changed independently [7].

This thesis design a two-degrees-of-freedom PID (TDOF PID) controller using a Genetic Algorithm (GA) as parameter estimation and controller tuning method. The controller has two independent transfer functions that allow achieving the two design objectives. The GA estimates the system model parameters and adjusts controller parameters. GA is a global search algorithm based on natural selection and developed by John Holland. It is a versatile optimizer and requires minimal prior assumptions on the nature of the problem. In contrast with other search strategies, GAs do not require differentiability, continuity, or other restrictive hypotheses on the objective function. Thus, they will lend themselves to practical performance-oriented control design problems [8].

The application of a controller on any system requires an understanding of its dynamic behavior or mathematical model, or Transfer function. However, it is difficult to consider all factors that influence the internal phenomenon of heating systems. In such cases, System Identification modeling can determine the relationship between the input and the output. System Identification is a methodology for building mathematical models of a dynamic system from an experimental setup, data acquisition, model estimation, and model validation [9] [10].

Furthermore, the implementation of a controller that possesses an integral action results in an Integral Windup. An Integral Windup accumulates errors for the deviation in setpoint even if the controller inputs saturate. This phenomenon brings overshoot and slow settling time, resulting in poor control performance. For this purpose, Anti-Windup (AW) controller scheme is implemented, enhancing the performance of the proposed controller.

1.2 Statement of the Problem

The two significant problems in temperature control design for Injera Cooking Machine (ICM) are setpoint tracking and disturbance rejection. The first aspect tracks the setpoint when the Injera Cooking Machine is raised to the cooking temperature at the start without giving excessive thermal stress. The second aspect is to keep the cooking temperature constant from the significant deviation mainly caused by the liquid dough on the plate. The setpoint tracking and disturbance rejections keep constant Injera cooking temperature. However, the setpoint tracking is by manual observation and an ON and OFF control mechanism. The Injera maker decides when to start baking through observation and experience. The cooking plate temperature is monitored by turning ON and OFF the heat energy source. The ON and OFF control strategy results in temperature fluctuation around the optimal cooking temperature. Solving this problem using the conventional or one-degree-of-freedom PID (1DOF PID) controller does not enhance simultaneous setpoint tracking and disturbance rejection.

This thesis designed a two-degrees-of-freedom PID (TDOF PID) controller incorporated with an Anti-Windup (AW) scheme and Genetic Algorithm (GA) for simultaneous setpoint tracking and disturbance rejection performance.

1.3 Objective of the Thesis

1.3.1 General Objective

The general objective is to design a GA-based TDOF PID controller incorporating an Anti-Windup scheme for temperature control of the Injera Cooking Machine to achieve simultaneous setpoint tracking and disturbance rejection.

1.3.2 Specific Objectives

- To obtain models of the ICM and develop a data logger for getting experimental data.
- To estimate the model parameters using experimental data, a parameter estimation technique, and a GA.
- To design a TDOF PID controller for the ICM.
- To tune the controller parameters optimally using a Genetic Algorithm to improve the setpoint tracking and disturbance rejection performance.
- To implement an Anti-Windup scheme to avoid the Integral Windup.
- To perform a set of simulations works to check the proposed method's effectiveness for simultaneous setpoint tracking and disturbance rejection response and compare its performance with PID controller.

1.4 Scope of the Thesis

This thesis focused on setting an experimental setup using software and hardware integration and measurement system for transfer function modeling from Input-output data. Simulation of GA-based model parameter estimation and proposed controller performance comparison with 1DOF PID controller and the effect of Integral Windup with and without Anti-Windup controller (AW) scheme implementation. MATLAB 2019b software implements GA-parameter estimation, controller parameters tuning, and performance measures for the proposed TDOF PID and 1DOF PID controller.

1.5 Limitations of the Thesis

This thesis is limited to implementing an experimental setup for system modeling incorporated with GA parameter estimation and control simulation using MATLAB 2019b software. This is because of the limitation in finance for procuring and purchasing the components in the Ethiopian Market. In this thesis, the Injera Cooking plate for system modeling and controller design simulation is for WassGrill-ICM because of its construction efficiency, availability, and flexibility than other existing cooking machines.

1.6 Significance of the Thesis

The thesis brings the following significance:

- The simultaneous setpoint tracking and disturbance rejection performance can improve the temperature fluctuation around the optimal cooking temperature caused by the ON and OFF controller.
- Protect overheating by maintaining optimal cooking temperature.
- Consistent temperature monitoring improves the test and quality of cooked Injera.
- The stepwise setpoint tracking performance allows the user to choose any optimal cooking temperature.
- It supports the reevaluation of the ON and OFF temperature controller.
- It promotes and supports research in temperature control design for ICM.

1.7 Thesis Organization

The thesis is organized into six chapters:

Chapter 1: Presents the introduction of the thesis works, statements of the problem, the objective of the thesis, scope, and limitation scope of the research work.

Chapter 2: Reviews recent research on the existing Injera cooking machines based on control strategy implementation and review closely related literature on PID temperature control.

Chapter 3: Describes the steps followed to achieve the system transfer function modeling.

Chapter 4: Presents the proposed TDOF PID controller design, Anti-Windup controller (AW) scheme Implementation, and optimal controller parameters tuning methods.

Chapter 5: Presents simulation result and discussion.

Chapter 6: Discusses the research work conclusion and recommendation.

CHAPTER 2

LITERATURE REVIEW

This chapter reviews recent works in an Injera Cooking Machine based on applied control strategies to regulate the optimal cooking temperature. The first section discusses working temperature and the gap in temperature control strategies to assess cooking temperature and ICM selection for system modeling and MATLAB control simulation. Then, a survey of PID controllers and related works on the proposed controller associated with the temperature control of the heating system and modeling are discussed.

2.1 Existing Injera Cooking Machine

The traditional cooking stoves use much firewood, and the cooking process is tedious and polluting. The Ethiopian Electric Power Authorities(ELPA) developed the first electric Injera Cooking plates; since then, the demands have increased due to electrification. However, the main problem is energy inefficiency because of their high heat load, construction efficiency, and temperature controller implementation. Researchers performed experimental investigations on alternative energy sources like solar and thermal cooking and temperature regulation methods to improve efficiency [1] [4] [6].

This section reviews the literature on solar and thermal and related works in temperature control implementation to assess cooking temperature selection and controller application limitation.

2.1.1 Solar and Thermal ICM

The author in [11] proposed the Solar Frayer-ICM, as depicted in Figure 2.1a. The system uses solar radiation through a mirror to heat the plate. Experimental investigation in the literature [11] shows a well-cooked Injera with an optimal cooking temperature of $180\,^{o}C$. The Injera Cooking plate withstands overheating $280\,^{o}C$-$290\,^{o}C$ for 30-min. However, the temperature regulation method is performed by manually tracking the solar radiation.

The author in [5] introduced a Solar-Thermal-ICM, as shown in Figure 2.1b; the ICM uses solar and thermal power to cook Injera. Solar energy is transferred to the kitchen through a circulating heat transfer fluid heated by solar energy concentrated by a parabolic through. The investigation in the literature [5] shows that the heat achieves a temperature of 180-220 $^{\circ}C$.

The author in [3] proposed a Steam-Based-Solar-Thermal-ICM as depicted in Figure 2.1c. The system uses pressurized steam heat transfer fluid circulating naturally. It generates steam by concentrating sun rays using a parabolic dish on the receiver. The steam flows to the cooking plate through a pipe and condenses by transferring heat to the baking pan in contact with steam on the steel. It illustrates the theory of boiling-condensing heat transfer in a closed-loop, and the system consists of a manual and automatic solar power tracker with a photodiode sensor [3].

The result of baked Injera in literature [3] with indirect steam at temperatures ranging from 135 $^{\circ}C$ to 160 °C was a key finding from this research. The indicated temperature was lower than the previous literature by other researchers [3] [4] [5] [11] [12].

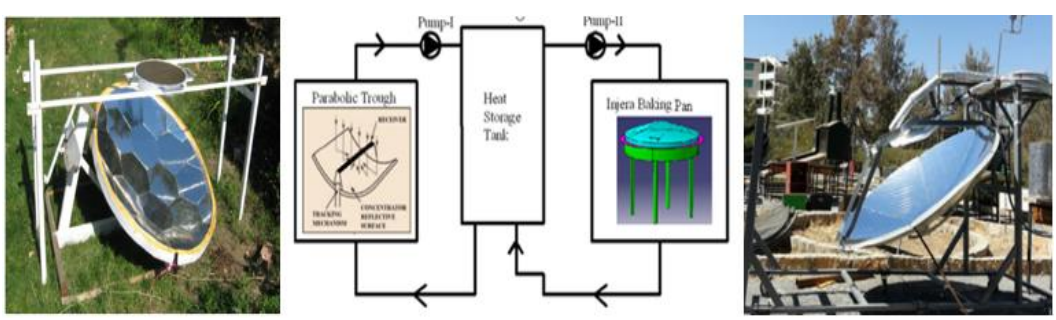

(a) (b) (c)

Figure 2. 1 (a) Solar Frayer [11] (b) Solar Thermal [3] (c) Steam Based Solar Thermal [5]

The existing solar Injera Cooking plates are seasonal because of solar energy dependency, and from the works of literature, their cooking temperature lies between 135 $^{\circ}C$ to 220 °C.

2.1.2 Temperature Regulation Methods In Electric ICM

The overheat and underheat problems are the main issues faced in the existing Injera Cooking plates. The leading causes are lack of temperature controller, standardized plates, and construction efficiency. This thesis focus on temperature controller application. There are research gaps in temperature regulator application to overcome overheat and under heat problems [6]. Few researchers have performed an ON and OFF controller to control the setpoint temperature.

The author in [12] proposed an Electromagnetic Induction Injera Machine (EMIM), as depicted in Figure 2.4a. The main components of EMIM are resonant inverter to generate high-frequency current, working coil, and cast-iron work peace [12]. An ON and OFF control mechanism is applied to maintain the optimum temperature using a microcontroller [13]. Figure 2.2 depicts the overall control block diagram of EMIM.

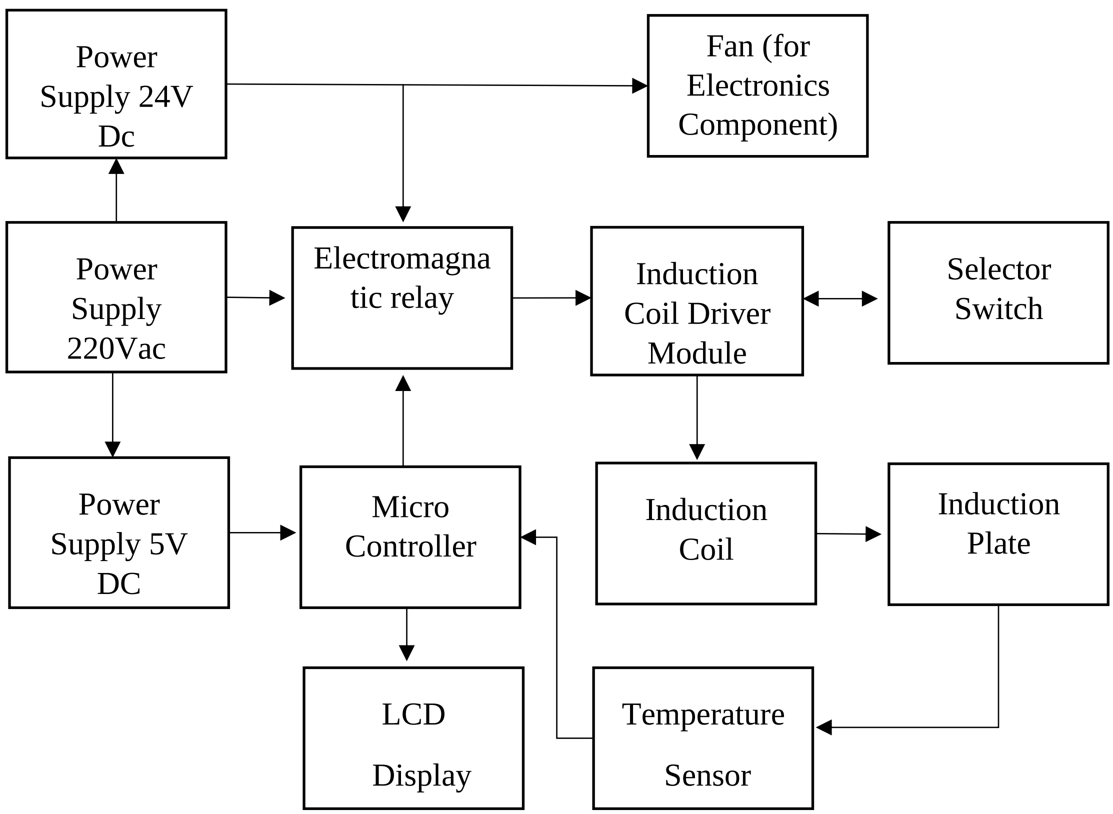

Figure 2. 2 Block diagram of the EMIM system [14]

From Figure 2.2, the electrical supply voltage is 220V at a 50Hz frequency. A 24V dc supply powers to the electromagnetic relay and the fan. The 5V dc supply power the microcontroller.

The fan protects the electronics components from high heat damage as a result of the baking process. During start-up, the selector switch controls the power flow to the coil.

The thermocouple placed on the cooking plate measures the temperature. It sends signals to the microcontroller programmed to switch ON and OFF the induction driver module via the electromagnetic relay. Once the induction plate temperature reaches $180\,^{o}C$ relay switches OFF, and when the temperature drops to $150\,^{o}C$, the relay is ON. The investigation in literature [13] [12] [14] shows that applying the ON and OFF control mechanism keeps the optimal cooking temperature between $150\,^{o}C$-$180\,^{o}C$.

The author in [15] introduced a resistive Electric Injera Cooking Machine equipped with a temperature monitoring device called a WassGrill-Injera Cooking Machine. Figures 2.4b and c depict WassGrill-ICM. The main parts of the ICM are the resistive coil, cooking iron plate, temperature control knop, thermostat, temperature sensor, and LED display unit [15]. The temperature is regulated based on the ON and OFF control mechanisms, as depicted in Figure 2.3.

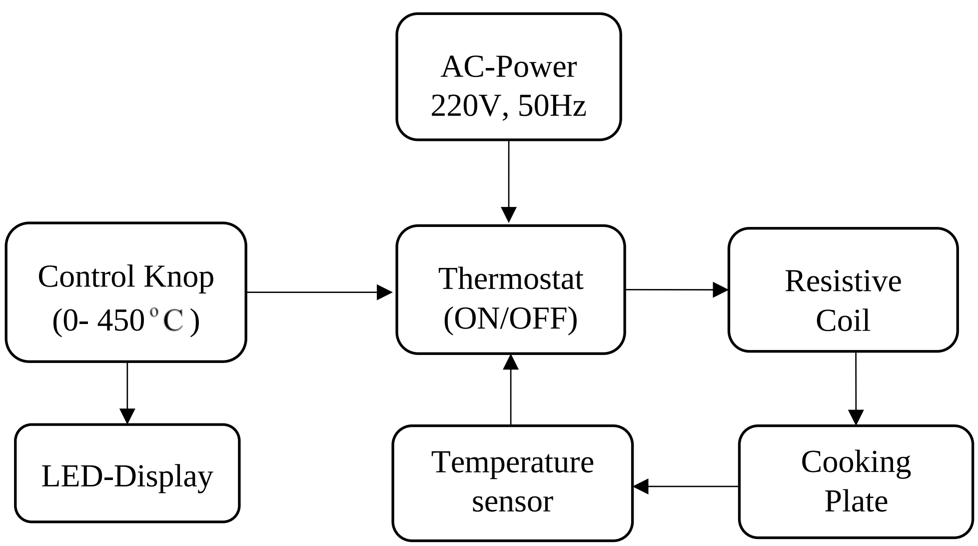

Figure 2. 3 Block diagram of the WassGrill cooking Machine

In WassGrill-ICM, the optimal temperature for cooking Injera is $121\,^{o}C$-$232\,^{o}C$. The control Knop followed by an LED-Display set the required cooking temperature.

The maximum recommended temperature that the control knob can adjust is 450 ^{o}C [2] [15]. The thermostat compares the error in setpoint temperature and actual temperature using a temperature sensor (thermocouple) placed at the center of the cooking plate [2] [15]. The thermostat switches OFF when the actual temperature reaches the setpoint and is ON when the actual temperature is below the setpoint.

(a) (b) (c)

Figure 2. 4 (a) EMIM [12] [13] (b) WassGrill ICM (c) WassGrill Component [2] [15].

Table 2.1 summarizes the optimal cooking temperature of solar and ON and OFF temperature-controlled electric ICM.

Table 2. 1 Summary of cooking temperature and control mechanism

Injera Cooking Plates	Energy Source	Temperature (^{o}C)	Controller
Solar Frayer	Solar	180	None
Solar Thermic	Solar-Thermal	180-220	None
Steam Based Solar Thermic	Solar-Thermal	130 -160	None
Electromagnetic Induction	Electrical	150-180	ON and OFF
WassGrill	Electrical	121-231	ON and OFF

In contrast with the existing Injera cooking heaters, WassGrill is the most popular because of its construction efficiency, availability, flexibility and allows a stepwise increase in temperature.

However, the ON and OFF control applications result in temperature fluctuation around optimal cooking temperature. In this thesis, WassGrill was selected for system modeling and proposed controller simulation.

2.2 Conventional Proportional Integral Derivative Controller (PID)

The most widely used single loop controller is the conventional or one-degree-of-freedom Proportional Integral Derivative (1DOF PID) controller. The degree-of-freedom (DOF) of a PID controller is the number of closed-loop transfer functions that can be altered independently [16] [17]. Figure 2.5 depicts the conventional PID controller structure.

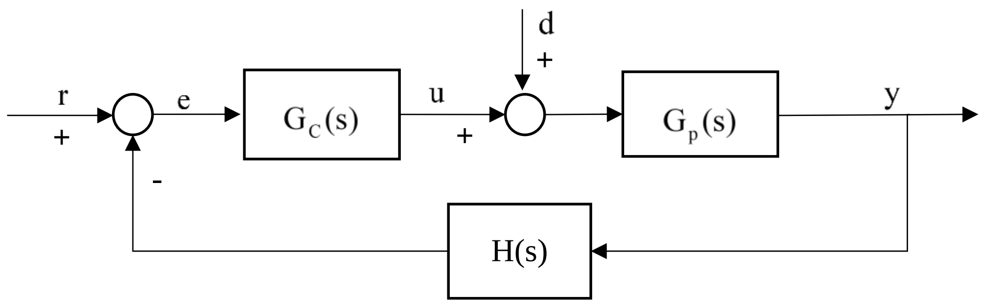

Figure 2. 5 Structure of the conventional PID controller.

Where r, e, u, y, H(s), $G_C(s)$, and $G_p(s)$ are setpoint input, error, controller output, feedback gain, plant output, PID controller, and plant transfer function model, respectively. The PID controller is a summation of three actions, namely Proportional, Derivative, and Integral, as shown in Equation (2.1).

$$G_C(s) = K_p(1 + \frac{1}{T_i s} + T_d s) \tag{2.1}$$

where, K_p, T_i and T_d are called proportional gain, integral and derivative time, respectively. The PID controller tuning determines those PID controller parameters [18].

The driving of the closed-loop transfer function for optimal setpoints and disturbance rejection is analyzed by setting the disturbance to zero for the optimal setpoint tracking and reference input to zero for optimal disturbance rejection. Taking unity feedback gain H(s), the closed-loop transfer function for optimal setpoint tracking $G_{yr}(s)$ and optimal disturbance rejection $G_{yd}(s)$ is given in Equations 2.2 and 2.3 [19].

$$G_{yr}(s) = \frac{Y(s)}{R(s)} = \frac{G_C(s)G_p(s)}{1+G_C(s)G_p(s)} \tag{2.2}$$

$$G_{yd}(s) = \frac{Y(s)}{D(s)} = \frac{G_p(s)}{1+G_C(s)G_p(s)} \tag{2.3}$$

The two closed-loop transfer functions in Equations (2.2) and (2.3) have only one tunable element $G_C(s)$. This fact results in the following difficulty. In optimizing the setpoint response, the disturbance becomes poor and vice versa. Some researchers gave two tables on their PID controller tuning methods, one for optimal disturbance rejection and another for setpoint tracking. The Chien, Hrones, Reswick, and Jan Cevjin methods can be mentioned. Those tuning methods are proposed for the first-order-plus-time-delay (FOPTD) system, as the FOPTD model can explain many processes [18] [20] [21] [22]. The general structure of the FOPTD process model is given as

$$G_p(s) = \frac{Ke^{-Ls}}{1+Ts} \tag{2.4}$$

where K, T, and L are the process's gain, time constant, and time delay (or transport delay).

2.2.1 The Chien, Hrones and Reswick Method (CHR)

The Chien, Hrones, and Reswick method focus on the experimental step response of the FOPTD process model as in Equation (2.4). The CHR method gives the response without overshoot 0% and 20 % overshoot and provides two tables for setpoint tracking and disturbance rejection [21].

Table 2. 2 CHR tuning rules for setpoint tracking

	0% Overshot			20% Overshot		
PID Controller Parameter	K_p	T_i	T_d	K_p	T_i	T_d
	$\frac{0.6T}{KL}$	T	0.5L	$\frac{0.6T}{KL}$	1.4 T	0.47L

Table 2. 3 CHR tuning rules for disturbance rejection

	0% Overshot			20% Overshot		
PID Controller Parameter	K_p	T_i	T_d	K_p	T_i	T_d
	$\frac{0.95T}{KL}$	2.4L	0.42L	$\frac{1.2T}{KL}$	2L	0.42L

2.2.2 The Jan Cevjin Method

The Cevjin Method gives a high degree of robustness for any value of the dead time parameters and provides two tables, one setpoint tracking and disturbance rejection, respectively [22]. For the FOPTD model in Equation (2.4).

Table 2. 4 Cvejin tuning rule for setpoint tracking response

	K_p	T_i	T_d
PID Controller Parameter	$\frac{1}{4K_p}(1+3\frac{\tau_p}{L})$	$\tau_p + \frac{L}{3}$	$\frac{L}{3+\frac{L}{\tau_p}}$

Table 2. 5 Cevjin tuning rule for disturbance rejection

	K_p	T_i	T_d
PID Controller Parameter	$\frac{1}{4K_p}(1+3.26\frac{\tau_p}{L})$	$\frac{3.9L\tau_p}{(3.9L+\tau_p)+L/3}$	$\frac{L\tau_p}{(3.26\tau_p+L)}$

2.3. Related Work on PID Controller and Heating System Modeling

Setpoint tracking and disturbance rejection are the most critical aspects of every process control application [7] [23] [24]. With the conventional one-degree-of-freedom PID controller (1DOF PID), it is difficult to achieve simultaneous setpoint tracking and disturbance rejection [24] [25].

The author in [26] shows that whenever the setpoint tracking is optimized, the disturbance rejection response becomes bad and vice versa. This situation leads researchers to find two alternative solutions. The first is to find the Pareto-optimal solution (Pareto-front), and the second is the TDOF PID controller, as illustrated in Figure 2.6.

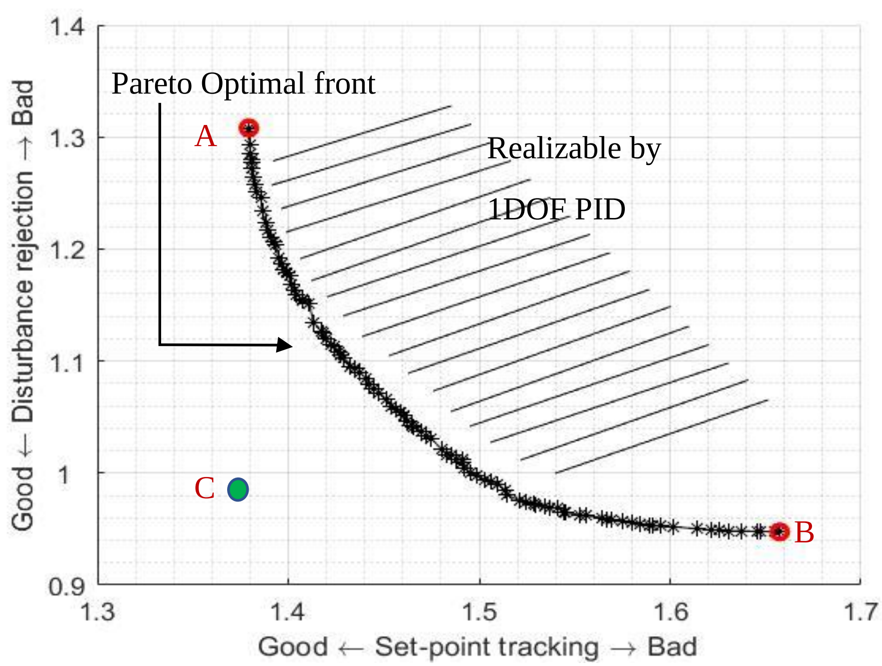

Figure 2. 6 Effects of the 1DOF PID and TDOF PID controllers

Pareto front stands for a set of solutions that are non-dominated to each other. However, they are superior to the rest of the solutions in the search space. Points A and B in Figure 2.6 are the optimal setpoints and disturbance rejection points, respectively. The shaded area is realizable by the 1DOF PID controller. The graph shows that the disturbance rejection becomes bad whenever the setpoint is optimized at point A. For optimized disturbance rejection at point B, the setpoint tracking becomes bad. There are two solutions to this problem; the first is to select one of the Pareto fronts. The second is to choose point C for simultaneous setpoint tracking and disturbance rejection response. In contrast, finding a solution at point C better meets the two controller objective than the Pareto-fronts line.

In this thesis, the optimal solution at point C is selected, which is realizable by two-degrees-of -freedom PID controller (TDOF PID) [7] [26] [27]. TDOF PID consists two closed-loop transfer functions or feedback control [26] [28] [29].

Transfer function provides the dynamic behavior of a system used to apply the controller. However, the heating process system dynamics depend on the condition in which they are being operated, which presents a challenge for modeling. System Identification solves such problems in transfer function modeling. System Identification is part of system control engineering that determines the plant's physical characteristics based on real-time measurement or experimental data [30].

The author in [30] applies a set of PC-based experimental setups to obtain the step-response of an electric oven for subsequent use in System Identification. Since the main control parameter in the heating system is the temperature, the author uses a thermocouple to record the open-loop response of the electric oven. The author adopted Auto Regression with exogenous input (ARX) parameter identification method to obtain system model transfer function. To validate the model, the author used the mean square error of the identified and actual response. Next, the author analyzes the application of conventional PID or 1DOF PID controllers, and the investigated result shows good setpoint tracking. In contrast, the TDOF PID performance test for heating systems is performed in the literature [31] [32].

The author in [31] performs a temperature control experimental setup for a heater and identifies the model by applying a step input to Solid-State Relays (SSR) connected to the heater coil for power regulation. The open-loop step-response is recorded on an excel datasheet for System Identification modeling. The author identified the FOPTD model using the MATLAB System Identification toolbox and applied the TDOF PID controller to analyze the closed-loop system response. The tested result shows good setpoint tracking and disturbance rejection response. The author in [32] performed the same System Identification modeling method for an experimental setup of a temperature process and applied a TDOF PID controller for optimal setpoint tracking and disturbance rejection.

The above authors in [30] [31] [32] use the classical gradient descent method Auto Regression with exogenous input (ARX) for parametric identification. However, the classical techniques have problems finding a global minimum solution; thus, this thesis designed a TDOF PID controller for the Injera Cooking Machine by incorporating a Genetic Algorithm (GA) as a global optimization tool. The GA estimates the model parameters of the WassGrill-ICM from the open-loop step response of measured data through experimental setup, and MATLAB implements the control simulation.

CHAPTER 3

SYSTEM MODELING AND PARAMETER ESTIMATION

This chapter deals with obtaining the model of a WassGrill-ICM as a controlled object and estimating its parameters. For this, a set of system identification procedures, such as getting a generic model structure, an experimental setup for data acquisition, parameter estimation, and validation, are carried out. Experimental setup integrates hardware and software components. A custom-developed data logger exports the measured data into an excel datasheet for subsequent use in parameters estimation and model validation.

The model parameter estimation uses measured data, model adjustment schemes, and Genetic Algorithm parameter estimation. The normalized-root-mean-square error (NRMSE) percentage fitting validate the estimated model.

3.1 Material

In this thesis work, the following software and hardware components are employed: MATLAB 2019b for the simulation; temperature sensor, signal conditioner, microcontroller, a custom-developed data logger, WassGrill-ICM, and step signal generator for setting the experimental setup.

3.2 Methodology

As portrayed in Figure 3.1, the block diagram summarizes the step followed to achieve the controller design objective. Based on the temperature controller design objective, the related work on the existing Injera Cooking Machine(ICM) and their optimal cooking temperature assess the ICM and operating temperature selection and PID controller. Genetic Algorithm (GA) parameters estimation requires input-output system response data; this data should be stored and analyzed for parameter estimation and model validation. For this purpose, an experimental setup from hardware and software integration and a custom-developed data logger was employed to record, display, monitor, and export the step response into an excel datasheet.

Then the GA estimates the generic model parameters of the controlled object from the exported measured data using a model adjustment scheme, and percentage fitting validate the estimated model parameters. Then a TDOF PID controller incorporating an Anti-Windup strategy is designed using GA as a controller parameter tuning method for simultaneous setpoint tracking and disturbance rejection response. Finally, MATLAB 2019b software implemented the proposed TDOF PID controller and compared its performance to the 1DOF PID controller based on the design objective.

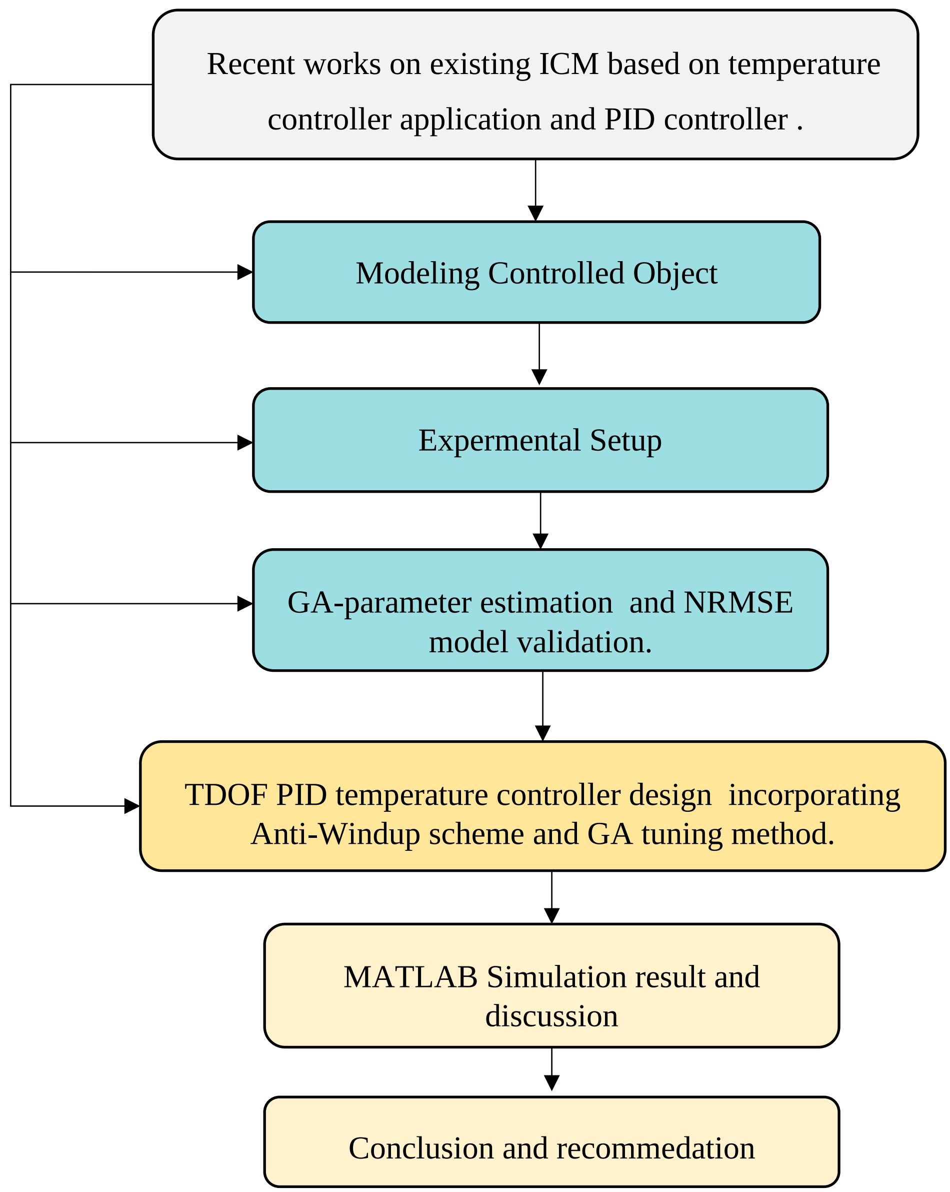

Figure 3. 1 Methodology block diagram

3.3 Modeling of the Controlled Object

Figure 3.2 depicts the block diagram of the proposed temperature control system. The error between the reference input (setpoint) and the Injera Cooking plate output is an input for the TDOF PID controller designed in Chapter 4. The controller generates the required control input signal. A Proportional Control Solid State Relay (SSR) generates an output power in response to the controlled input signal as an electrical power Actuator. The power Actuator operates with a limited controlled input signal; because of this, it is necessary to limit the control input signal for protection.

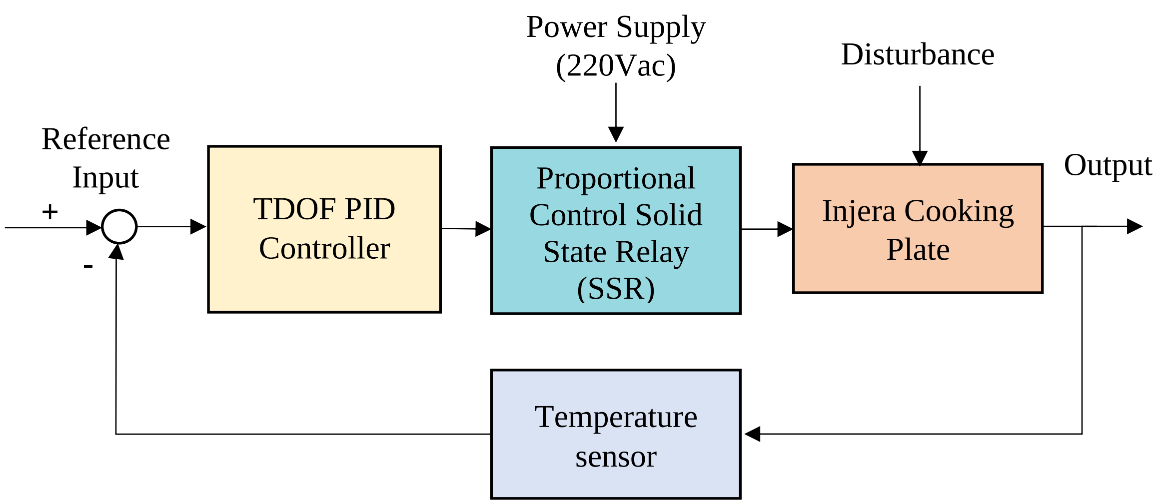

Figure 3. 2 Block diagram of the proposed temperature control system

As seen in Figure 3.2, the control system is roughly divided into two parts: the controller and the controlled object. The controlled object consists of the electric power Actuator, Injera Cooking plate, and the sensor, as in Figure 3.3.

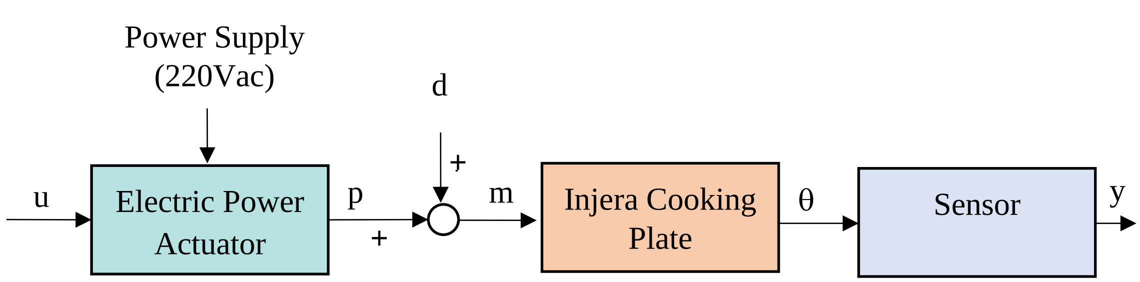

Figure 3. 3 Block diagram of the controlled object

In Figure 3.3, u denotes the control input, p power Actuator output, d disturbance, m power applied to the Injera Cooking plate, θ the temperature of the cooking plate and y the measured temperature. The sudden change in temperature while pouring the liquid dough on the plate introduces a step disturbance input.

In the subsequent sections, the model of each component that constitutes the controlled object is discussed.

3.3.1 Electric Power Actuator

The electric power Actuator plays the role of supplying the electric power. It controls the cooking temperature by regulating the $220V_{ac}$ input signal V_s in response to the controller output signal. This thesis uses the Proportional Control Phase Angle Analog Voltage Solid-State-Relay (PCPAAV-SSR) as a power Actuator. PCPAAV-SSR is a type of Solid-State Relay (SSR) that provides proportional power to the load based on the values of an analog signal applied to 0 to $10V_{dc}$. In the PCPAAV-SSR, the input signal is controlled by triggering a pulse of output at a particular phase of the input's modulation cycle, usually at the half-cycle in response to 0-10 V_{dc} analog input signal [33] [34] [35]. Figure 3.4 depicts the phase angle control at the triggering angle δ.

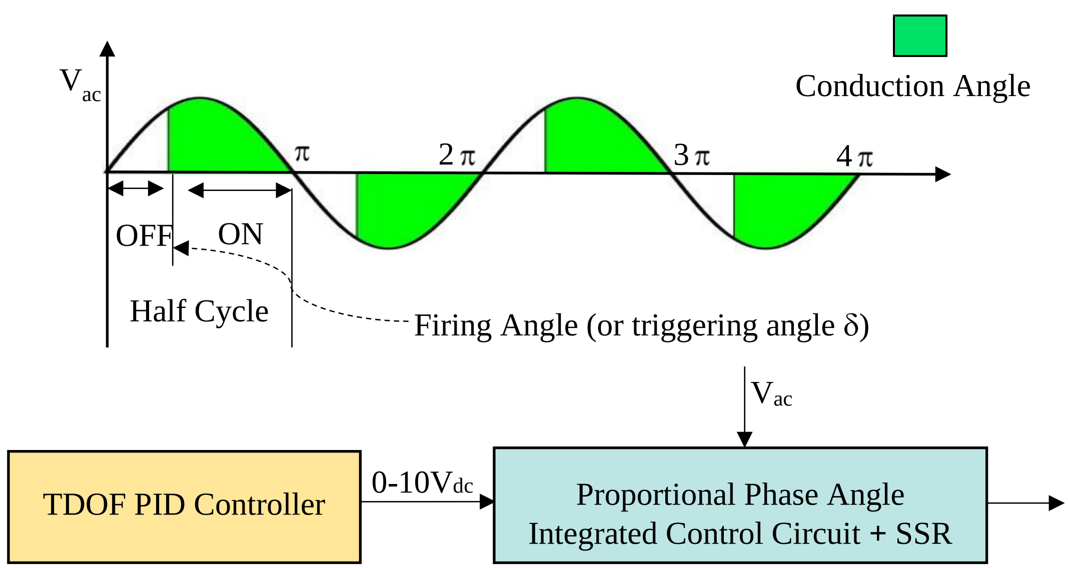

Figure 3. 4 Proportional Control Phase Angle SSR [36]

The SSR uses a silicon-controlled rectifier (SCR) or triode-for-alternating-current (TRIAC) for full-wave control and provides a variable average voltage output. The average value of the output load voltage is controlled by varying the triggering angle. For proportional phase angle controlled SSR, the conduction angle depends on the triggering or firing angle δ varying from 0 to π corresponding to the control input signal 0~10V_{dc} enabling high accuracy temperature control [33] [37].

The supply voltage V_s in terms of the maximum value of phase voltage V_m is

$$V_s = V_m \sin(\omega t) \tag{3.1}$$

Driving the average or DC-value of the phase angle control SSR for full-wave control output voltage in terms of the firing angle δ as follows [37]. For any waveform, the DC-Value is given by

$$V_{DC} = \frac{1}{T}\int_0^T V_s(t)dt \tag{3.2}$$

where T is the period.

From Figure 3.4

$$\begin{aligned} V_{SSRdc} &= \frac{1}{\pi}\int_\delta^\pi V_s(t)dt \\ &= \frac{V_m}{\pi}\int_\delta^\pi \sin(\omega t)dt \\ &= \frac{V_m}{\pi}(-\cos(\omega t))\Big|_\delta^\pi \\ &= \frac{V_m}{\pi}(-\cos(\pi)+\cos(\delta)) \\ &= \frac{V_m}{\pi}[\cos(\delta)+1] \end{aligned} \tag{3.3a}$$

Where

$$V_m = \sqrt{2}V_s \tag{3.3b}$$

Equation (3.3) shows the input-output relation between the firing angle δ and the average DC value. The maximum DC output voltage is delivered to the load at the triggering angle δ= 0. Substituting δ= 0 to Equation (3.3)

$$V_{SSRdc} = \frac{\sqrt{2}V_s}{\pi}[\cos(0)+1] = \frac{2\sqrt{2}V_s}{\pi} \tag{3.4}$$

The minimum DC-Value at $\delta = \pi\,(180°)$ results:

$$V_{SSRdc} = \frac{\sqrt{2}V_s}{\pi}[\cos(\pi)+1] = 0 \tag{3.5}$$

The PCAAV-SSR has an internal circuit that controls and linearizes the phase angle δ to provide a proportional output power for the corresponding control signal from 0 -10V_{dc} [34] [35].

Zero input voltage(0V_{dc}) corresponds to no switching or $\delta = 180^{o}$, and control input voltage 10V_{dc} corresponds to a maximum of 100 % power or $\delta = 0^{o}$ [35]. Table 3.1 and Figure 3.5 show power transfer characteristics between control input u(t) and phase angle operation [35].

Table 3. 1 Transfer characteristics output power in terms of the control input [35]

Control Input (0 -10V_{dc})	0	2.5	5	7.5	10
Percentage Power %	0%	25%	50%	75%	100%

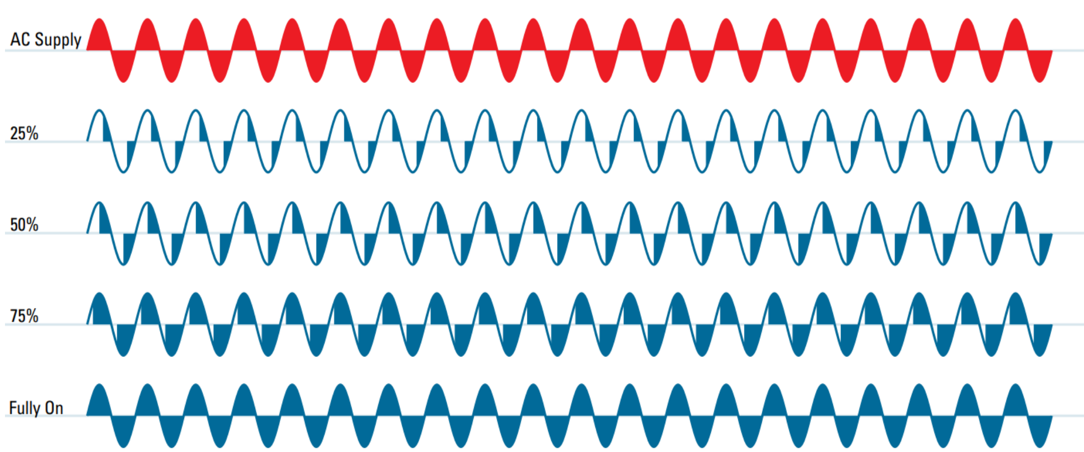

Figure 3. 5 Power Actuator control input and percentage power output [38]

The blue-colored area in Figure 3.5 depicts the percentage output power to the load. The figure clarifies that by linearly increasing the control input signal from 0V to $10V_{dc}$, the power to the Injera Cooking plate is controlled. As the control input increase from 0 to $10V_{dc}$, the firing angle decrease from 180^{o} to 0^{o}. Figure 3.6 depicts control and firing angle characteristics.

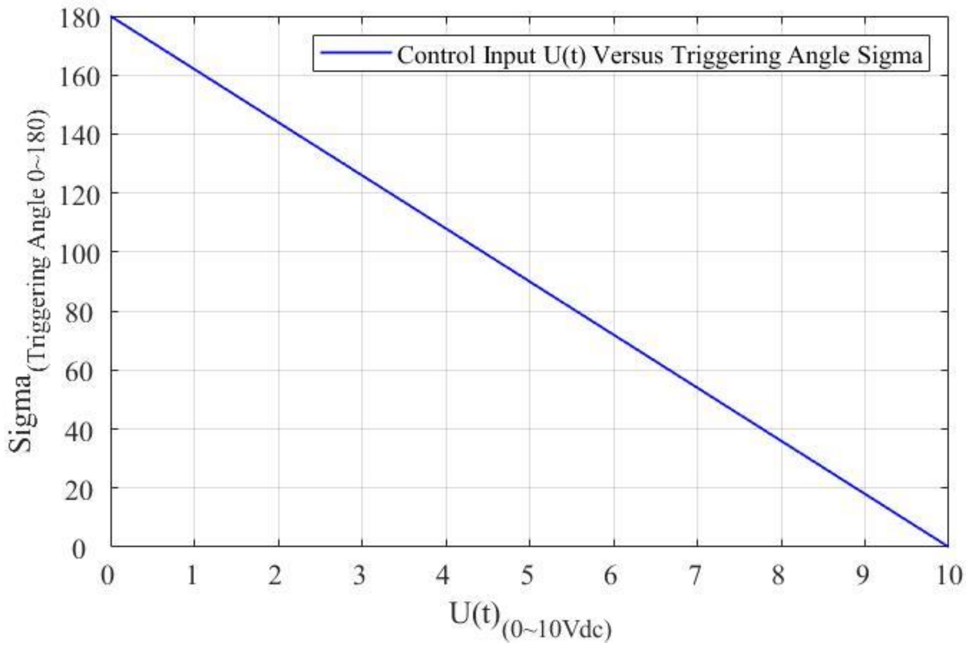

Figure 3. 6 Control input u(t) and firing angle characteristics

The relationship between control input and firing angle is a straight line having a negative slope. From the Equation of a line

$$\delta = \mathrm{mu(t)} + \mathrm{b} \qquad (3.6a)$$

where m is slope and b is the y-intercept from Equation (3.6a) and Figure 3.5.

$$\delta = -\frac{\pi}{10}\mathrm{u(t)} + \pi \qquad (3.6b)$$

By substituting Equation (3.6) into (3.3), the control input signal u(t) and the average or DC-value are related as

$$V_{SSRdc} = \frac{\sqrt{2}}{\pi} V_s[\cos(-\frac{\pi}{10} u(t) + \pi) + 1]$$
$$= \frac{\sqrt{2}}{\pi} V_s[1 - \cos(-\frac{\pi}{10} u(t))] \quad (3.7)$$

Figure 3.7 depicts the characteristics plot of the control input u(t) versus output DC voltage.

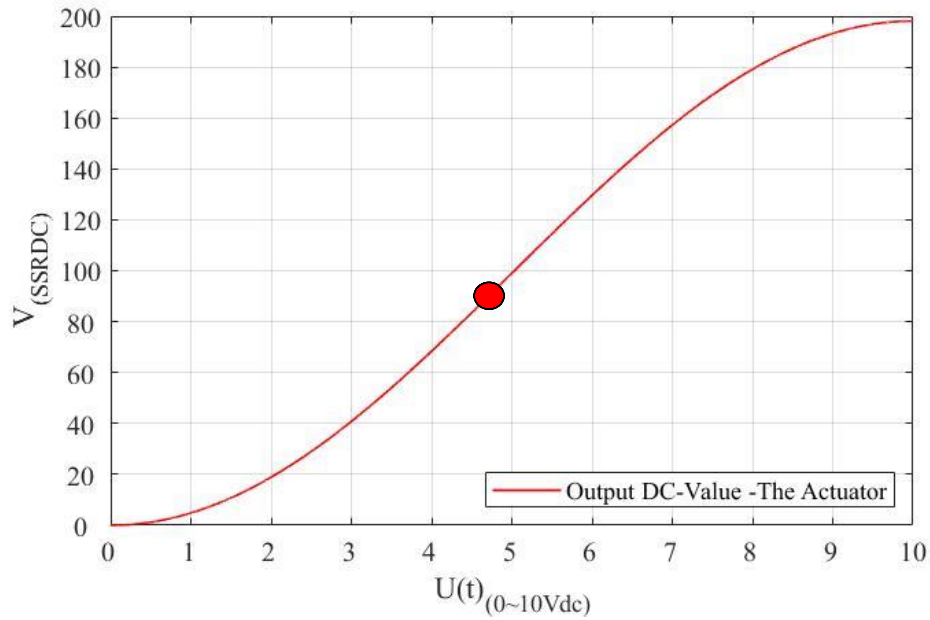

Figure 3. 7 Transfer characteristics control input versus output DC-Value

As seen in Figure 3.7, the PCAAV-SSR shows a linear relationship around the system's operating point. It responded too fast compared to the Injera Cooking plate with a significant time constant. So, in this study, the PCAAV-SSR is considered as a simple gain.

$$\frac{P(s)}{U(s)} = K_a \quad (3.8a)$$

$$K_a = \left. \frac{V_{SSRMAX} - V_{SSRMIN}}{U_{SSRMAX} - U_{SSRMIN}} \right|_{V_s = 220V} \quad (3.8b)$$

where V_{SSRMAX} maximum DC-voltage value at 0^o firing angle or 10Vdc control input signal, V_{SSRMIN} the minimum or DC-Voltage for 180^o triggering angle, or zero voltage($0V_{dc}$) control input, U_{SSRMAX}, and U_{SSRMIN} are the maximum and minimum analog control input voltage for the PCAAV-SSR, respectively, For WassGrill-ICM considering the primary supply voltage 220Vac

$$V_{SSRMAX} = \frac{\sqrt{2}}{\pi} V_s [1 - \cos(\frac{\pi}{10} u(t))] \Big|_{\substack{\delta=0 \\ u(t)=10Vdc}} = 198V \tag{3.9a}$$

$$V_{SSRMIN} = \frac{\sqrt{2}}{\pi} V_s [1 - \cos(\frac{\pi}{10} u(t))] \Big|_{\substack{\delta=180 \\ u(t)=0Vdc}} = 0V \tag{3.9b}$$

Substituting values of Equation (3.9) into (3.8) yields

$$\begin{aligned} K_a &= \frac{V_{SSRMAX} - V_{SSRMIN}}{U_{SSRMAX} - U_{SSRMIN}} \Big|_{V_s=220V} \\ &= \frac{198-0}{10-0} = 19.8V \end{aligned} \tag{3.10}$$

3.3.2 Injera Cooking Plate

The Injera Cooking plate used in this thesis comprises a resistive heater coil, an iron plate, and a covering lid. Figure 3.8 depicts the thermal elements of the cooking plate.

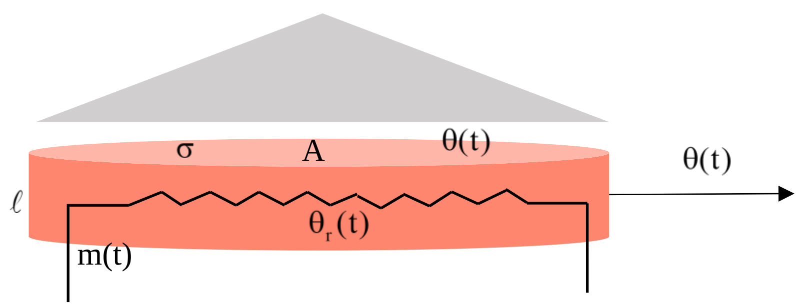

Figure 3. 8 Injera Cooking Plate

In the figure, ℓ denotes the length of the cooking iron plate (cm), σ thermal conductivity (W cm^{-1} ^{o}C^{-1}), A the effective heat transfer area (cm^2), $\theta_r(t)$ resistive coil temperature, $\theta(t)$ iron plate temperature, and m(t) electrical power source defined by

$$m(t) = p(t) + d(t) \tag{3.11}$$

If there is no disturbance, m(t)= p(t).

The physical element in the Injera Cooking plate is thermal resistance R_p ($^{o}CW^{-1}$) and thermal capacitance C_p ($J^{o}C^{-1}$). The thermal resistance is analogous to electrical resistance, and it is the plate resistance to the rate of heat inflow. Thermal capacitance is a measure of how much heat is stored in the iron plate. The plate receives the power from the electric power Actuator-controlled output signal m(t), which induces thermal energy that cooks the Injera. The electric power Actuator heats the cooking plate via the resistive coil embedded in the iron plate, then leaks heat from the cooking plate to the Injera. In this thesis, a model of the Injera Cooking plate is obtained by lumping all thermal properties.

The concept of energy balance states that the rate of heat inflow is equal to the summation of heat outflow and the rate of heat stored [39]. The rate of heat outflow to the surrounding is too low than the heat stored in the iron plate; a generic model of the Injera Cooking plate is obtained as

$$Q_{in} = Q_{sp} \tag{3.12}$$

where Q_{in} heat transfer rate from the resistive coil to the iron plate and Q_{sp} rate of heat stored in the plate.

The rate of heat inflow from the resistive coil to the iron plate in terms of the thermal resistance R_p is

$$Q_{in} = \frac{\theta_r(t) - \theta(t)}{R_p} \tag{3.13}$$

and heat energy stored in terms of thermal capacitance:

$$Q_{sp} = C_p \frac{d\theta(t)}{dt} \tag{3.14}$$

From Equation (3.12)

$$\frac{\theta_r(t)-\theta(t)}{R_p}=C_p\frac{d\theta(t)}{dt}$$
$$\frac{\theta_r(t)}{R_p}=\frac{\theta(t)}{R_p}+C_p\frac{d\theta(t)}{dt} \tag{3.15}$$

Applying Laplace transform at zero initial condition Equation (3.13) become

$$\frac{\Theta_r(s)}{R_p}=\frac{\Theta(s)}{R_p}+C_p s\Theta(s)$$
$$=(\frac{1}{R_p}+C_p s)\Theta(s) \tag{3.16}$$

Rearranging Equation (3.16) yields the relationship between the iron plate temperature and the resistive coil temperature as

$$\frac{\Theta(s)}{\Theta_r(s)}=\frac{1}{(1+C_pR_ps)} \tag{3.17}$$

When thermal energy physically moves in the cooking plate, a time delay occurs related to the movement, and it is translated by a transport delay L as

$$\theta(t)=\theta_r(t-L) \tag{3.18}$$

The transfer function of Equation (3.16), considering the time delay, is rewritten by

$$\frac{\Theta(s)}{\Theta_r(s)}=\frac{e^{-Ls}}{1+C_pR_ps} \tag{3.19}$$

The input thermal energy to the resistive coil provided by the controller input signal m(t) to the resistive heater coil is proportional to the electrical power dissipated by the resistive coil.

$$\theta_r \propto m$$
$$\Theta_r(s)=K_hM(s) \tag{3.20}$$

The product of thermal capacitance and resistance has the dimension of time T_h. The thermal resistance is given by

$$R_p = \frac{\ell}{A \cdot \sigma} = \frac{cm}{cm^2 (Wcm^{-1})^o C^{-1}} = \frac{^oC}{W} \tag{3.21}$$

From Equation (3.19)

$$C_p R_p = \frac{^oC}{W} \cdot \frac{J}{^oC} = \frac{J}{W} = T_h \tag{3.22}$$

Finally, Equation (3.19) gives the first-order-plus-time-delay(FOPTD) model.

$$G_h(s) = \frac{\Theta(s)}{M(s)} = \frac{K_h e^{-Ls}}{1 + T_h s} \tag{3.23}$$

where T_h and K_h are the steady-state gain and the time constant of the Injera Cooking plate, respectively.

3.3.3 Temperature Sensor

A thermocouple sensor measures the Injera Cooking plate temperature $\theta(t)$. The fundamental component of the thermocouple is placed at the center of the cooking plate, as portrayed in Figure 3.9.

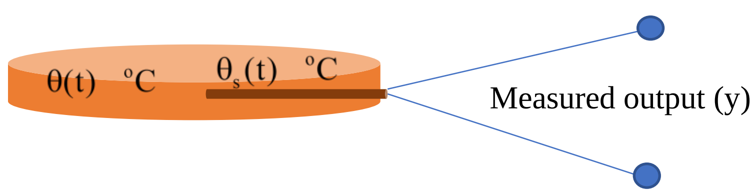

Figure 3. 9 Temperature sensor at the center of the cooking plate

In the figure, $\theta_s(t)$ the temperature of the sensor, Q_s rate of heat inflow to the sensor, and y the measured output temperature. At t=0, the temperature of the sensor and cooking plate temperature is equal $\theta(0) = \theta_s(0)$.

When the cooking plate temperature changes suddenly, the sensor temperature is no longer at a steady state. The heat inflow rate to the sensor will be proportional to the temperature difference from the energy balance equation [39].

$$Q_{in} = Q_{sp} \tag{3.24}$$

The heat inflow rate to the sensor

$$Q_{in} = UA[\theta(t) - \theta_s(t)] \tag{3.25}$$

The proportional constant U is the overall heat transfer coefficient between the cooking plate and sensor ($Wcm^{-2}\ {}^{o}C^{-1}$), and A is the effective heat transfer area (cm^2).

And the increased heat content of the senor

$$Q_{Stored} = C_s \frac{d\theta_s(t)}{dt} \tag{3.26}$$

The differential equation that governs the sensor temperature change

$$\begin{aligned} UA[\theta(t) - \theta_s(t)] &= C_s \frac{d\theta_s(t)}{dt} \\ \theta(t) - \theta_s(t) &= \frac{C_s}{UA} \frac{d\theta_s(t)}{dt} \end{aligned} \tag{3.27}$$

Laplace transforming Equation (3.27) with the initial condition to zero gives

$$\Theta(s) - \Theta_s(s) = \frac{C_s}{UA} s\Theta_s(s) \tag{3.28}$$

The coefficient C_S / UA has a time unit as

$$\frac{J.{}^{o}C^{-1}}{W.{}^{o}C^{-1}} = \frac{J}{W} = T_s \tag{3.29}$$

where T_S is the time constant. Rearranging Equation (3.28), the transfer function that relates the change in sensor temperature to the difference in the cooking plate temperature is driven as

$$\frac{\Theta_s(s)}{\Theta(s)} = \frac{1}{1 + T_s s} \tag{3.30}$$

and the measured output temperature y is proportional to the change in temperature.

$$y \propto \theta_s \tag{3.31a}$$

$$Y(s) = K_s \Theta_s(s) \tag{3.31b}$$

The proportional constant K_s is the sensitivity gain of the temperature sensor. From Equation (3.30), the transfer function from the change in measured output y to the cooking plate temperature θ becomes

$$G_s(s) = \frac{Y(s)}{\Theta(s)} = \frac{K_s}{1+T_s s} \tag{3.32}$$

The temperature sensor sensitivity gain and time constants depend on the construction and types of thermocouple used.

3.4 Experimental Setup

The parameters of the model obtained in the previous section are estimated from the actual response. For this, the input-output data is measured from the response of the experimental equipment.

This stage includes selecting the Injera Cooking plate, temperature sensor, signal conditioner, processing unit and data logger development, and hardware and software integration to obtain the step response of the cooking plate. The required components are selected based on the following experimental setup structure, as depicted in Figure 3.10.

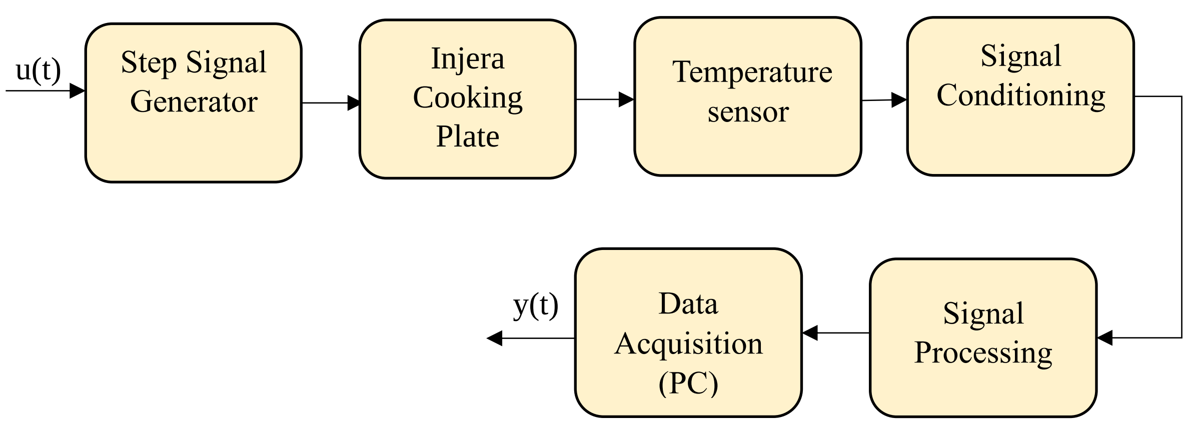

Figure 3. 10 Block diagram of the experimental setup flow

The experimental setup is organized by integrating the hardware and software components. The cooking iron plate and the resistive heating coil constitute an open circuit. Furthermore, the ungrounded K-type thermocouple is fixed to the center of the cooking plate as depicted in Figure 3.11b, and the output terminals are connected to the MAX31856 and Arduino-Uno for signal conditioning and processing, respectively. Finally, the processed signal from the Arduino to the computer is configured by the developed data logger with a 9600 baud rate and 0.5 second sampling time. Figure 3.11a depicts the experimental setup for system parameter estimation.

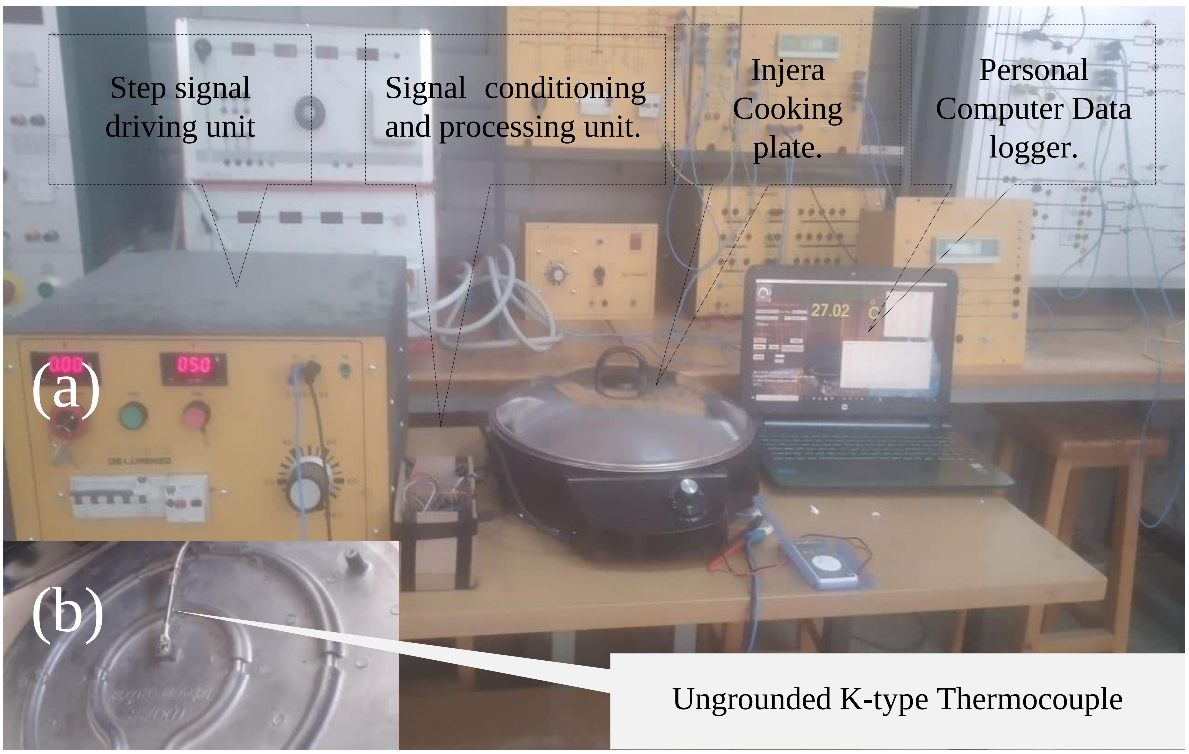

Figure 3. 11 Experimental setups (a) organization (b) Sensor position

3.4.1 Injera Cooking Machine

As mentioned earlier in Section 2.1, WassGrill-ICM is selected as a controlled object because of its ON and OFF temperature controller application, construction efficiency, availability, and flexibility. The controller part of the WassGrill-ICM was removed and the iron plate, the resistive heater, covering lid, and chassis were kept to analyze the open-loop response.

Figure 3. 12 A WassGrill-ICM

3.4.2 Thermocouple Sensor

The thermocouple is a sensor that measures the system output, that is, the temperature of the cooking plate. A thermocouple comprises two dissimilar metal wires connected at one junction, and the change in temperature of the metal wire stimulates the voltage signal or electromotive force (emf). There are three tip configurations in manufacturing the thermocouple, exposed, grounded, and ungrounded type, as in Figure 3.13 [40].

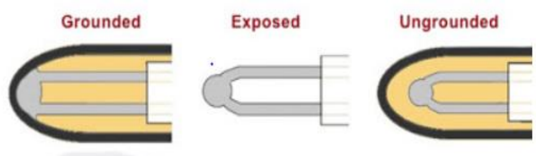

Figure 3. 13 Types of thermocouples based on construction [40].

There is no covering or protection for the welded bead and the wire tips; thus, they are prone to mechanical damage. Their signal is susceptible to electrical noise. The grounded-type thermocouple wire tips and welded bead are in physical contact with the thermocouple sheath. They have less electrical noise than the exposed type. However, the sensing tip is also in physical contact with the sheath; noise can also affect signals. The edge is inside the thermocouple sheath on ungrounded-type thermocouples, and it can handle external electrical interference [40] [41].

The recommended maximum capacity of the cooking plate from Section 2.1 is 450 °C [15]. Choosing a suitable thermocouple focuses on the demerit and merits of each of the three types of thermocouples and temperature ranges. In this thesis, because of its high accuracy, insulation from electrical noise, and popularity. An ungrounded K-type thermocouple, having a temperature range of 0 to 600 ^{o}C, 6mm $\times$100mm(Diameter$\times$Length) with sensitivity gain $\frac{40uV}{^{o}C}$ or $\frac{0.04mv}{^{o}C}$, is selected.

Figure 3. 14 Ungrounded K-type thermocouple

In Section 3.3.3, this thermocouple was modeled as the first-order system

$$\frac{Y(s)}{\Theta(s)} = \frac{K_s}{1+T_s s} \tag{3.33}$$

Since the steady-state sensitivity gain of the selected ungrounded K-type thermocouple has a $0.04[mv/^{o}C]$, K_S becomes

$$K_s = 0.04 \tag{3.34}$$

The time constant T_S depends on the probe diameter and the types of thermocouples used. The time constant for the three types of thermocouples with their respective probe diameter in inch is given in Figure 3.15.

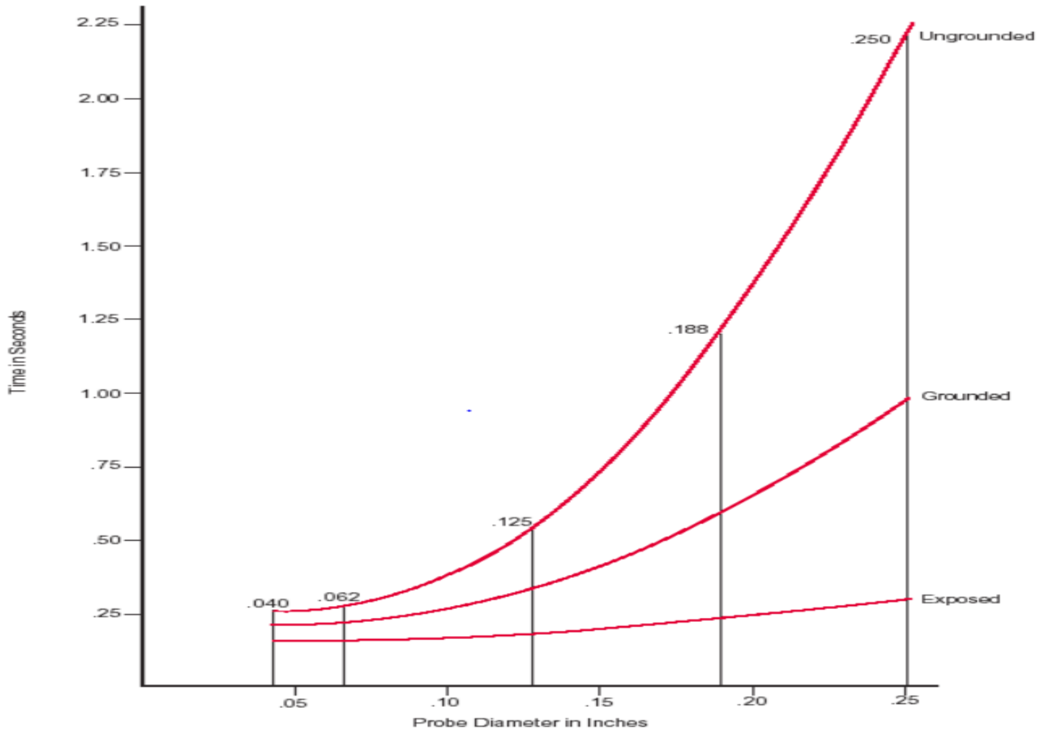

Figure 3. 15 Time constant exposed, grounded, ungrounded with a probe diameter [42]

Selecting the ungrounded K-type thermocouple of a 6mm diameter (or a 0.236 inch) from Figure 3.15, the time constant as

$$T_s = 1.28\,\text{sec} = 0.0213\,\text{min} \tag{3.35}$$

3.4.3 Signal Conditioning

The output voltage signal obtained from the ungrounded K-type thermocouple is too small. It needs further amplification for subsequent use in signal processing and data acquisition. A MAX31856 Precision Thermocouple to Digital Converter with linearization integrated IC is used to manipulate signals for further processing. Detect open thermocouples, Over and Under Temperature Fault, and has 50Hz/60Hz Noise Rejection Filtering [43].

Figure 3. 16 MAX31856 Integrated IC signal conditioner [43]

3.4.4 AtMega16 Microcontroller

After signal conditioning, the next step is signal processing, which changes the signal into helpful information for data acquisition. In this thesis, an AtMega16 microcontroller (Arduino) performs signal processing and data communication with a personal computer. The controller works using the C++ programming language, and the code is loaded on the controller using a universal serial bus (USB).

3.4.5 DC Power Supplier

A DC voltage supplier is used as an input to analyze the dynamics of the Injera Cooking plate. It consists of a control knop and LED indicator for controlling step input u(t); the control knop adjusts the step signal magnitude. The LED displays allow monitoring step input magnitude.

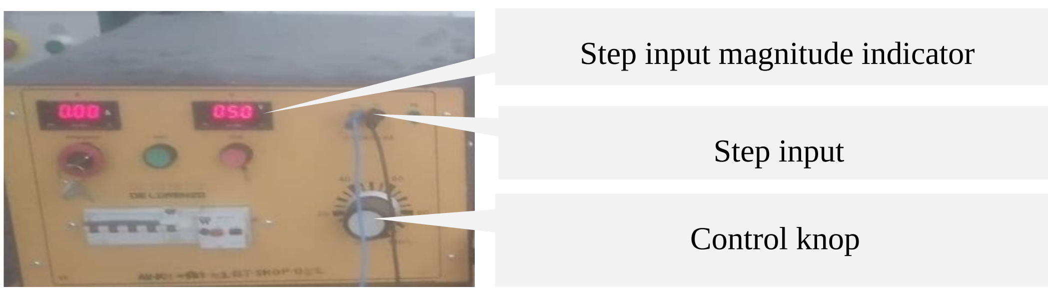

Figure 3. 17 Step signal DC voltage supplier

3.4.6 Data Acquisition

Data acquisition is generally related to acquiring signals, analyzing, presenting, and saving data. The response of the ICM to the change in the step signal is stored for subsequent use in model parameter estimation and validation. In this thesis, a data logger is developed, considering the following criterion.

1. It must acquire the required signals from the Injera Cooking plate.
2. It must provide an effective man-machine interface or Graphical User Interface (GUI).
3. It must store data for further analysis.

The data logger based on Graphical-User-Interface (GUI) comprises serial communication, control, real-time temperature displays, temperature versus time graph, and data saver sections. Figure 3.18 depicts the custom-developed data logger GUI.

Figure 3. 18 Custom-developed data-logger

The commands for data transfer between the microcontroller and the personal computer are carried out through the serial communication section and contain three buttons. The scan port button scans the detected communication port of the microcontroller. The baud rate button selects the data transfer speed on the serial line; it is measured in bits per second(bps), allowing the standard baud rates as selection options: 1200, 2400, 4800, 9600,19200, 38400, 57600, and 115200.

The connect button selects the parameters and creates communication between the computer and the microcontroller.

The control section is used to record, clear, stop and export saved data to an excel datasheet and set step input magnitude. The real-time temperature, graph, sampling time, and amount of sampled data are displayed during the experiment on their respective real-time temperature versus time graph and data saver sections to track the response. The maximum sampling time of the data logger is 0.125 sec (eight sampled responses per second). The data logger stores data in an excel datasheet column arrangement of {N, t, u(t), y(t)}, that is, in the order of the index of sampled data N, sampling time t, input signal u(t), and measured output signal y(t).

3.5 Step Response of the WassGrill-Injera Cooking Plate

In parameter estimation, various types of input signals are in general use. The step signal is frequently used since it is sufficient for analyzing the main essential characteristics of a process, such as a process gain, time constant, and time delay [44] [45] [46].

In this thesis, by employing WassGrill and the cooking temperature assessment Table 2.1, the cooking temperature is considered 190 ^{o}C . A corresponding input was applied to change the temperature from 100 ^{o} C to its optimal cooking temperature to obtain the system's dynamic behavior near the cooking temperature. The cooking plate is first allowed to achieve its steady-state at 100 ^{o} C by a gradual change in step input, and then a positive step change is applied from its steady-state value. Figure 3.19 depicts the response.

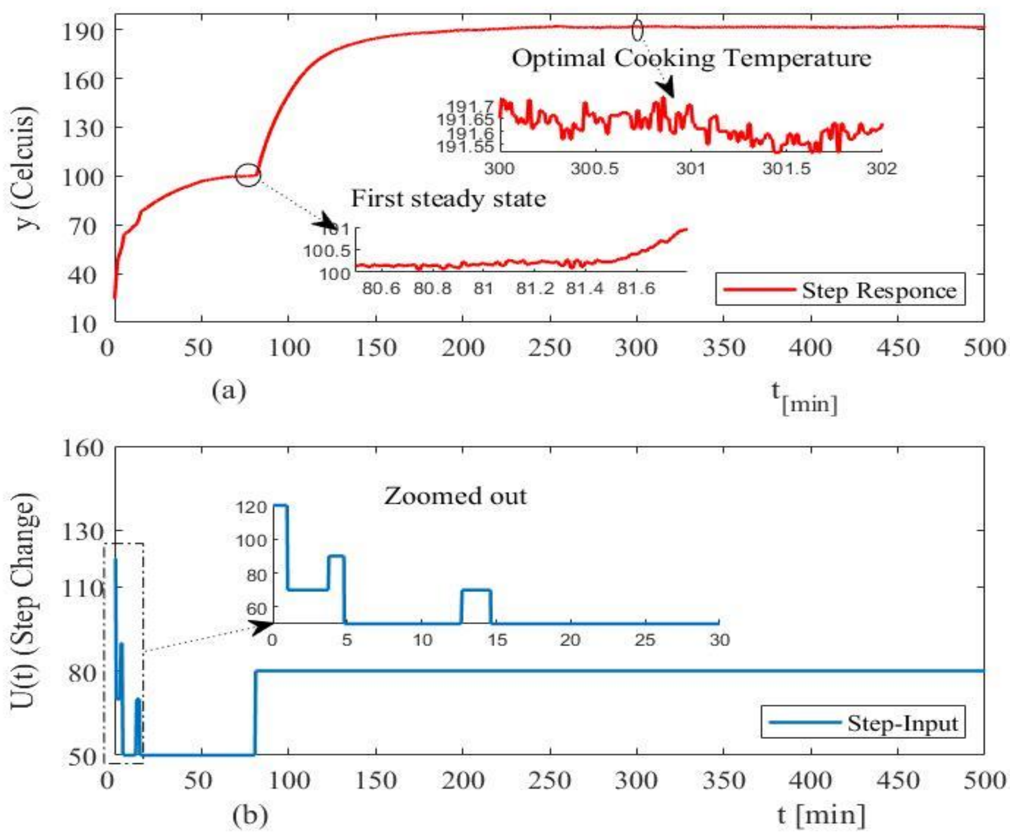

Figure 3. 19 Measured data step up (a) Output y(t) (b) Control input u(t)

As in Figure 3.19, when the response reaches the steady-state of 100 ^{o}C for applying a step input magnitude of 50V, a step signal of 30V is applied for a time equal to twice the transient time ($t_{st} \geq 2t_{rt}$).

The system dynamics may be slightly different when the input increases and decreases; another experiment was conducted by changing the temperature from 190°C to 100°C, Figure 3.20 depicts response.

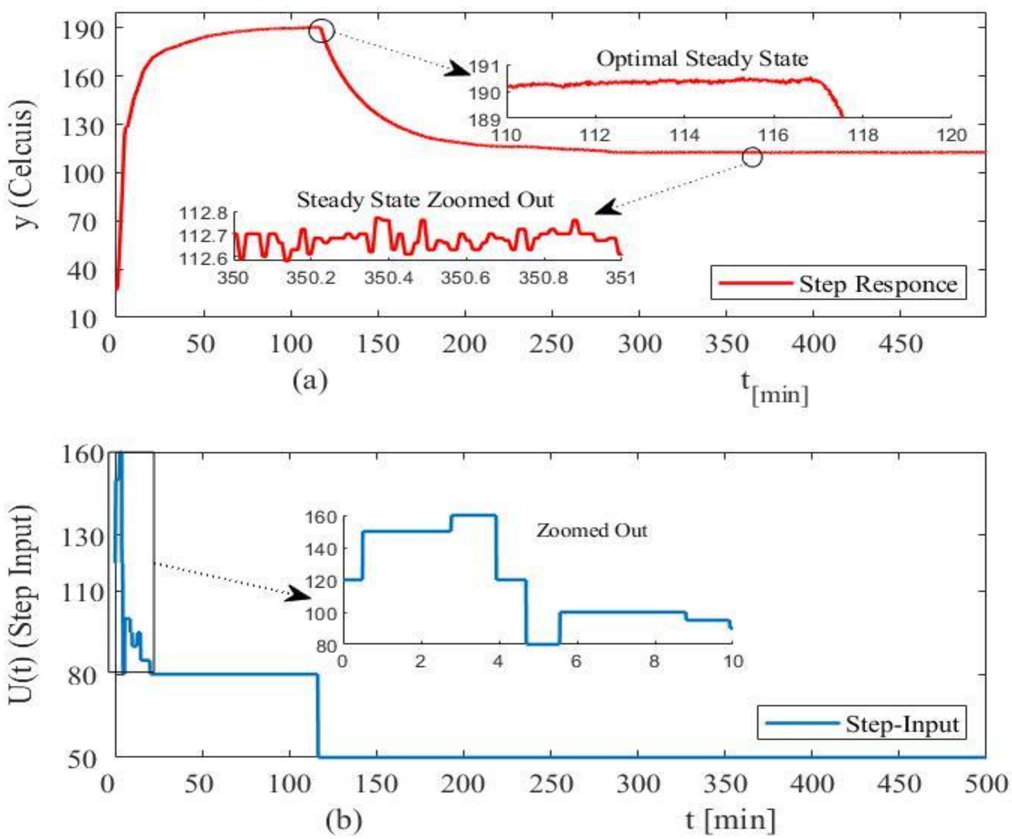

Figure 3. 20 Measured data step down (a) Output y(t) (b) Control input u(t)

In a decreasing step change, first, the system output temperature is kept at operating temperature at a step signal of 80V, and a step input of the same magnitude with the positive step-change is applied. The system's responses for both increasing and decreasing step input from their respective steady-state temperature are depicted in Figures 3.21 and 3.22.

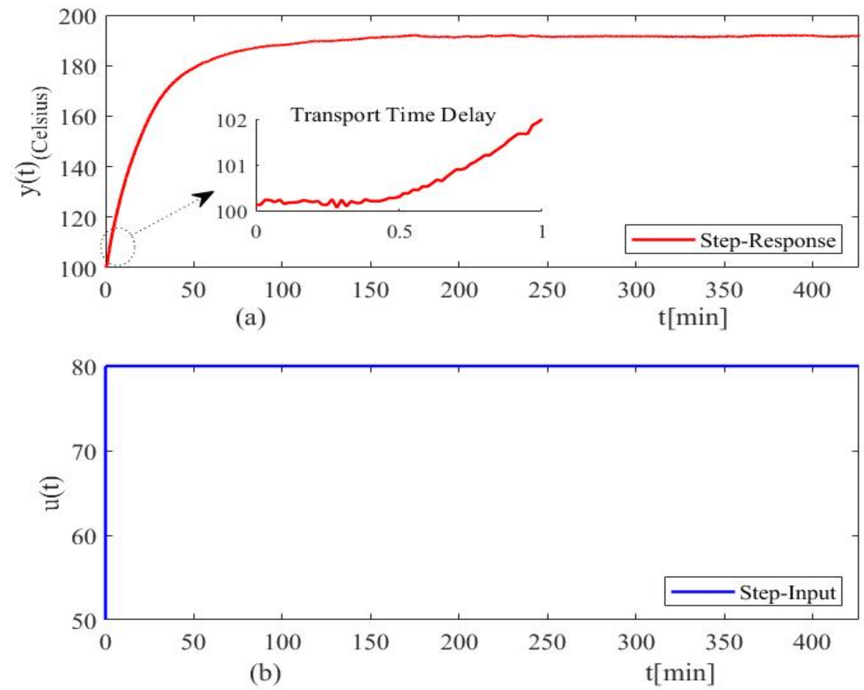

Figure 3. 21 Controlled object (a) Step response (b) Positive step input

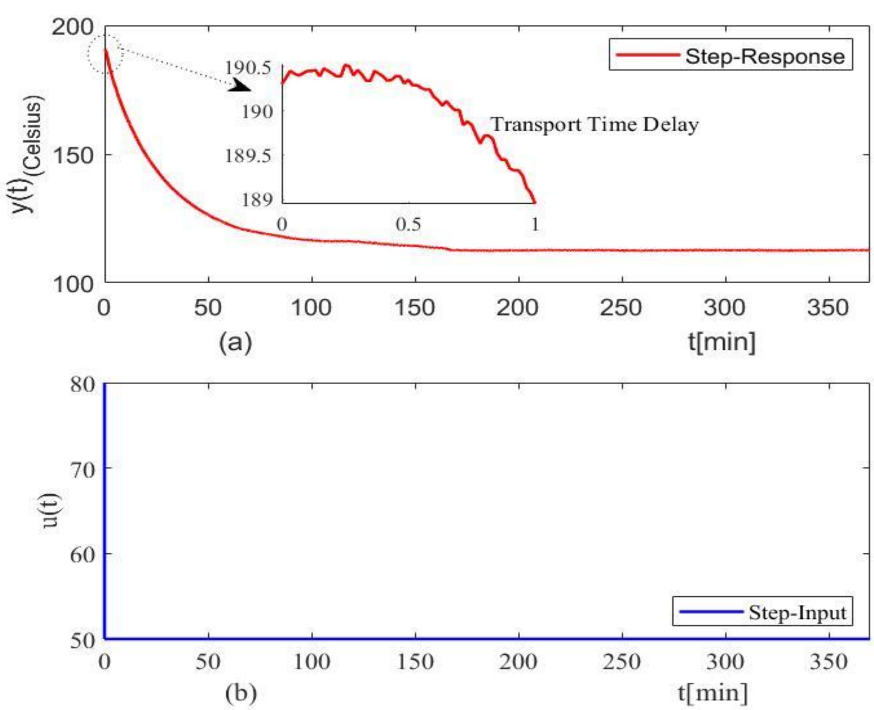

Figure 3. 22 Controlled object (a) Step response (b) Negative step input

As depicted in Figures 3.21 and 3.22, the steady-state time response (t_{st}) has more than twice the transient time (t_{rt}), giving sufficient time response and increasing the accuracy of the model parameters in representing the system's dynamic behavior. The temperature does not respond instantly to a sudden change in step input because of a physical, thermal energy movement; this effect is illustrated by the zoomed-out transport delay plot in Figures 3.21 and 3.22. From the response, there is a slight time delay.

3.6 Genetic Algorithm as an Optimization Tool

Parameter estimation is the process that estimates the model parameters using the given model and measurement data. In this process, an optimization problem occurs, and a genetic algorithm is applied for model parameter estimation.

GA is a global search algorithm based on natural selection and biology that falls under the umbrella of evolutionary algorithm (EA). GA has a pool with a subset of all possible solutions to the given problem. The population for GA is analogous to the human being population. The candidate's solution representing human beings is applied instead of human beings in GA. The chromosome in GA is one such solution to the given objective function. They are an encoded representation of all parameter solutions, and a gene is one element position of the chromosome. These solutions are then subjected to recombination and mutation as in natural genetics, resulting in new offspring. The process continues to iterate throughout generations. Like the Darwinian theory of survival of the fittest, each candidate solution will have a fitness value. Furthermore, the fitter individuals are assigned a higher probability to mate and produce fitter individuals [47] [48]. Figure 3.22 depicts the basic structure of GA.

The GA starts by initializing a population with a random population consisting of 20-100 individuals. The accuracy and time to convergences are affected by the scale of the original population. Small populations represent small parts of the search space; the time for generation is short since further generations are needed to converge. A large population distribution occupies a large portion of the search space, necessitating fewer generations. The time per generation, on the other hand, is increased.

The next step after population initialization is fitness calculation. An objective function helps to determine the fitness value of all chromosomes in each generation. The fitness evaluation step in GA decides how good the solution is concerning the objective function. Generally, it is the guide to an optimal solution. After the fitness evaluation, the selection operation determines the following population based on the fitness value.

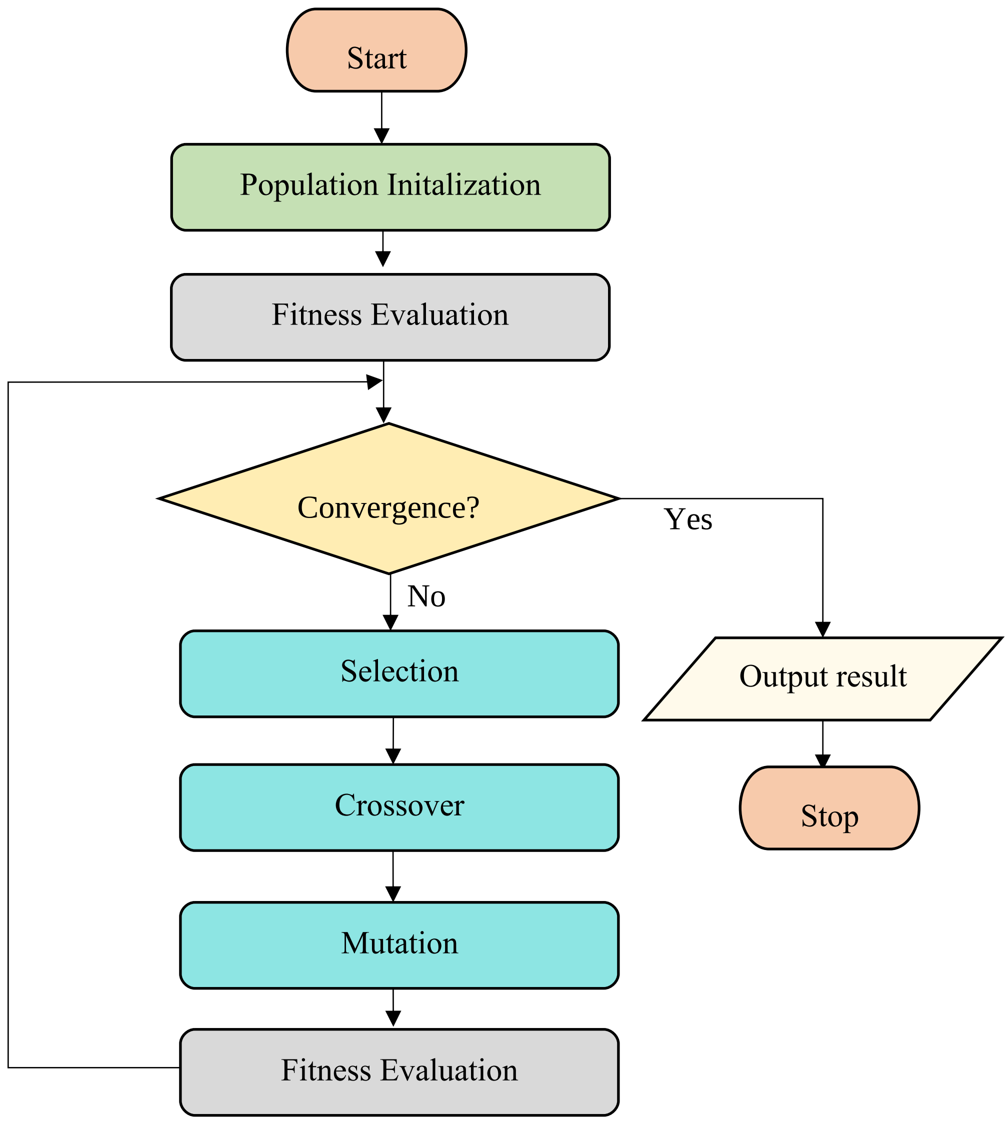

Figure 3. 23 Basic structure of a GA

The selected group is called the mating pool. In the crossover, the stage focuses on swapping certain parts of the mating pool strings to capture the good details of old chromosomes create new ones. Each pair of strings is subjected to the following crossover: An crossover point k is chosen randomly within the length L of the chromosome. Swapping of the tail parts between k+1 and L results in two new sequences [47] [49]. A crossover operation takes place with probability. Having the likelihood of 0 means that the offspring will be exact copies of their parents. A chance of 1 means that each generation will be composed of entirely new offspring. At random, the freshly replicated strings in the mating pool are paired in the single-point crossover.

For maintaining genetic diversity from generation to generation, one or more genes in a chromosome are changed from their initial state; this stage is known as mutation. The mutation operation alters each gene with a low probability because a high mutation rate destroys fit genes [47]-[49]. This series of operations is repeated until the stop condition is satisfied.

3.7 Parameter Estimation Using a GA

In this section, a model adjustment scheme for continuous-time parameter estimation is used for model parameter estimation. Figure 3.24 depicts the block diagram of the model adjustment scheme.

This scheme composes the mathematical models obtained in Subsection 3.3.2 and 3.3.3 and the measured data set from the step response of the Injera Cooking plate and a GA as an adaptive mechanism. In this thesis, the control input u(t) and the measured temperature y(t) signals as the data set are taken for GA parameter estimation. The measured output temperature comprises both the cooking plate and temperature sensor as a second-order-plus-time-delay (SOPTD) process model shown in Equation (3.36).

$$\begin{aligned} Y(s) &= G_a(s)G_h(s)G_s(s)U(s) \\ &= \frac{K_aK_sK_he^{-Ls}}{(1+T_ss)(1+T_hs)}U(s) \\ &= \frac{K_me^{-Ls}}{(1+T_ss)(1+T_hs)}U(s) \end{aligned} \tag{3.36}$$

where K_m denotes the total gain with $K_m = K_aK_sK_h$.

As previously known from the analysis of the electrical power unit and the selected ungrounded K-type thermocouple specifications, the three parameters K_a, K_s, and T_s are *a priori* known as

$$K_a = 19.8,\ K_s = 0.04,\ T_s = 1.28 \tag{3.37}$$

Unknown parameters to be estimated are only K_h, T_h, and L. The same input signal collected via the experiment is applied to the model, and the model output is compared to the WassGrill output to produce the error.

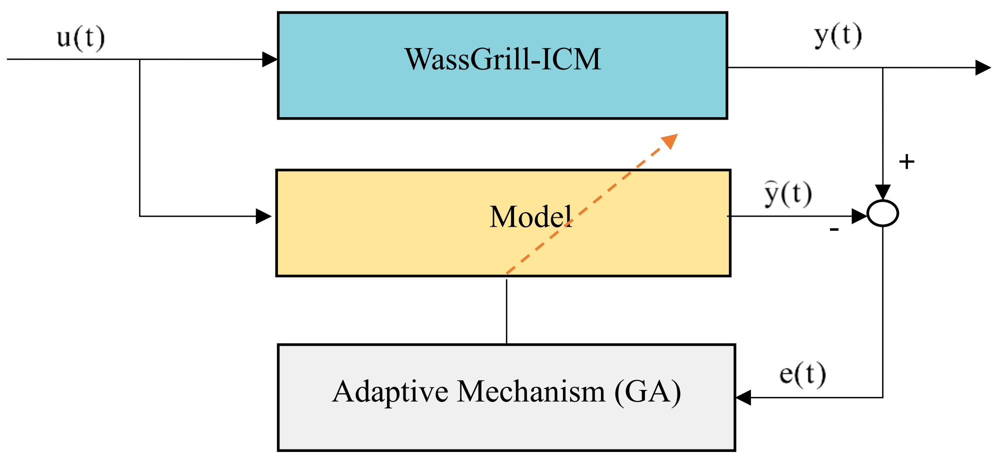

Figure 3. 24 Block diagram of the model adjustment scheme

Then, the GA adjusts the model parameters by minimizing the Integral of Absolute Error (IAE) criterion [50] as

$$IAE = \int_0^{\infty} |e(t)|\, dt \tag{3.38}$$

where $\hat{y}(t)$ is the model output and $e(t) = y(t) - \hat{y}(t)$. The model parameters for both step-up and step-down responses are taken into account since there may exist some nonlinearity in the real system. The estimated model parameters using the scheme in Figure 3.24 are listed in Table 3.2.

Table 3. 2 Parameters estimated using the model adjustment scheme

Response Type	Parameter		
	K_h	T_h	L
Step-up	59.825	24.117	0.0207
Step-down	56.320	28.772	0.0205

Finally, their mean value in Table 3.2 is considered as the estimate. Taking the mean gives the following values:

$$K_h = 58.072,\ T_h = 26.445\text{-min, and } L = 0.021\text{-min} \quad (3.39)$$

3.8 Model Validation

The estimated system model parameters are validated using normalized-root-mean-square-error (NRMSE) percentage fitting. The NRMSE is used to generate the percentage fit number, and it is a measure of how much better the model is in reproducing the observed data relative to the mean of the data [42] [43]. The NRMSE and percentage fit calculation are given in Equation 3.39.

$$\begin{aligned} \text{NRMSE} &= \frac{\|\text{ ICM Response } - \text{ Model Response }\|_2^2}{\|\text{ ICM Response } - \text{ Mean (ICM Response) }\|_2^2} \\ &= \frac{\|\, y(t) - y_m(t) \,\|_2^2}{\|\, y(t) - \text{Mean }(y(t)) \,\|_2^2} \end{aligned} \quad (3.39a)$$

$$\text{Percentage FIT} = (1 - \text{NRMSE}) \times 100 \quad (3.39b)$$

The estimated model provides an NRMSE value of 0.053 for a step-up input. A good model should have an NRMSE value of less than 0.25 to fit more than 75% [46]. The validation shows that the estimated model has a 94.80% percentage fitting with the observed positive step response of the system, implying the best-estimated model parameters as depicted in Figure 3.25. And for the step-down response, the validation shows a 93.50% percentage fitting (0.065 NRMSE values) for the SOPTD model verifying best-estimated model parameters as depicted in Figure 3.26 [46].

Figures 3.25 and 3.26 depict the corresponding model validation of the transfer function modeling for both step-up and step-down inputs.

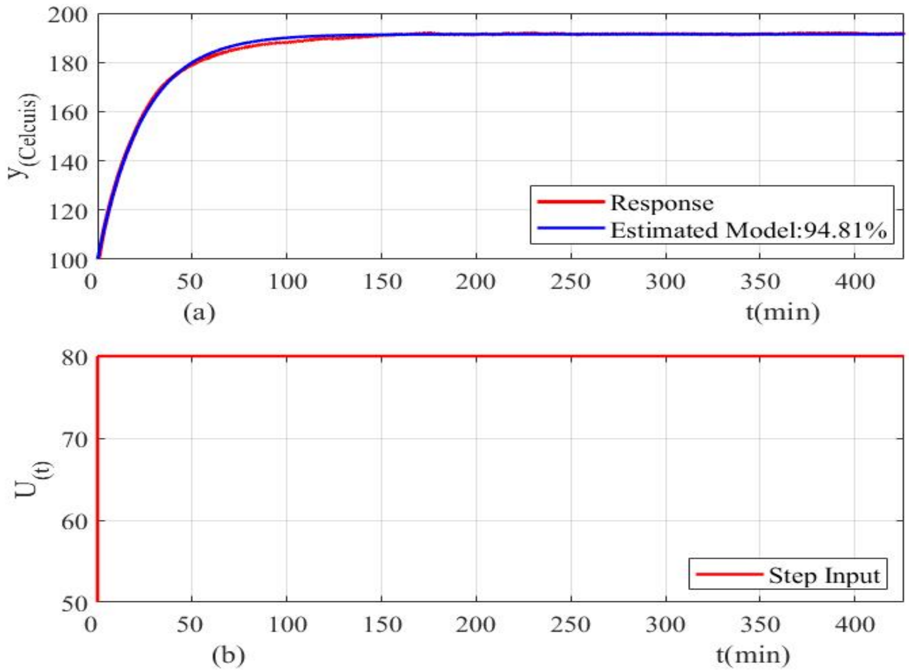

Figure 3. 25 Model validation for the step-up input

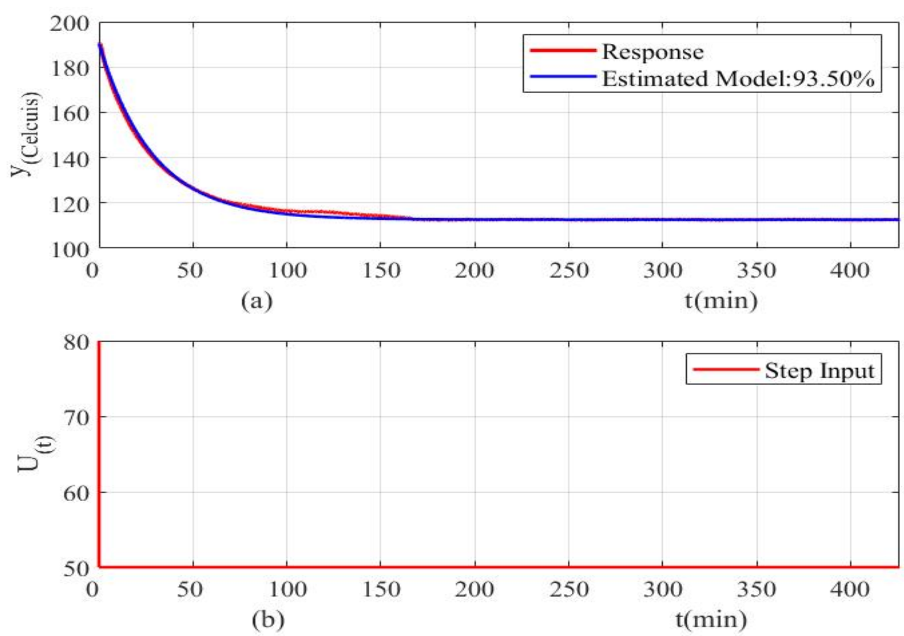

Figure 3. 26 Model validation for the step-down input

The blue and red lines in Figures 3.25 and 3.26 depict the model response $\hat{y}(t)$ and the WassGrill step response $y(t)$, respectively. The slight difference in percentage fitting for step-up and step-down response indicates a considerable heating and cooling coefficient difference.

CHAPTER 4

DESIGN OF A TWO-DEGREES-OF-FREEDOM PID CONTROLLER FOR AN INJERA COOKING MACHINE

This chapter deals with designing the two-degree-of-freedom (TDOF) PID controller for the Injera Cooking Machine (ICM), incorporating an Anti-Windup scheme, and tuning its parameters optimally. The first two sections discuss the design and steady-state of the closed-loop system comprising the TDOF PID controller and the controlled object reflecting the process dynamics. The third and fourth sections analyzed the equivalent structural transformation of the controller for simulation and Anti-Windup (AW) scheme implementation. Finally, a discussion on the optimal tuning of controller parameters for simultaneous setpoint tracking and disturbance rejection responses.

4.1 Temperature Control System for the ICM

Figure 4.1 depicts the block diagram of the TDOF PID controller for the proposed temperature control discussed in Chapter 3.

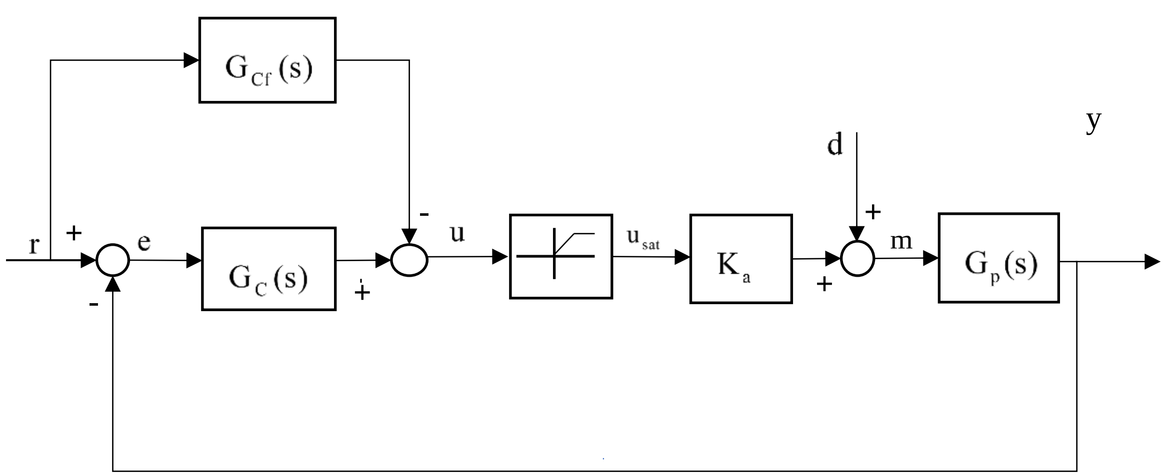

Figure 4. 1 Proposed TDOF PID control system for the ICM

The overall control system consists of five parts: the feedback controller $G_C(s)$, the feedforward controller $G_{Cf}(s)$, the power Actuator $G_a(s)$, processes model $G_p(s)$, and input saturation. r denotes the reference input, e the error, u controller input, u_{sat} the saturated input, m the Injera Cooking plate input, d the disturbance, and the measured output y.

4.1.1 Feedback and Feedforward Controllers

The TDOF PID controller used in this thesis comprises the PID-type feedback controller $G_C(s)$ and the PD-type feedforward controller $G_{Cf}(s)$. The two controllers have the following form [19] [26].

Feedback controller

$$G_C(s) = K_P[1 + \frac{1}{T_i s} + T_d D'(s)] \tag{4.1a}$$

or

$$G_C(s) = K_P + \frac{K_i}{s} + K_d D'(s) \tag{4.1b}$$

Feedforward controller

$$G_{Cf}(s) = -K_p[\alpha + \beta T_D D'(s)] \tag{4.2a}$$

or

$$G_{Cf}(s) = -[\alpha K_p + \beta K_d D'(s)] \tag{4.2b}$$

where K_p is the proportional gain, K_i is the integral gain, K_d is the derivative gain, T_i is the integral time with $T_i = K_p/K_i$, T_d is the derivative time with $T_d = K_d/K_p$, and α and β are the parameters of the feedforward control called two-degree-of-freedom (TDOF) parameters. The input to the feedback controller is the error e and it is the difference between the output y and the reference input r, and the input to the feedforward controller is r.

The $D'(s)$ term in Equations (4.1) and (4.2) is the approximate derivative whose denominator has a first-order polynomial of s and is given by [19] [26]

$$D'(s) = \frac{s}{1 + \tau_d s} \tag{4.3}$$

where $\tau_d = T_d / N$ and N is the derivative factor. If N→∞, Equation (4.3) becomes the ideal derivative. The ideal derivative is of no use in practical applications due to the phenomena known as *derivative kick*. Derivative kick occurs because there is a sudden jump in error at the moment that the setpoint changes. This jump of the error causes its derivative to be instantaneously large. It limits the control input to the upper or lower value for some cycles and potentially disturbs the overall control system. For this reason, the form of Equation (4.3) is used.

Since a computational experiment has demonstrated that changing parameter N does not alter the optimum values of other parameters. It is customary to use fixed values according to the noise environment [19] [26]. In this thesis, N is set to 10.

4.1.2 Input Saturation

In most real systems, several Actuators are used as the power driving devices, such as hydraulic, pneumatic, stepper motors, and so on. The existence of inherent physical limits on the Actuators always leads to saturation on the control input. Saturation can have many forms: a valve that reaches its fully opened or closed position, a motor driver that limits the maximum allowable current, or a car handle that reaches the left or rightmost angle [51].

Saturation can be symmetrical or asymmetric. The proposed ICM is a good example for asymmetrical saturation: the element can only heat, and the heater power has an upper limit dictated by the driving signal, but a reverse demand (i.e., cooling ICM) as control action is impossible. The machine has to wait until it cools down by convection and reaches that temperature.

Saturation in this thesis limits the controller output signal within a range of u_{min}~ u_{max} V_{dc} to protect the Actuator from its physical limit, which is modeled by a saturation input as

$$u_{sat} = \begin{cases} u_{max} & u > u_{max} \\ u & u_{min} < u \le u_{max} \\ u_{min} & u \le u_{min} \end{cases} \tag{4.4}$$

In this thesis, a u_{min} and u_{max} are set to 0 and 10, respectively.

4.1.3 Controlled Object

The input signal from the power Actuator controls the output temperature. The Actuator supplies proportional voltage to the ICM in response to the controller output signal resulting in controlled output temperature. From Section 3.7, the ICM process model is given by:

$$G_p(s) = G_h(s)G_s(s) = \frac{K_h K_s}{(1+T_h s)(1+T_s s)} e^{-Ls} \tag{4.5}$$

Where K_h and T_h are the gain and time constant of the process model, respectively, and K_S and T_s are the gain and time constant of the temperature sensor, respectively.

The feedback gain is unity as the temperature sensor is part of the process model, as shown in Equation (4.5). The disturbance d enters before $G_p(s)$ because pouring the liquid dough changes the dynamic behavior of the cooking plate before the sensor observes its effect.

4.2 Steady-State Analysis of the Closed-Loop System

When the system in Figure 4.1 operates within the linear range of the power Actuator, the closed-loop transfer functions from r to y and disturbance d to y are expressed by

$$E(s) = R(s) - Y(s) \tag{4.6a}$$

$$U(s) = G_{Cf}(s)R(s) + G_C(s)E(s) \tag{4.6b}$$

$$Y(s) = G_p(s)[K_a U(s) + D(s)] \tag{4.6c}$$

Substituting Equations (4.6a) and (4.6b) to (4.6c) yields:

$$Y(s) = G_p(s)\{K_a[G_{Cf}(s)R(s) + G_C(s)(R(s) - Y(s))] + D(s)\} \tag{4.7}$$

Rearranging Equation (4.7):

$$Y(s) = \frac{K_a G_p(s)[G_{Cf}(s) + G_C(s)]}{1 + K_a G_C(s)G_p(s)} R(s) + \frac{G_p(s)}{1 + K_a G_C(s)G_p(s)} D(s) \tag{4.8a}$$

$$= G_{yr}(s)R(s) + G_{yd}(s)D(s) \tag{4.8b}$$

Where the two transfer functions $G_{yr}(s)$ and $G_{yd}(s)$, are:

$$G_{yr}(s)=\frac{K_aG_p(s)[G_{Cf}(s)+G_C(s)]}{1+K_aG_C(s)G_p(s)}$$
$$G_{yd}(s)=\frac{G_p(s)}{1+K_aG_C(s)G_p(s)} \quad (4.9)$$

4.2.1 Setpoint Tracking Response

The steady-state error is derived for a setpoint assuming zero disturbance (d= 0). Obtaining the error e(s) in terms of r(s) gives

$$\begin{aligned}E(s)&=R(s)-Y(s)\\&=R(s)-\frac{K_aG_p(s)[G_{Cf}(s)+G_C(s)]}{1+K_aG_C(s)G_p(s)}R(s)\end{aligned} \quad (4.10)$$

For a step input $R(s)=\frac{a}{s}$ $(a\neq 0)$, the steady-state error e_{ss} is given by:

$$e_{ss}=\lim_{s\to 0}s\cdot E(s) \quad (4.11a)$$

$$=\lim_{s\to 0}\{a-\frac{aK_aG_p(s)[G_{Cf}(s)+G_C(s)]}{1+K_aG_C(s)G_p(s)}\} \quad (4.11b)$$

$$=\lim_{s\to 0}\{a-\frac{aK_aG_p(s)[\frac{G_{Cf}(s)}{G_C(s)}+1]}{\frac{1}{G_C(s)}+K_aG_p(s)}\} \quad (4.11c)$$

From Equations (4.1) -(4.3) and (4.5), since the following conditions are satisfied

$$\lim_{s\to 0}G_C(s)=\lim_{s\to 0}K_P[1+\frac{1}{T_is}+\frac{T_Ds}{1+\tau_Ds}]=\infty \quad (4.12a)$$

$$\lim_{s\to 0}\frac{G_{Cf}(s)}{G_C(s)}=\frac{\lim_{s\to 0}\{-K_p[\alpha+\beta T_DD(s)]\}}{\lim_{s\to 0}G_C(s)}=0 \quad (4.12b)$$

$$\lim_{s\to 0} G_p(s) = K_h K_a \neq 0 \quad (4.12c)$$

Hence, Equation (4.11c) becomes zero, that is, $e_{ss} = a - a = 0$.

4.2.2 Disturbance Rejection Response

Like the previous case, the steady-state error derived for a step-type disturbance assuming zero setpoints (r= 0). Obtaining e(s) in terms of $d(s)$ yields

$$\begin{aligned} E(s) &= R(s) - Y(s) \\ &= -\frac{G_p(s)}{1 + K_a G_C(s) G_p(s)} D(s) \end{aligned} \quad (4.13)$$

For a step-type disturbance $D(s) = \frac{b}{s}$ $(b \neq 0)$, the steady-state error e_{ss} is given by

$$e_{ss} = \lim_{s\to 0} s \cdot E(s) \quad (4.14a)$$

$$= \lim_{s\to 0} \{-\frac{bG_p(s)}{1 + K_a G_C(s) G_p(s)}\} \quad (4.14b)$$

$$= \lim_{s\to 0} \{-\frac{b\frac{G_p(s)}{G_C(s)}}{\frac{1}{G_C(s)} + K_a G_p(s)}\} \quad (4.14c)$$

Applying Equation (4.12) to Equation (4.14) results in the zero steady-state error, that is, $e_{ss}= 0$. The proposed control system makes the steady-state error zero robustly for step-type setpoint and step-type disturbances. The step-type setpoint and disturbance response correspond to a change in step magnitude from the initial to cooking temperature and a sudden change in temperature because of the liquid dough.

4.3 Equivalent Structure of the TDOF PID Controller

As shown in Figure 4.1 and the transfer function of Equations (4.1) and (4.2), the two controllers have the same proportional and derivative terms; in implementing those terms, calculations duplicate unnecessarily. Therefore, obtaining the equivalent transfer function is convenient to implement.

From Equation (4.6b)

$$U(s) = G_{Cf}(s)R(s) + G_C(s)[R(s) - Y(s)] \tag{4.15a}$$

$$= [G_{Cf}(s) + G_C(s)]R(s) - G_C(s)Y(s) \tag{4.15b}$$

Substituting Equations (4.1) and (4.2) to Equation (4.15) gives:

$$U(s) = \{-K_p[\alpha + \beta T_D D'(s)] + K_P[1 + \frac{1}{T_i s} + T_D D'(s)]\}R(s) - K_P[1 + \frac{1}{T_i s} + T_D D'(s)]Y(s) \tag{4.16a}$$

By rearranging standard terms

$$\begin{aligned} U(s) &= [(1-\alpha)K_P + \frac{K_p}{T_i s} + (1-\beta)K_p T_D D'(s)]R(s) - [K_P + \frac{K_p}{T_i s} + K_p T_D D'(s)]Y(s) \\ &= K_p\{[(1-\alpha)R(s) - Y(s)] + \frac{1}{T_i s}[R(s) - Y(s)] + T_D D'(s)[(1-\beta)R(s) - Y(s)]\} \end{aligned} \tag{4.16b}$$

Equation (4.16) translates the TDOF PID into a component separated structure as a summation of three outputs u_p, u_i, and u_d multiplied by K_p.

$$U(s) = K_p[U_p(s) + U_i(s) + U_d(s)] \tag{4.17a}$$

Where

$$\begin{aligned} U_p(s) &= (1-\alpha)R(s) - Y(s) \\ U_i(s) &= \frac{1}{T_i s}[R(s) - Y(s)] \\ U_d(s) &= T_D D'(s)[(1-\beta)R(s) - Y(s)] \end{aligned} \tag{4.17b}$$

Figure 4.2 depicts the equivalent structure of the TDOF PID controller.

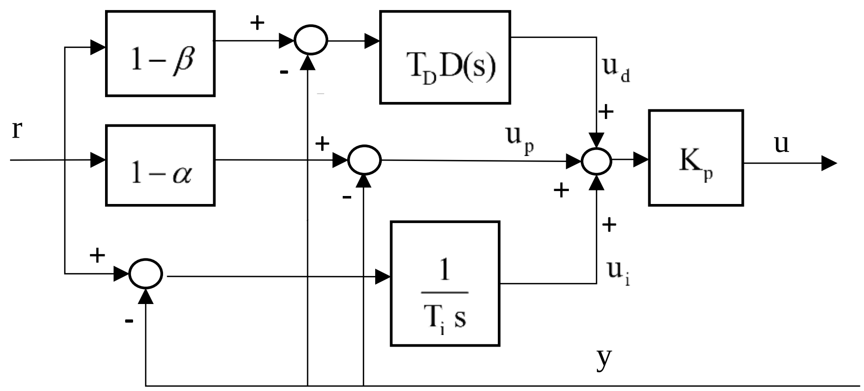

Figure 4. 2 Equivalent structure of the TDOF PID controller

4.4 Anti-Windup (AW) Scheme

In the proposed TDOF PID controller for Injera Cooking Machine, the input to the PCAAV-SSR or Actuator is limited to its saturation(0-10V_{dc}). From Section 4.2, the integral action in the TDOF PID controller is responsible for the setpoint tracking with no steady-state error. When a controller with integral receives an error signal for a significant period, the integral term of the controller will increase at a rate governed by the integral time of the controller, causing the Actuator to reach its 100% or 0% percent of its scale or 10V_{dc}-0V_{dc}. When the control output is equal to the reference value, the error sign will take a long time to integrate backward, resulting in an extended overshoot. This effect is known as an Integral Windup. The system performance is affected if the Integral Windup is not taken correctly at controller design. The Anti-Windup controller (AW) scheme ensures the integral at a proper value as the Actuator saturates. The controller can restart operations as soon as the control error changes. The component separated structure of the TDOF PID controller in Figure 4.2 is suitable to implement a parallel form or a back-calculation [52] Anti-Windup scheme, as depicted in Figure 4.3.

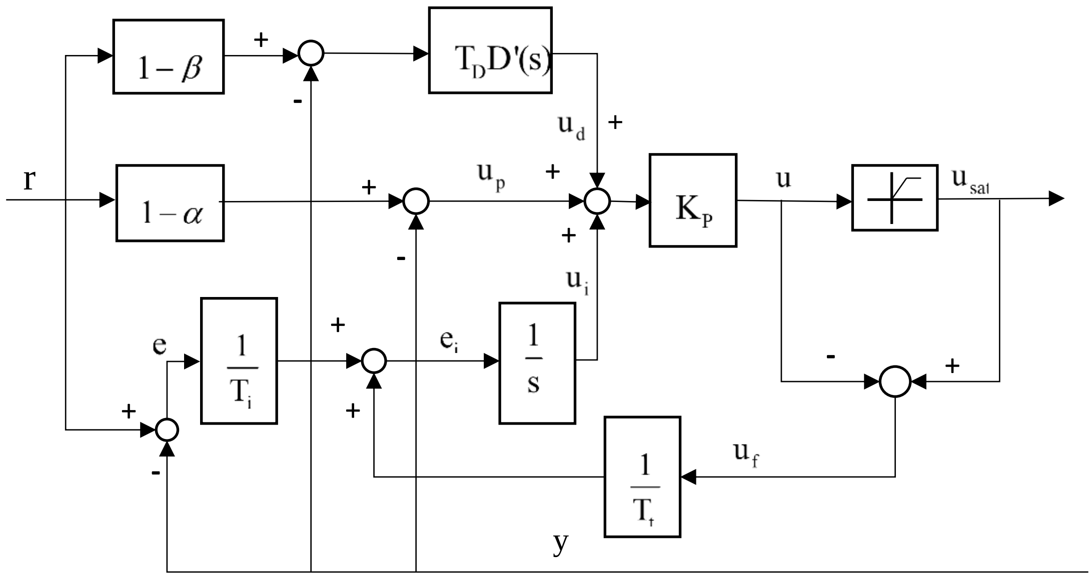

Figure 4. 3 TDOF PID controller with the back-calculation AW scheme

The input saturation works with

$$u_{sat} = \begin{cases} 10 & u(s) > 10 \\ u(s) & 0 < u(s) \le 10 \\ 0 & u(s) \le 0 \end{cases} \tag{4.18}$$

The difference between the controller output $u(s)$ and saturation output u_{sat} is given by:

$$u_f(t) = u(t) - u_{sat}(t) \tag{4.19}$$

The scheme has no effect as long as the Actuator input is equal to the controller output. When the Actuator reaches saturation, the Anti-Windup controller is activated, and the integral value is changed to prevent an integrator output from reaching saturation [52] [53]. As depicted in Figure 4.8, the integrator error signal is fed back to the controller by an integrator with a constant monitoring time called time tracking constant T_t. The general rule for setting T_t is choosing values between the integral time T_i and derivative time T_d or using the rule of thumb, suggesting $T_t = \sqrt{T_i \cdot T_d}$ [54] [55]. The other method is to use global search algorithms. In this thesis, GA tuned the tracking time constant T_t.

Computing the integrator error signal e_i

$$e_i(t) = \frac{1}{T_i} e(t) + \frac{1}{T_t}[u_{sat}(t) - u(t)] \tag{4.20}$$

If the P and D actions are zeros, that is, $u_p = 0$ and $u_d = 0$, the internal loop from e to u is manipulated as

$$U = \frac{K_p}{s} E_i(s) \tag{4.21}$$

Substituting Equation (4.20) to Equation (4.21) yields

$$U = \frac{K_p}{s}\{\frac{1}{T_i} E(s) + \frac{1}{T_t}[U_{sat} - U]\} \tag{4.22}$$

Rewriting Equation (4.22) gives

$$U = \frac{\frac{T_t}{T_i}}{1 + \frac{T_t}{K_p} s} E(s) + \frac{1}{1 + \frac{T_t}{K_p} s} U_{sat} \tag{4.23}$$

where T_t / K_p is the time constant, and in the special case where $T_t = T_i$, the time constant becomes $1/K_i$.

4.5 Parameter Tuning of the TDOF PID Controller

As seen in Figure (4.2), there are six tuning parameters, that is, five parameters $\{K_p, K_i, K_d, \alpha, \beta\}$ for the TDOF PID controller and one parameter T_t for the AW scheme. Those parameters require proper tuning for better performance. The authors in [26] proposed a two-step tuning method for the TDOF PID controller without an AW scheme. They are first optimizing the feedback PID controller parameters $\{K_p, K_i, K_d\}$ for disturbance rejection. Second, by fixing the PID controller parameters optimizing setpoint tracking by adjusting the parameters $\{\alpha, \beta\}$ for the feedforward controller. However, this two-step tuning method may not guarantee the optimal solution because the first step determines the significant characteristics $\{K_p, K_i, K_d\}$. If setting $G_C(s)$ goes too excessively, tuning of $G_{Cf}(s)$ at the second step becomes difficult, resulting in an inadequate setpoint response; For this reason, in this thesis, the overall controller parameters, including AW time tracking constant, are adjusted simultaneously.

The problem of adequately tuning those parameters for optimal performance requires an optimization algorithm and performance criterion(or an objective function). The Integral Absolute Error (IAE) criterion is employed as an objective function for the proposed method. The IAE criterion is of the form [50]

$$IAE = \int_0^{\infty} | e(t) | \, dt \tag{4.24}$$

The error e(t) is the difference between the reference input r and the output y.

$$e(t) = r - y \tag{4.25}$$

As can be inferred from Equations (4.1),(4.2), and (4.22), tuning the six parameters causes a multi-parameter optimization problem. The objective function can be multimodal in which several local solutions and the global solution may exist together in some cases. This thesis uses a Genetic Algorithm (GA) as an optimization tool discussed in Section 3.6. Figure 4.4 depicts pseudocode for a GA.

```
Set k= 0;
Initialize a population P(k) randomly;
Evaluate the fitness of the chromosomes in P(k);
While (termination criteria is not reached) do
        Set k= k+1;
        Select the off spring from their parents and setup P(k);
        Crossover the chromosomes in P(k);
        Mutate the chromosomes in P(k);
        Evaluate the fitness of the chromosomes in P(k);
 end
```

Figure 4. 4 GA pseudocode

CHAPTER 5

RESULT AND DISCUSSION

This chapter presents the simulation result to assess the effectiveness of the proposed TDOF PID controller with AW scheme implementation for optimal temperature control of the ICM. The response of the proposed controller is compared to that of the conventional PID controller to assess setpoint tracking and disturbance rejection performances. The results of controller parameters tuned by CHR, CVJIN, and GA for optimal setpoint tracking performance (PID-SP) and disturbance rejection response (PID-DIS) in 1DOF PID assess the comparison with the TDOF PID tuned by GA. Also, this chapter presents the simulation results to evaluate the effectiveness of the AW scheme implementation for the TDOF PID controller in handling the effects of the Integral Windup. The time-domain specification measures demonstrate the capability of the proposed controller in achieving the multi-objective performance. A tabular and graphical representations present the result of the calculated quantitative performance measures. MATLAB-2019b software used implements the simulation.

5.1 Parameter Values of the Controlled Object

In chapter 3, Dealing with system modeling and parameters of the controlled object, the gain of the Actuator is obtained in Subsection 3.3.1, and parameters of the Injera Cooking plate are found from the step response and GA for parameter estimation in Section 3.5 and 3.7, respectively. The SOPTD model validation in Section 3.8 shows a 94.80% and 93.50% percentage fitting for a step-up and step-down response, respectively.

Table 5.1 lists the summary of the model parameters.

Table 5. 1 Model parameters of the controlled object

Parameter name	Parameter	Value
Injera Cooking plate gain	K_h	58.072
The time constant of the cooking plate	T_h	26.445
Time delay	L	0.021
Sensor gain	K_s	0.04
Sensor time constant	T_s	0.0213
Actuator gain	K_a	19.8

The actuator saturation limit U_{min}=0 and U_{max}=10 are set.

5.2 Parameter Settings for the TDOF PID Controller and the AW Scheme

Chapter 4 dealt with the design of the proposed controller and its optimal tuning of the six parameters K_p, K_i, K_d, α, β, and T_t. Tuning the parameters was implemented by GA Toolbox software on MATLAB 2019b, using the following parameters.

- Number of Population: 30
- Number of Generation: 40
- Lowerbound (LB): $[0\ \ 0\ \ 0\ \ 0\ \ 0\ \ \ 0]^T$
- Upperbound (UB): $[35\ \ 10\ \ 5\ \ 1\ \ 1\ \ 5]^T$

Figure 5.1 depicts the convergency curve for the best and mean fitness values of the GA tuning.

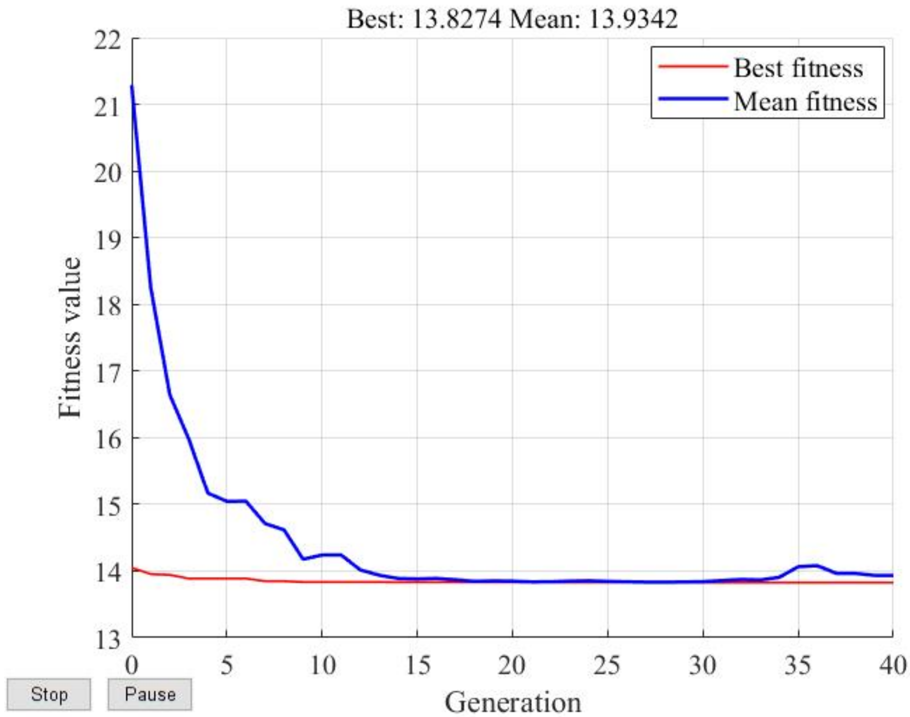

Figure 5. 1 Convergence characteristics of the GA

The convergency curve has the best fitness value of 13.827, and Table 5.2 lists the result of optimally tuned parameters.

Table 5. 2 GA tuned controller parameters

Parameters	Parameter name	Parameter symbol	Values
PID	Proportional gain	K_p	33.794
	Integral gain	K_i	8.947
	Derivative gain	K_d	3.521
TDOF	Alpha	α	0.863
	Beta	β	0.678
Anti-Windup	Time tracking	T_t	1.358

5.3 Parameter Setting for 1DOF PID Controller

This section presents the controller parameter tuning of the 1DOF PID controller to assess the effectiveness of the proposed controller. Three controller tuning methods evaluate the comparison Chien, Hrones, and Reswick (PID-CHR), Jan Cevjin (PID-CEVJIN), and GA tuned method (PID-GA). The first section discusses the required FOPTD approximation of the SOPTD model for PID-CHR and PID-CEVJIN methods. Then in the second section, the result of the tuned parameter is presented.

5.3.1 FOPTD Approximation of the Controlled Object

The PID-CHR and PID-CVEJIN methods discussed in Section 2.2 need the S-curve response of the system as a FOPTD approximation. For this purpose, a GA approximates the controlled object obtained in Equation (3.36) into the required FOPTD model in Equation (2.4). Figure 5.2 depicts the block diagram of model reduction using GA.

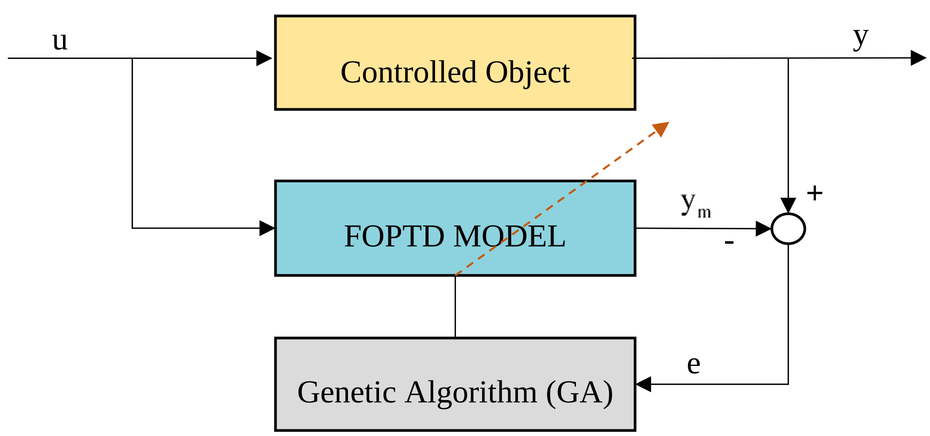

Figure 5. 2 GA model approximation from SOPTD to FOPTD model

The FOPTD parameters discussed in Section 2.2 are time constant T, process gain K, and time delay L. GA adopts the FOPTD model parameters by minimizing the error between the two outputs. The Integral Absolute Error (IAE) error criterion is implemented as an objective function.

$$IAE = \int_0^\infty |e(t)|\,dt \tag{5.2}$$

where the error e(t) is the difference between the output y of the controlled object and the model output y_m with

$$e(t) = y(t) - y_m(t) \tag{5.3}$$

The model approximation was implemented by GA toolbox software on MATLAB 2019b, using the following parameters.

- Number of Population: 30
- Number of Generation: 40
- Lower bound (LB): $[0 \quad 0 \quad 0]^T$
- Upper bound (UB): $[3 \quad 30 \quad 0.1]^T$

Figure 5.3 depicts the result of the GA convergency curve for the GA approximation.

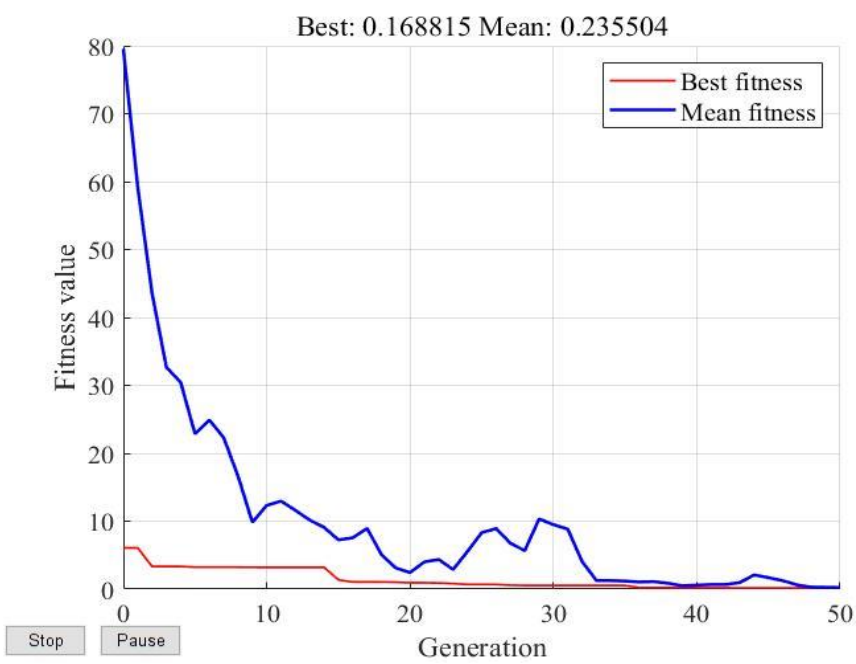

Figure 5. 3 GA approximation convergency curve

The convergency curve has the best fitness value of 0.168. Table 5.3 lists the resulting FOPTD model parameter approximation.

Table 5. 3 GA approximation result FOPTD model parameters

Model	Model Parameters		
	K	T	L
FOPTD	2.323	26.456	0.062

The approximated FOPTD model is validated using percentage fitting as depicted in Figure 5.4.

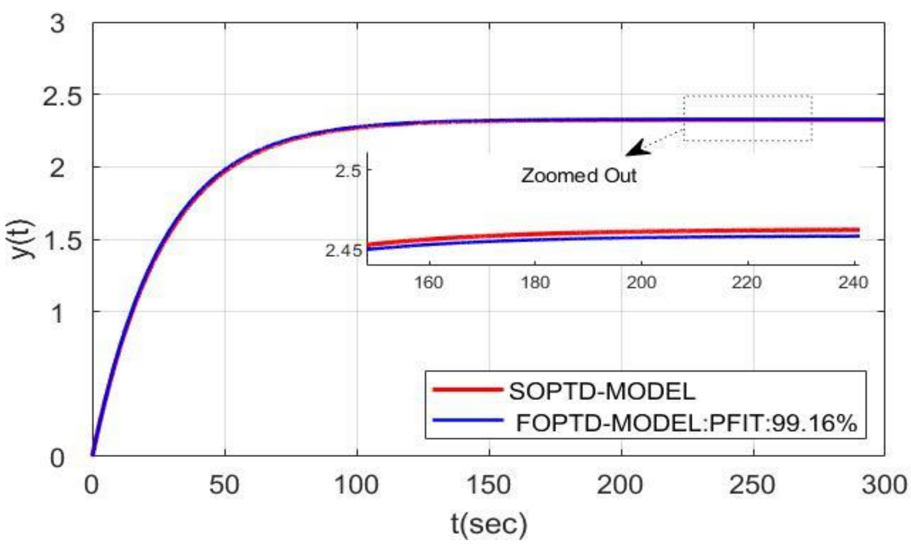

Figure 5. 4 GA model approximation validation

The FOPTD model fit 99.16% with the SOPTD system model, implying validated model reduction.

5.3.2 Parameter Setting of the 1DOF PID Controllers

This section discusses 1DOF PID controller parameter settings using three PID tuning methods CHR, CEVJIN, and GA. The parameters tuned by CHR and CEVJIN methods are obtained based on Tables 2.2 and 2.3, respectively, and two-step tuning methods for PID-GA. For setpoint tracking (PID-GA-SP), the setpoint was changed from $100\,^{o}C$ to $190\,^{o}C$, while setting the disturbance d zero. For disturbance rejection (PID-GA-DIS), a step-type disturbance that changes the dynamic behavior to deviate about 47% from its steady-state value was altered while the temperature is maintained steady-state at 190 °C . The simulation is implemented on MATLAB 2019b GA-tool box software by the following GA parameter setting.

- Number of Population: 30
- Number of Generation: 40
- Lower bound (LB): $[0 \;\; 0 \;\; 0]^T$
- Upper bound (UB): $[35 \;\; 10 \;\; 5]^T$

Figure 5.5 depicts the convergency curve for PID-GA-SP and PID-GA-DIS, respectively.

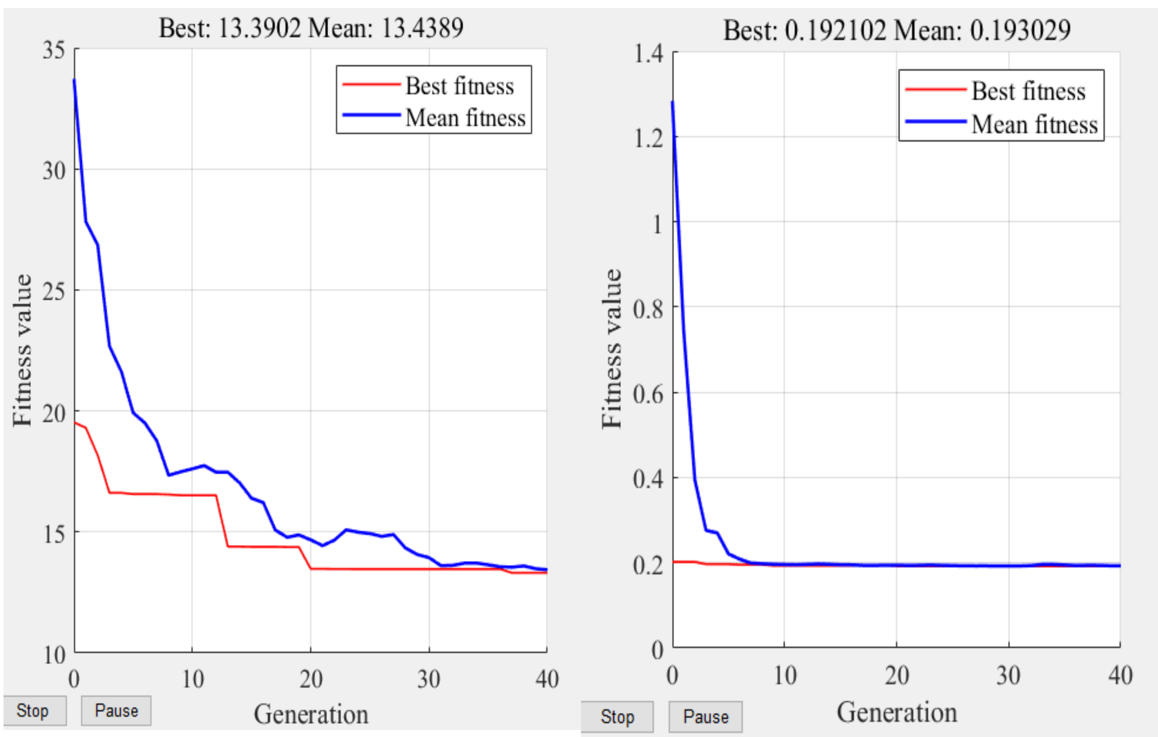

(a) Setpoint tracking (b) Disturbance rejection

Figure 5. 5 GA convergency curve PID-GA

Tables 5.4 and 5.5 summarize the parameters tuned by the CHR, CEVJIN, and GA methods.

Table 5. 4 PID controller parameters tuned for setpoint tracking

Tuning method	Controller parameters		
	K_p	K_i	K_d
PID-GA-SP	34.887	0.1570	0.029
PID-CHR-SP	5.584	0.211	0.173
PID-CVEJIN-SP	6.986	0.264	0.144

Table 5. 5 PID controller parameters tuned for disturbance rejection

Tuning method	Controller parameters		
	K_p	K_i	K_d
PID-GA-DIS	34.998	9.99	0.113
PID-CHR-DIS	8.842	59.614	0.229
PID-CVEJIN-DIS	7.591	29.258	0.143

5.4 Controller Performance Test

This section discusses the effectiveness of the proposed controller for simultaneous set-point tracking and disturbance rejection. Three controller tuning methods demonstrate the robustness of the proposed TDOF PID controller, namely GA, CHR, and CVEJIN methods tuned for setpoint tracking (PID-SP) and disturbance rejections (PID-DIS). The controller parameters in Table 5.4 and Table 5.5 assess the controller objective for both simultaneous setpoint tracking and disturbance rejection. Time-domain specifications measure the performance evaluation of the system. Furthermore, the last subsection discusses the effect of Integral Windup and its corresponding Anti-Windup (AW) scheme implementation.

5.4.1 Setpoint Tracking Response

In this section, the single-point tracking and setpoint variation assess the performance of the proposed controller. The first subsection discusses the proposed controller setpoint tracking response for a single point step change to the optimal Injera cooking temperature compared to the conventional PID controller. The following subsection discusses the result of the proposed controller for tracking input commands for the setpoint variations.

5.4.1.1 Response to Single Setpoint Tracking

The PID controller parameters tuned for setpoint tracking and disturbance rejection assess the setpoint tracking performance. In the first case, Table 5.4 of PID controller parameters tuned for setpoint tracking (PID-SP) contrasts with the proposed controller. Table 5.5 of PID controller parameters tuned for disturbance rejection (PID-DIS) compared to the proposed controller in the second case. The two instances assess the performance of each tuning method for setpoint tracking performance.

Figure 5.6 depicts the setpoint tracking response of the ICM for the proposed and 1DOF PID controller parameters tuned for setpoint tracking performance (PID-SP).

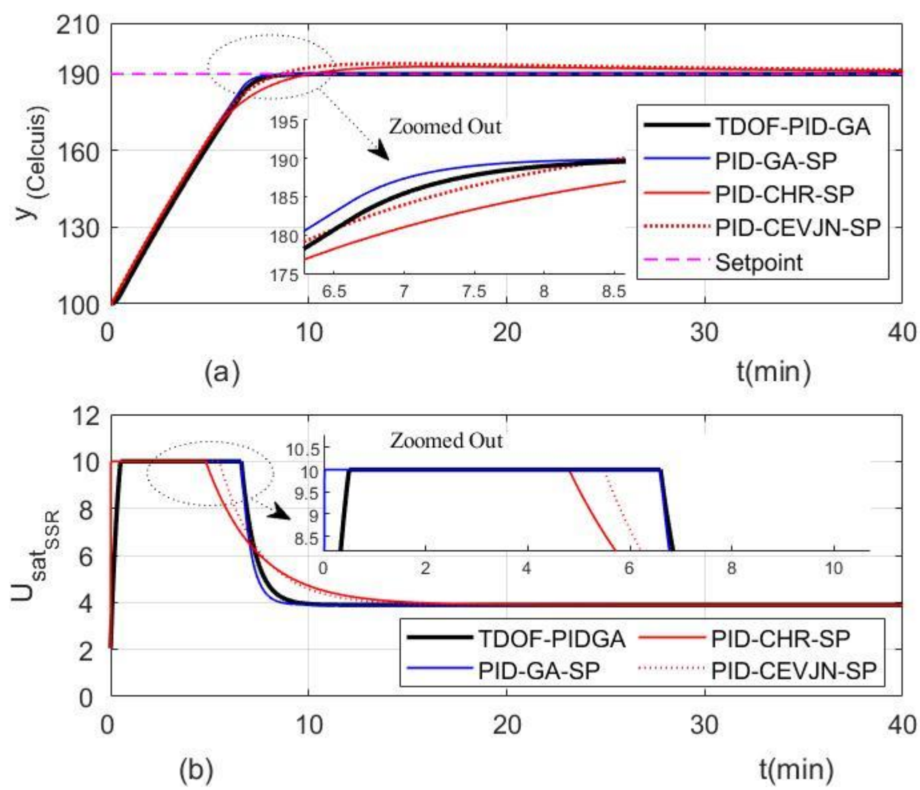

Figure 5. 6 TDOF PID and PID-SP (a) Setpoint tracking response (b) Controlled signal saturation

In Figure 5.6, all methods track the setpoint, but the TDOF PID and PID controller tuned by GA for setpoint tracking (PID-GA-SP) reach faster than other tuning methods with a short settling time and zero overshoot. The controlled signal saturation response illustrates that the controller output signal is in the range of the Actuator physical limit (U_{max} and U_{min}). The quantitative performance measures by time-domain specifications like overshoot (M_p), rise time (t_r), settling time(t_s), and the Integral Absolute Error (IAE) assess the effectiveness of the proposed controller, and the smallest value is better. Table 5.6 lists the result of the calculated performance measures.

Table 5. 6 Quantitative setpoint tracking performance measure of proposed and PID-SP

Controller	Rise time(t_r)	Overshoot (M_p)	Settling time(t_s)	IAE
TDOF PID	6.459	0	7.632	5.481
PID-GA-SP	6.384	0	7.194	5.191
PID-CHR-SP	7.724	3.244	32.062	6.789
PID-CEVJIN-SP	6.946	4.568	38.037	7.137

From Table 5.6, Comparing each performance measure, First, in terms of rising time(t_r), the PID-GA-SP has the smallest value(t_r=6.384-min). In relative to the shortest rising time(t_r), the TDOF PID, PID-CHR-SP, and PID-CEVJIN-SP have a delay of 0.075-min,1.34-min, and 0.562-min, respectively. Second, in terms of Overshoot (M_p), the proposed TDOF PID(M_p=0%) and PID-GA-SP(M_p=0%) have zero overshoot than PID-CHR-SP(Mp=3.244%) and PID-CEVJIN-SP(M_p=4.568%). Third, in terms of settling time(t_s), PID-GA-SP (t_s=7.194-min) has a smaller value and a slight difference from the TDOF PID (t_s=7.632-min) and settle before the proposed controller leading in a 0.438-min and a significant difference to the PID-CHR-SP (t_s=32.062-min) and PID-CVEJIN-SP (t_s=38.037-min) which have a delay of 24.868-min and 30.843-min, respectively. Finally, IAE evaluation, a smaller value in PID-GA-SP(IAE=5.836) than TDOF PID, PID-CHR-SP, and PID-CEVJIN-SP having a difference of 0.456,0.852 and 1.266, respectively.

The quantitative performance measures indicate that the GA-tuned for optimal setpoint tracking has better performance than the other. In contrast, the proposed controller is ranked second with a slight difference from PID-GA-SP. Furthermore, Figure 5.7 depicts a graphical illustration of the performance measure.

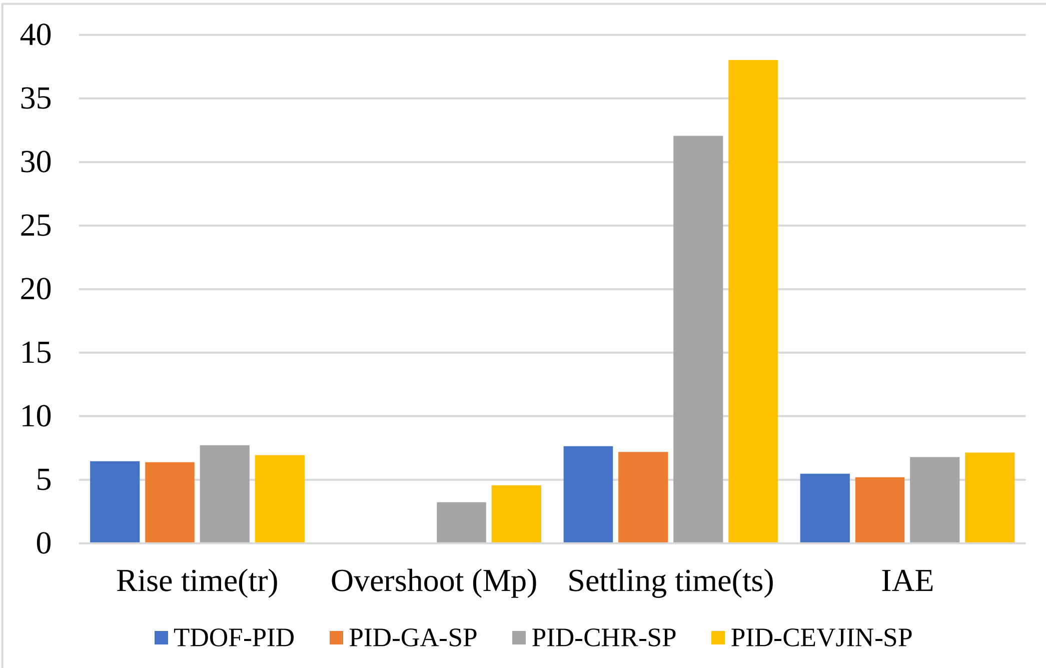

Figure 5. 7 Setpoint tracking performance measure TDOF PID and PID-SP

The graphical representation in Figure 5.7 reveals a slight difference in rising time and IAE and settling time between PID-GA-SP and TDOF PID controller. The significant overshoot and extensive settling time(t_s) for the PID-CHR-SP and PID-CVJIN-SP are inappropriate. The PID-GA-SP and TDOF PID have good setpoint tracking performance with a considerable slight difference. However, further measures are required to assess the simultaneous setpoint tracking and disturbance rejection.

Figure 5.8 depicts the setpoint tracking response of the proposed and 1DOF PID controller tuned for disturbance rejection performance (PID-DIS).

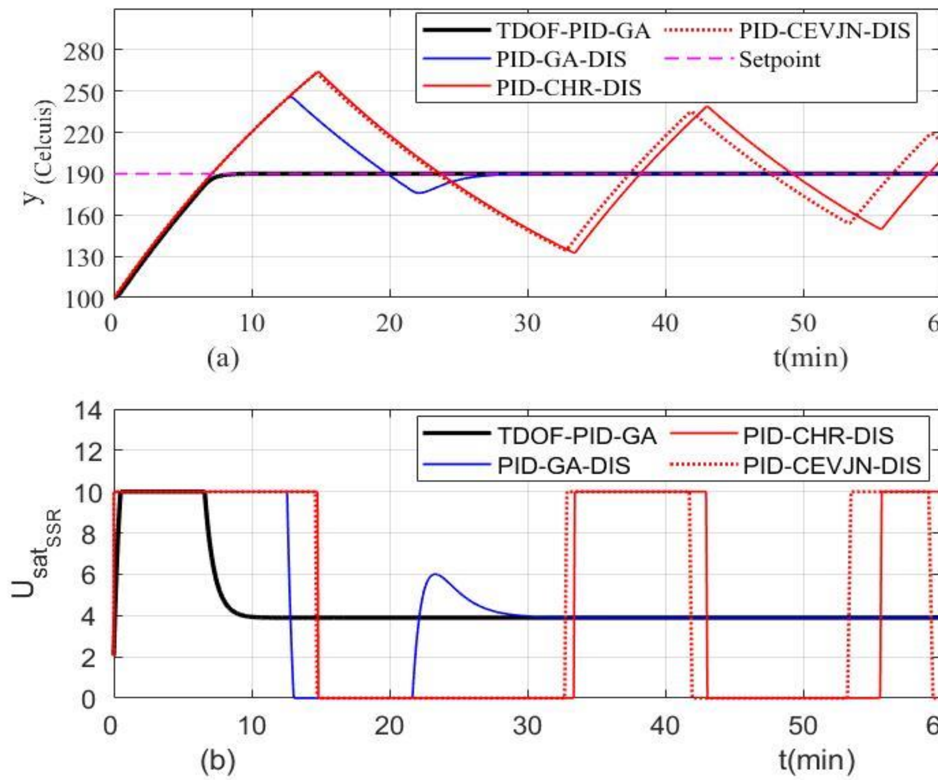

Figure 5. 8 TDOF PID and PID-DIS (a) Setpoint tracking response (b) Controlled signal saturation

For the result in Figure 5.8, all the PID controller parameters tuned for optimal disturbance rejection result in higher overshoot and settling time. The PID controller tuned by GA, CHR, and CVEJIN for disturbance rejection performance (PID-DIS) results in bad setpoint tracking. The PID-GA-DIS sends a maximum controller input signal to the Actuator after the response reaches the setpoint, resulting in a high overshoot. The input saturation response of PID-CVEJN-DIS and PID-CHR-DIS turns ON and OFF between U_{max} and U_{min}, resulting in temperature fluctuation at the setpoint. In contrast, the proposed TDOF PID controller reaches faster to the setpoint with zero overshoot than the others.

Furthermore, Table 5.7 lists the quantitative setpoint tracking performance measures of the proposed TDOF PID controller and 1DOF PID controller tuned for optimal disturbance rejection (PID DIS).

Table 5. 7 Quantitative setpoint tracking performance measure proposed and PID-DIS

Controller	Rise time(t_r)	Overshoot (M_p)	Settling time(t_s)	IAE
TDOF PID	6.459	0	7.632	5.481
PID-GA-DIS	6.372	61.984	26.634	11.989
PID-CHR-DIS	6.372	82.457	109.840	39.419
PID-CEVJIN-DIS	6.372	81.162	85.067	32.764

The performance measure in Table 5.7 reveals that the proposed controller lag with considerable rising time(t_r) by 0.0867-min compared to the others, and the proposed controller has a smaller settling time(t_s=7.632-min), zero overshoot (0%), and IAE=5.481. In contrast, other controllers have extensive settling time(t_s), more than 20% overshoot (M_p), and large IAE values. Figure 5.9 depicts a pictorial representation.

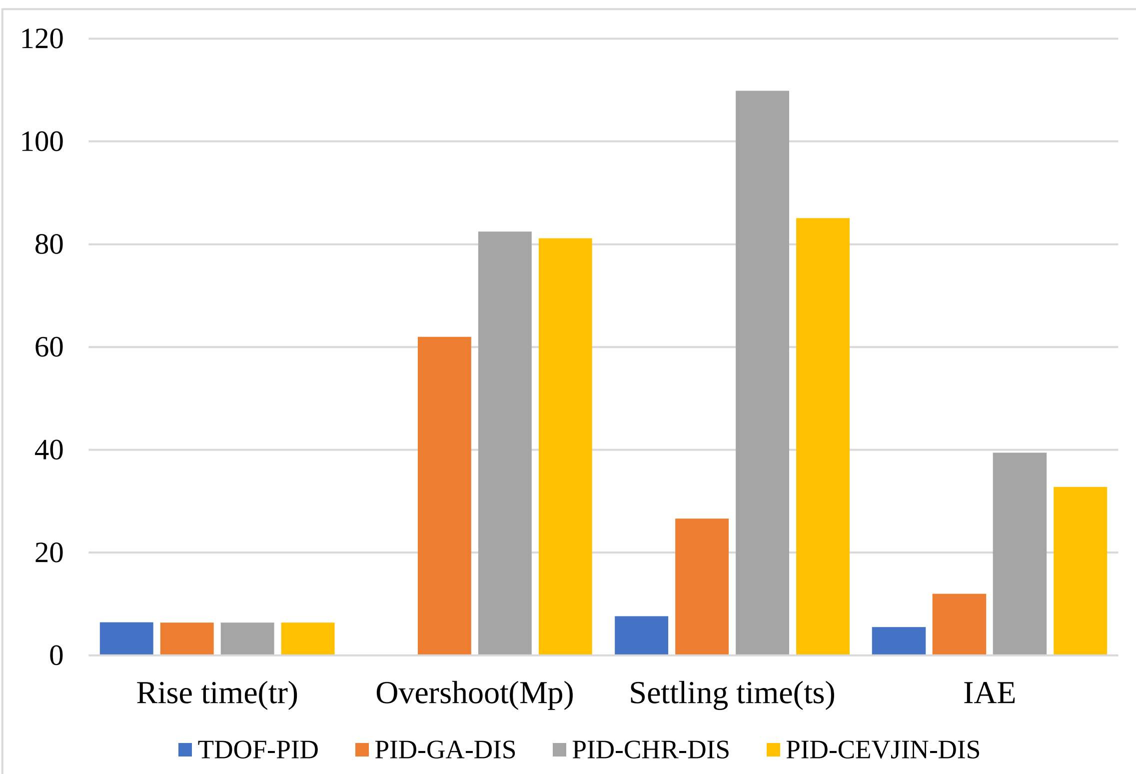

Figure 5. 9 Setpoint tracking performance measure TDOF PID and PID-DIS

A result of long settling time and more than 20%overshoot in PID-CHR-DIS, PID-CVJIN-DIS, and PID-GA-DIS reveals that lots of time are required to reach its setpoint, and a high overheat above the optimal cooking temperature, which is unacceptable. In return, the TDOF PID controller matches the setpoint with 0% overshoot and fast settling time(t_s=7.632). Figure 5.9 illustrates that the proposed controller has better performance measures with all performance comparing to PID-DIS for setpoint tracking response.

The setpoint performance test for PID controller parameters tuned for optimal setpoint tracking (PID-SP) ascertains controller PID-GA-SP and the proposed TDOF PID have better setpoint tracking performance. However, the PID controller parameters tuned for optimal disturbance rejection (PID-DIS) have more than 20% overshoot, a long settling time, and high IAE values. In contrast, the proposed TDOF PID controller has a reasonably good setpoint tracking response. The result in PID-DIS for GA tuned for disturbance rejection assures that only PID-GA-SP is capable of setpoint tracking. Implementing GA tuned for disturbance rejection can not enhance simultaneous setpoint tracking and disturbance rejection.

5.4.1.2 Response to Setpoint Tracking for Step Input Variation

The step variation tracking allows a step increase in temperature from an initial value to the optimal cooking temperature. The setpoint variation in the start and stop mode assesses input command tracking. From the previous discussion, the PID-GA-SP and TDOF PID controllers result in good setpoint tracking performance than the others; for this reason, GA tuned PID controller parameters, and the proposed controller is used to assess the stepwise increase in setpoint. The stepwise variation to the optimal cooking temperature starts from 30 to $80\,^{o}C$, then 80 to $140\,^{o}C$, and 140 to $190\,^{o}C$.

Figure 5.10 depicts the setpoint variation response.

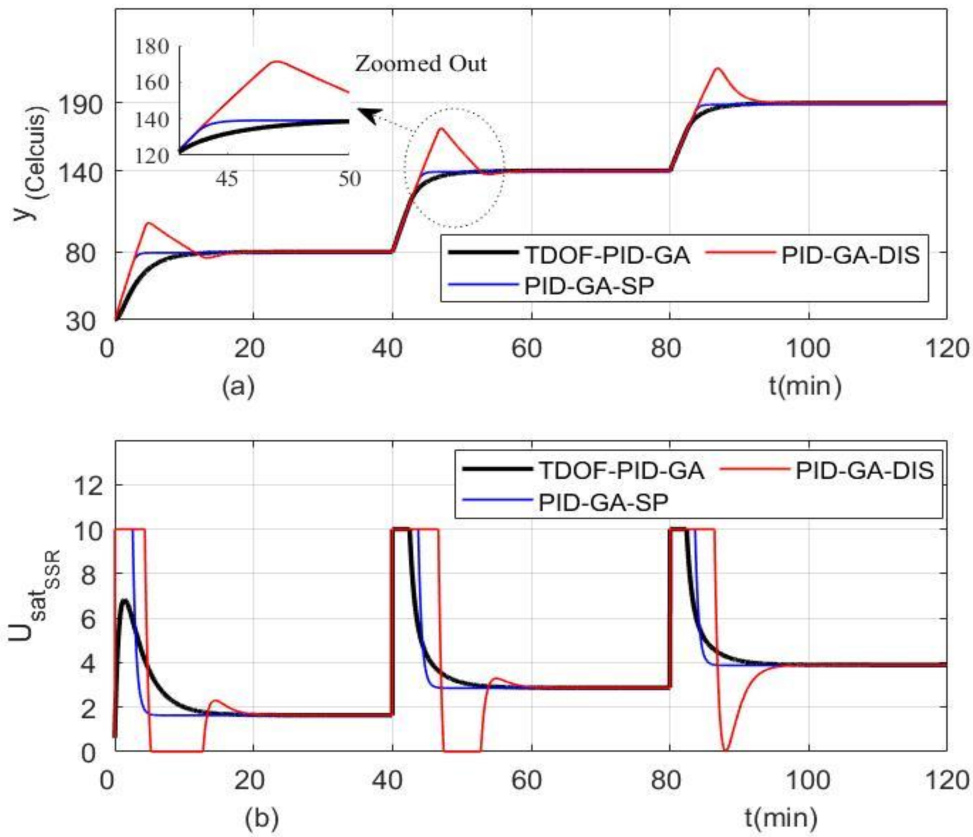

Figure 5. 10 Setpoint variation (a) Input command tracking (b) Controller signal saturation

The PID-GA-DIS attains reference temperature with a high overshoot; in contrast, the PID-GA-SP and TDOF PID follow the input command with zero overshoot.

The controller input signal decreases from U_{max} to U_{min} for PID-GA-DIS to bring the overshoot back to the input command, resulting in a slow tracking response. However, for the TDOF PID and PID-GA-SP, the controller signal adjusts and tracks considerately. The undesired overshoot and slow tracking response by PID tuned for disturbance rejection are insufficient for setpoint variation.

5.4.2 Disturbance Rejection Response

In this section, a step and pulse disturbance assess the performance of the proposed controller. The first subsection discusses the disturbance rejection response of the proposed controller for the negative temperature deviation from steady-state. The second subsection discusses the simulation result of the proposed controller for disturbance variation.

5.4.2.1 Response to Step Disturbance

The PID controller parameters for PID-SP and PID-DIS for GA, CHR, and CVJIN tuning methods assess the effectiveness of the proposed controller for disturbance rejection. In the first case, PID-DIS controller parameters with the proposed controller. In the second case, PID tuned for setpoint tracking performance to assess fast disturbance rejection capability and evaluate simultaneous setpoint tracking and disturbance rejection response.

Figure 5.11 depicts the disturbance rejection response of the proposed TDOF PID and PID controller parameters tuned for optimal disturbance rejection by GA, CHR, and CVJIN.

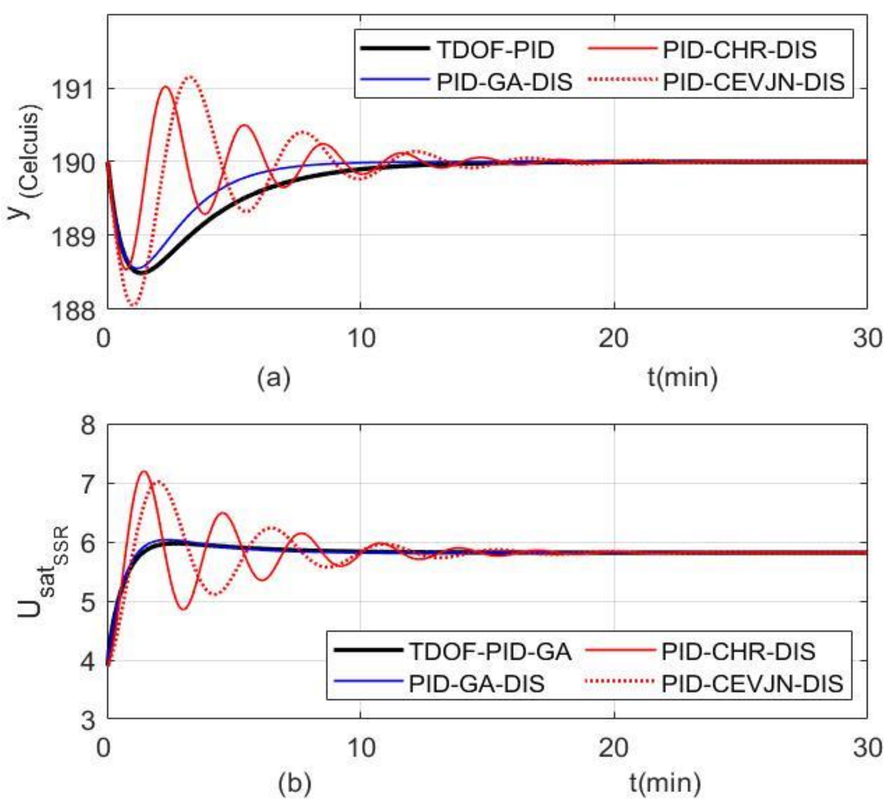

Figure 5. 11 TDOF PID and PID-DIS (a) Disturbance rejection (b) Controlled signal saturation

From the result in Figure 5.11, there is a slight deviation from steady-state temperature. The temperature deviates to the minimum 188.1^{o}C and maximum 191.1^{o}C temperatures. The PID-CHR-DIS and PID-CVJIN-DIS responses fluctuate towards the optimal cooking temperature starting from 188.5-191.6^{o}C and 188.1-191.1^{o}C, whereas the TDOF PID and PID-GA-SP deviate to 188.9^{o}C and 190.6^{o}C, respectively. The PID-GA-DIS and TDOF PID controller recover faster than the PID-CHR-DIS and PID-CVJIN-DIS.

The quantitative performance measures peak time(t_p), recovery time(t_{rcy}), and Integral Absolute Error (IAE) assess the effectiveness of the proposed controller. Table 5.8 list the quantitative performance measures.

Table 5.8 Quantitative step disturbance performance measure for the proposed and PID-DIS

Controller	Peak time(t_p)	Recovery time(t_{rcy})	IAE
TDOF PID	1.350	13.592	0.115
PID-GA-DIS	1.200	8.806	0.104
PID-CHR-DIS	0.750	16.658	0.101
PID-CVEJIN-DIS	1.033	17.071	0.111

From Table 5.8, contrasting each performance, In the case of peak time(t_p) and IAE, the PID-CHR-DIS (t_p=0.75-min, IAE=0.101) has the smallest value, and relative to peak time, the PID-GA-DIS, PID-CVJIN-DIS, and the proposed TDOF PID delays with 0.6-min, 0.45-min, and 0.28-min. In terms of recovery time(t_{rcy}), PID-GA-DIS (t_{rcy}=8.806-min) has the smallest recovery time(t_{rcy}), and PID-CHR-DIS (t_{rcy}=16.659-min) and PID-CVJIN-DIS (t_{rcy}=17.071-min) delays with 7.852-min and 8.265-min. The proposed controller has a significant recovery time compared to the PID-CHR-DIS and PID-CVJIN-DIS and recovers faster than the two-controller, leading with 3.066-min and 3.479-min.

Figure 5.12 depicts the graphical representation of the quantitative measures.

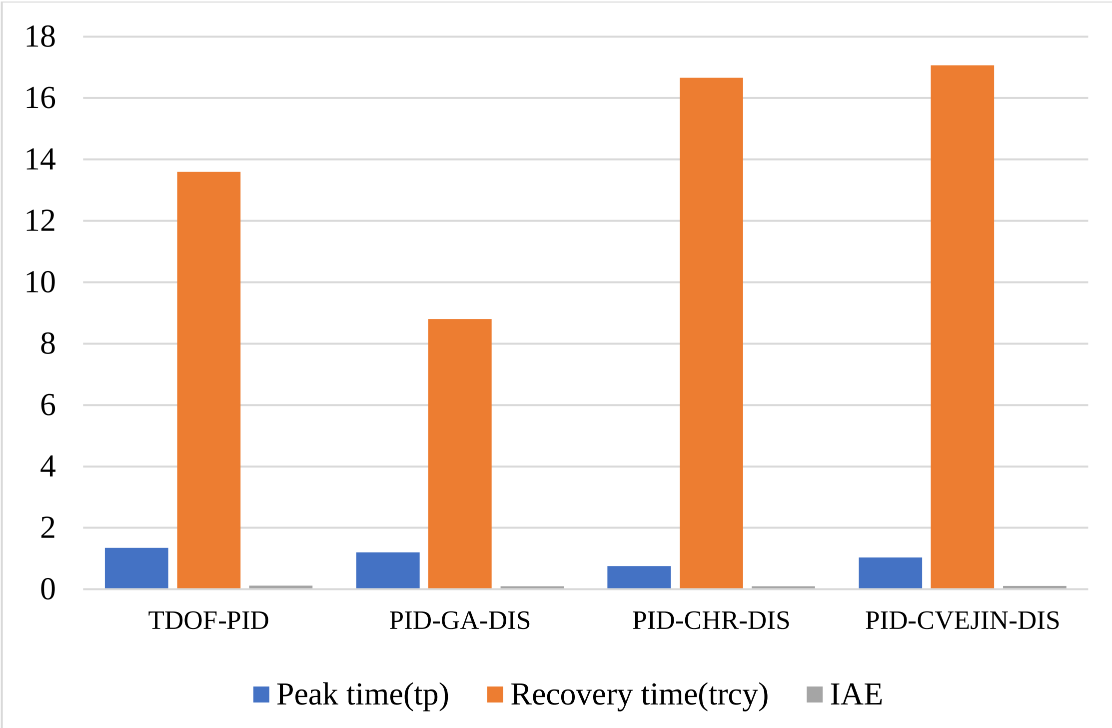

Figure 5. 12 Proposed and PID-DIS disturbance rejection performance measure

The peak time(t_p) is the time required by the response to reach its first peak, and the maximum peak value for the deviation from the steady-state is 1.9°C because of this reason, the slight change in peak time between each controller is considerable. Considering recovery time as the primary evaluation measure, the proposed TDOF PID controller ranked second next to the PID-GA-DIS method.

From the quantitative measure, the PID-GA-DIS has good disturbance rejection performance. However, comparing PID-DIS controller parameters for setpoint tracking performance from Table 5.7, the PID-GA-DIS, PID-CHR-DIS, and PID-CVEJIN-DIS have bad setpoint tracking performance measures having 61.984%, 82.457%, and 81.162% overshoot(M_p), and 26.634-min,109.840-min, and 85.067-min settling time(t_s), respectively. The significant overshoot and settling time assures high overheat and prolonged tracking performance. Since the controller design objective is simultaneous setpoint tracking and disturbance rejection, the PID-GA-DIS, PID-CHR-DIS, and PID-CEVJIN-DIS are ineffective and inappropriate.

Figure 5.13 depicts the disturbance rejection response of the proposed TDOF PID and PID-SP controller parameters.

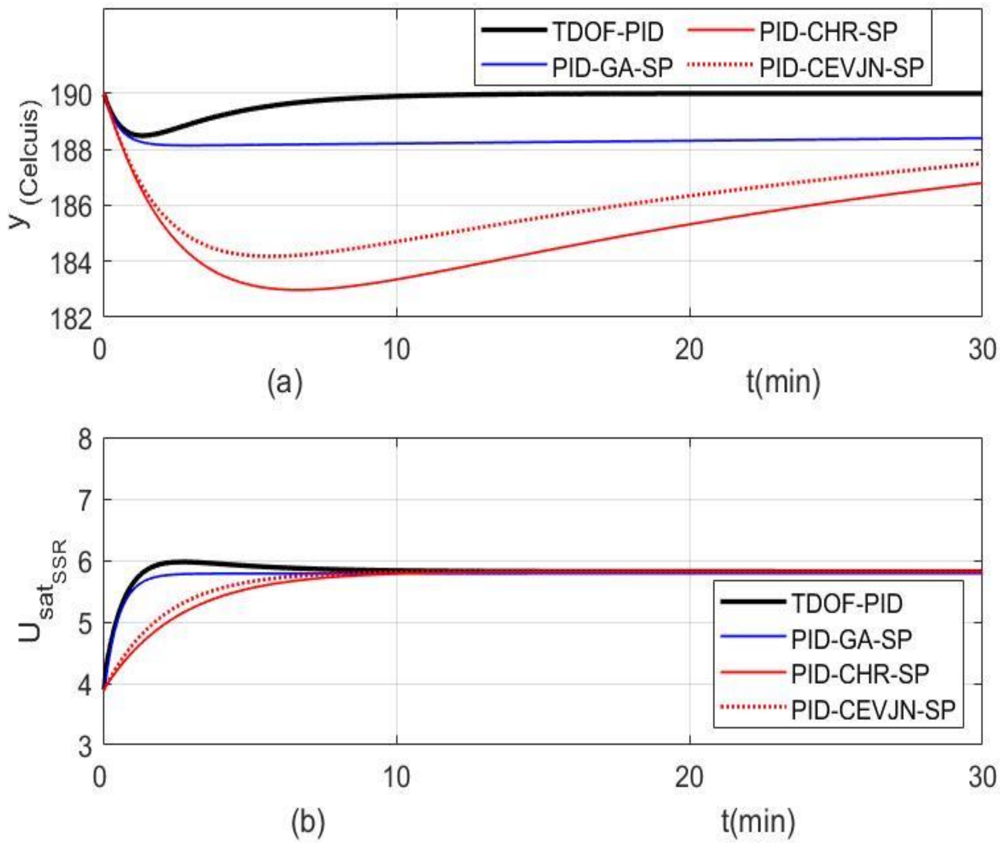

Figure 5. 13 Disturbance rejection (a) TDOF PID and 1DOF PID-SP response (b) controlled signal saturation

The response in Figure 5.13 reveals that the 1DOF PID-SP controllers have a prolonged recovery time from the deviation but, the TDOF PID controller sustains the steady-state temperature faster. The controller signal rises to its U_{max} of 6V and starts to decrease smoothly to bring the ICM to its steady-state temperature. The quantitative time-domain specification performance measure like peak time(t_p), recovery time(t_{rcy}), and Integral Absolute Error (IAE) evaluate the effectiveness of the proposed controller. Table 5.9 lists the proposed and PID-SP controller parameters for disturbance rejection response.

Table 5. 9 Quantitative step disturbance performance measure for the proposed and PID-SP

Controller	Peak time(t_p)	Recovery time(t_{rcy})	IAE
TDOF PID	1.350	13.592	0.1154
PID-GA-SP	2.950	639.4	4.1837
PID-CHR-SP	6.6667	111.875	3.9506
PID-CVEJIN-SP	5.7000	110.503	3.1605

From Table 5.9, the proposed controller has the smallest value in peak time (t_p=1.350-min), recovery time (t_{rcy}=13.592), and IAE values (IAE=0.1154). The overlong recovery time by PID-GA-SP(t_{rcy}=639.4-min) is unnecessary, resulting in improper disturbance rejection response. The PID-CHR-SP and PID-CVEJIN-SP also have a long recovery time(t_{rcy}), which is undesirable even if they recover before the PID-GA-SP.

Figure 5.14 depicts the graphical representation of the proposed and PID-SP performance measures in terms of peak time(t_p) and IAE.

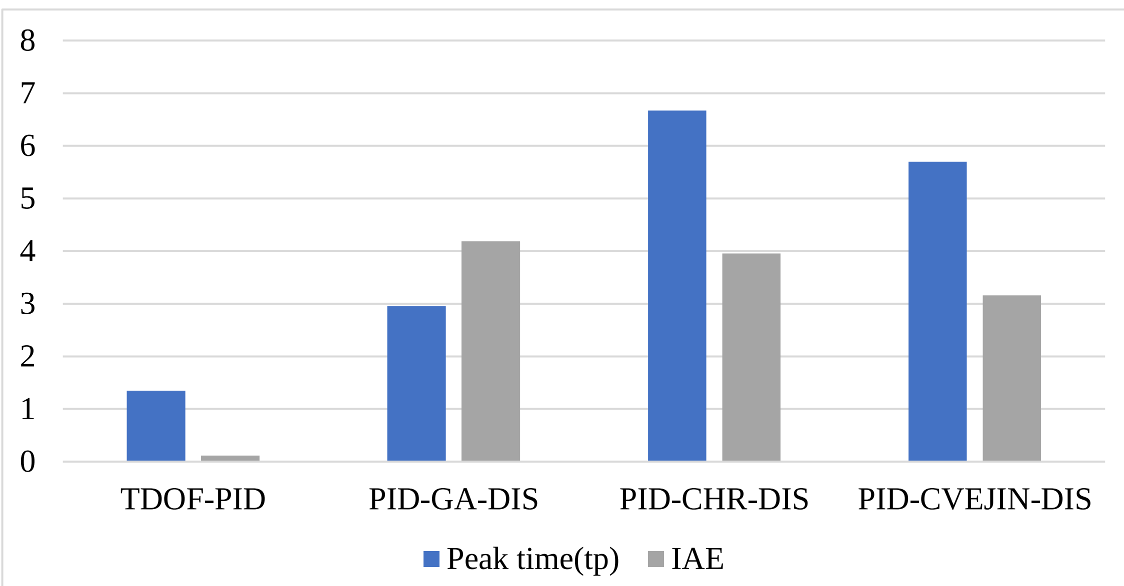

Figure 5. 14 Proposed and PID-DIS disturbance rejection performance measure

From the quantitative measure in Table 5.9 and Figure 5.13 and 5.14, the TDOF PID controller has the best disturbance rejection response with all criteria compared to controller parameters tuned for disturbance rejection (PID-SP).

The result obtained for setpoint tracking and disturbance rejection performance shows that even if the PID-GA-SP has good setpoint tracking, its disturbance rejection response is undesirable. In return, the PID-GA-DIS has good disturbance rejection and inappropriate setpoint tracking performance. The CHR and CVEJIN methods result in bad setpoint tracking, and disturbance rejection response than the proposed and GA tuned PID-DIS and PID-SP.

The result and discussion in Sections 5.4.1 and 5.4.2 illustrate using conventional or 1DOF PID controller for setpoint tracking results in bad disturbance rejection and vice versa. In contrast, the TDOF PID controller has a reasonable better setpoint tracking and disturbance rejection response. Since the main controller design objective is simultaneous setpoint tracking and disturbance rejection response. The TDOF PID controller can simultaneously track and reject the setpoint and disturbance for the Injera Cooking Machine (ICM), respectively.

5.4.2.2 Response to Pulse-type Disturbance

Injera cooking process takes 2 to 4-minute starting from pouring the dough on the plate up to delivering a cooked Injera. Step pulse variation assesses the response of the proposed controller for a pulse disturbance rejection. Five consistent pulse variations with a duration of 1-min zero disturbance and one pulse for 1.5-min are applied to the system to assess the response. The pulse magnitude is varied with a 47.37%,52.63%,63.63%,57.89%, and 55.26% temperature deviation in an open-loop system from the steady-state temperature of $190\,^{\circ}C$, respectively.

Figure 5.15 depicts pulse disturbance response.

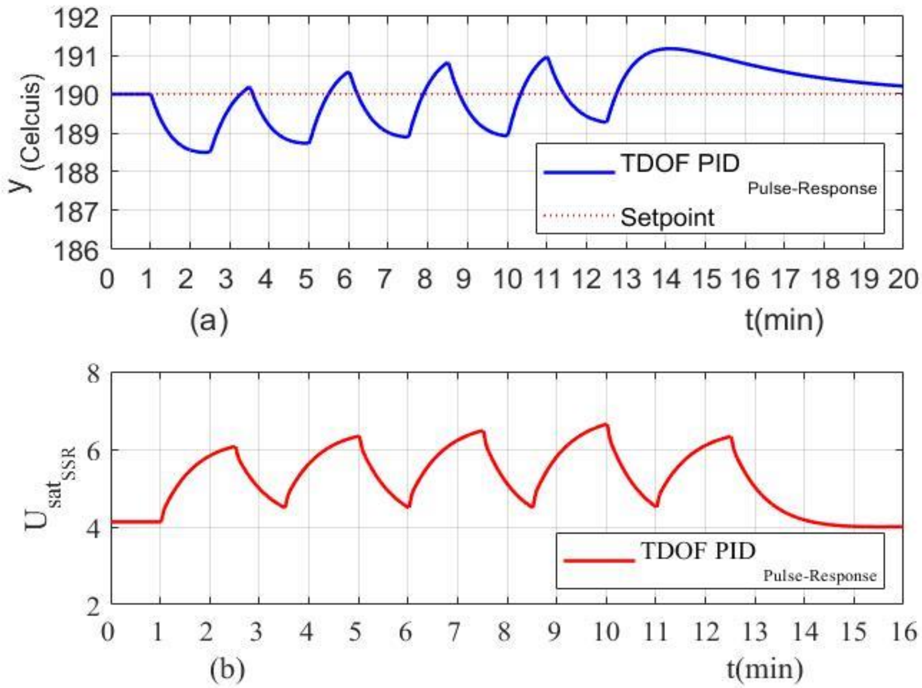

Figure 5. 15 (a) Pulse variation response (b) Control signal saturation

The constant temperature at 190°C for the first 1-min shows the retainment of steady-state. The baking process starts once the ICM reaches a steady state. The first pulse disturbance stays for 1.5-min or 1-2.5min, and the response rejects the deviation with a considerable variation. After 2.5-min a zero disruption is introduced, meaning the cooked Injera is removed from the ICM, and the ICM keeps on rising to the optimal cooking temperature. The process continues in the same ways for all pulse disturbance inputs. The controller output signal adjusts in response to the desired output temperature.

5.4.3 Effect on the AW Scheme

A positive setpoint change above the optimal cooking temperature is introduced for assessing the effect of Integral Windup and the corresponding Anti-Windup (AW) scheme discussed in Section 4.4. The setpoint is changed suddenly from an initial temperature of 100°C to 220°C above the optimal cooking temperature.

Figure 5.16 depicts the response of the TDOF PID controller without and with AW scheme implementation.

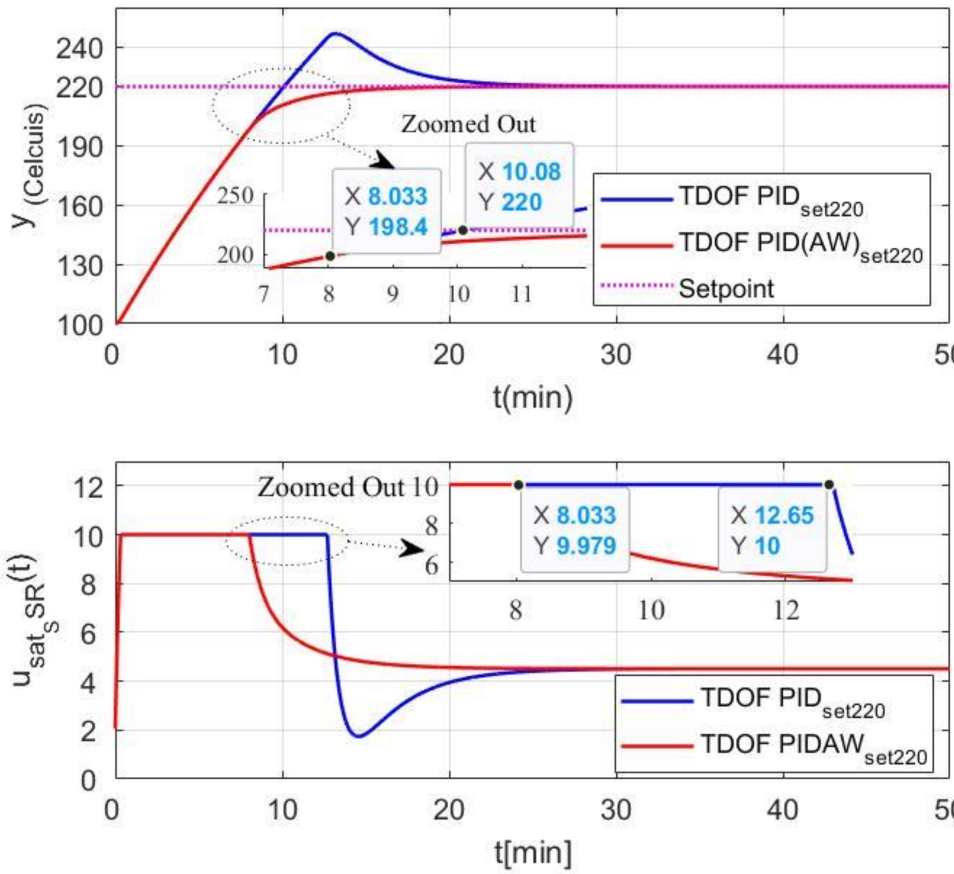

Figure 5. 16 TDOF PID (a) Without and with AW scheme (b) Controller signal saturation.

From the result in Figure 5.16, the TDOF PID without AW scheme increases above the setpoint temperature even if the control input saturates. The control is expected to resume at least the temperature rise reaches in 10.08-min or 220 °C . However, because of an increase in the integral of the error (Integral Windup), the controller input saturation resumes at 12.65-min. The input saturation waits for a delay of 2.57-min until the Windup decrease. In return, the TDOF PID with AW scheme implementation keeps on comparing the actual and saturation input. When the controller input is more significant than the saturation limit, integrating the error is reduced. For the same control input and Actuator input, there is no effect or regular operation. As depicted in Figure 5.16, the Actuator input or input saturation U_{sat} starts to decrease at 8.033-min or before 10.08-min, and the response rises in time slowly and settles without overshoot. Further quantitative measures like settling time(t_s), overshoot (M_p), and Integral of Absolute Error (IAE) assess the performance measure. Table 5.10 lists the quantitative performance measures of the proposed TDOF PID with and without the AW scheme.

Table 5. 10 Anti-Windup scheme implementation quantitative measure

Controller	Overshoot ($M_{p\%}$)	Settling time(t_s)	IAE
TDOF PID With AW scheme	0	13.962	10.2302
TDOF PID Without AW Scheme	22.264	21.041	12.0393

From Table 5.10, the TDOF PID controller with AW scheme implementation has better values with all performance measures. The Integral Windup overshoot (M_p=22.264%) is reduced to zero percent overshoot (M_p=0%), and settling time(t_s) leads the Windup by 7.079-min. Furthermore, the error plot depicted in Figure 5.17 reveals the capability of AW scheme implementation to remove the undesired integral error.

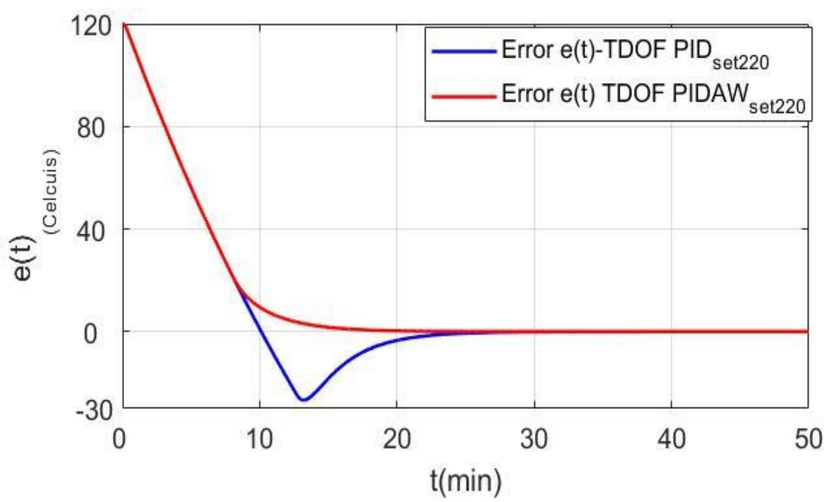

Figure 5. 17 Error e(t) TDOF PID With AW and TDOF PID without AW scheme

6 CONCLUSION AND RECOMMENDATION

6.1 Conclusion

The application of temperature controller strategies improves performance. The Injera Cooking Machine(ICM) requires simultaneous setpoint tracking and disturbance rejection response. The existing ICM operates either through observation or ON and OFF controller strategies, which results in temperature fluctuations around the optimal cooking temperature. Solving the issue with a one-degree-of-freedom (1DOF) PID controller does not enhance the multi-objective problem.

This thesis presents a scheme of designing a two-degrees-of-freedom (TDOF) PID controller incorporating an Anti-Windup (AW) technique and a Genetic Algorithm (GA) for simultaneous setpoint tracking and disturbance rejection response. The GA used in this thesis performed two main tasks; controlled object model parameter estimation and controller parameter optimization. GA estimates the cooking plate's second-order-plus-time-delay (SOPTD) transfer function model parameters from the actual step response. The experimental setup record and export the step response into an excel datasheet for GA parameter estimation. The normalized-root-mean-square-error (NRMSE) percentage fitting for positive and negative step responses shows that the GA estimated model parameters fit with the actual step response by 94.81% and 93.50%, respectively, implying a validated model parameter estimation.

Further GA approximates the SOPTD controlled object model to FOPTD fitted with 99.16%, a validated model reduction. The presented TDOF PID controller overshoot (Mp=0%), settling time($t_{s=}$7.632-min), and recovery time(t_{rcy}=13.592-min) revealed the capability of the proposed controller to track the setpoint without overheating and under heating issue and good disturbance rejection response compared to the 1DOF PID controller.

In the 1DOF PID controller, good setpoint tracking results in a bad disturbance rejection response vice versa. The disturbance rejection response results in extensive recovery time(t_{rcy}) whenever the setpoint tracking performance becomes good, and the setpoint tracking response results in undesirable percentage overshoot (>20%) and settling time(t_s) if the disturbance rejection becomes good. However, the proposed TDOF PID controller is robust enough for simultaneous setpoint tracking and disturbance rejection performance.

The AW back-calculation scheme implementation for the proposed controller handles the significant overshoot (M_p) and settling time(t_s) caused by the Integral Windup. The quantitative performance measure results of the proposed controller with and without AW scheme reveals that with AW scheme implementation, the significant overshoot (Mp=22.264%) and long settling time(t_s=21.041-min) result of the TDOF PID without AW scheme are reduced by a zero percent overshoot (Mp=0%) and settling time(t_s=13.962-min). The TDOF PID with AW scheme reaches steady-state with zero overshoot leading to a 7.079-min.

The designed TDOF PID controller with Anti-Windup scheme implementation for ICM can handle Integral Windup and enhance a simultaneous setpoint tracking and disturbance rejection response.

6.2 Recommendation

The ON and OFF controller, adopted on the currently existing Injera Cooking Machine in the Ethiopian Market, can be replaced by the proposed controller to increase the efficiency of the ICM by regulating the temperature. The PID controller solves 90% of control problems and is cost-effective. These advantages allow the proposed controller to be affordable at the household level. Improving the cooking plate structure and construction efficiency also enhances the temperature regulation method by reducing heat loss by radiation. The sensor position used in this thesis for WassGrill is from the company selection; further research on setting the temperature sensor at the optimal heat distribution point increases the efficiency of the ICM. The GA for parameter estimation method also works for other cooking systems as a transfer function modeling. And can be utilized to set and conduct a laboratory test for postgraduate and undergraduate students in transfer function modeling from the actual response of measured data using an electric oven or any heating system with a short time constant to manage the laboratory session to one and up to three hours. There is a research gap in controller strategies application in the existing Injera Cooking Machine (ICM); the thesis opens further study in temperature controller design.

Research Fund Acknowledgment

This research project is funded by Adama Science and Technology University under the grant number of ASTU/SM-R/160/20, Adama, Ethiopia.

REFERENCES

[1] K. D. A. D. A. Adem, "A review of injera baking technologies in Ethiopia: Challenges and gaps," *Energy for Sustainable Development,* vol. 41, pp. 69-80, 2017.

[2] M. Tadesse, "The Developmental Patterns of Injera Baking Stoves: Review on the Efficiency, and Energy Consumption In Ethiopia," *SSRG International Journal of Mechanical Engineering,* vol. 7, no. 1, pp. 7-16, 2020.

[3] O. J. N. B. Asfafaw Haileslasie, "Design and Development of Solar Thermal Injera Baking: Steam Based Direct Baking," *ISES Solar World Congress,* vol. 57, no. 14, pp. 2946-2955, 2013.

[4] Ethiopian Energy Agency (EEA), "Electric Injera Mitad Energy Efficiency Standards & Labeling, challenges, and prospects," in *VIENNA ENERGY FORUM 2017,* VIENNA, 2017.

[5] S. B. K. M. W. Abdulkadir A. Hassen, "Design and manufacturing of thermal energy based Injera baking glass pan," in *Africa-EU Renewable Energy Research and Innovation Symposium*, Tlemcn, 2016.

[6] *Project Document On Electric Injera Mitad Energy Efficiency Standards and Labeling,* 2015.

[7] T. K. J. P.Febina Beevi, "Two Degree of Freedom Controller Design by AGTM\AGMP," in *Global Colloquium in Recent Advancement and Effectual Researches in Engineering, Science and Technology,* Kerala, 2016.

[8] A. Devanshu, "Genetic Algorithm Tuned PID Controller for Process Control," in *International Conference on Inventive Systems and Control(ICISC),* 2017.

[9] P. a. H. L.D.Vijay Anand, "SYSTEM IDENTIFICATIONOF A TEMPERATURE PROCESS," *International Journal of Pure and Applied Mathematics,* vol. 118, no. 20, pp. 3845-3850, 2018.

[10] H. D. L.D.Vijay Anand, "REAL-TIME SYSTEM IDENTIFICATIONOF THERMAL PROCESS," *International Journal of Mechanical Engineering and Technology (IJMET),* vol. 9, no. 11, p. 2076–2084, 2018.

[11] A. Gallagher, "A solar fryer," *A solar fryer*, vol. 3, no. 85, pp. 496-505, 2011.

[12] D. V. H. O. Feleke Fanta, "Design and development of Electromagnetic Induction Injera Mitad," *International Research Journal of Engineering and Technology (IRJET)* , vol. 07, no. 04, pp. 56-72, 2019.

[13] F. Fanta, "Improving Performance of Electromagnetic Induction Injera Mitad," *International Research Journal of Engineering and Technology (IRJET),* vol. 07, no. 4, pp. 56-72, 2020.

[14] F. F. M, "Design and Development of Microcontroller Based Electromagnetic Induction Mitad Prototype," *International Journal of Recent Technology and Engineering (IJRTE),* vol. 9, no. 4, pp. 2277-3878, 2020.

[15] Wassie, "Wass Electronics." USA Patent WASS-US-GRL, 2016.

[16] M. V. S. S. Gopi krishna rao P V, "Study on PID Controller Design and Performance Based on Tuning Techniques," in *International Conference on Control, Instrumentation, Communication and Computational Technologies (ICCICCT)*, Nagercoil, 2014.

[17] V. Y. R. V. K. T. P. C. Palaniyappan T K, "PID Control Design for a Temperature Control System," in *International Conference on Power Energy, Environment and Intelligent Control (PEEIC)*, Noida, 2018.

[18] A. O'Dwyer, HANDBOOK OF PI AND PID CONTROLLER TUNING RULES, London: Imperial College Press, 2009.

[19] K. Ogata, Modern Control Engineering Fifth Edition, New Jersey: Prentice-Hall, 2010.

[20] A. E. B. C.R. Madhuranthakam, "Optimal tuning of PID controllers for FOPTD, SOPTD and SOPTD with lead processes," *Chemical Engineering and Processing 47,* p. 251–264, 28 November 2008.

[21] M. S. a. A. Zomorrodi, Comparison of PID Controller Tuning Methods.

[22] J. Cvejn, "Simple PI/PID Controller Tuning Rules for FOPDT Plants with Guaranteed Closed-Loop Stability Margin," *Acta Montanistica Slovaca*, vol. 1, no. 16, pp. 17-25, 2011.

[23] M. E. A. N. Moslem Amirinejad, "Automatic PID Controller Parameter Tuning using bee colony algorithm," *International Journal of Scientific & Engineering Research (ISSN),* vol. 5, no. 8, pp. 24-28, 2014.

[24] G. C. W.-J. Hu Wuhua Xiao, "PID Controller Design Based on Two-Degrees-of-Freedom Direct Synthesis," in *IEEE 2011 23rd Chinese Control and Decision Conference (CCDC),* Mianyang, 2011.

[25] R. I. M. N. K. S. M. H. a. KISHORE BINGI, "A comparative study of 2DOF PID and 2DOF fractional-order PID controllers on a class of unstable systems," *Archives of Control Sciences,* vol. 28, no. 04, p. 635–682, 2018.

[26] M. A. a. H. Taguchi, "Tutorial Paper Two-Degree of PID Controller," *International Journal of Control, Automation, and Systems,* vol. 1, no. 4, pp. 401-412, 2002.

[27] R. V. Víctor M. Alfaro, Model-Reference Robust Tuning of PID Controllers, Switherland: Springer, 2016.

[28] R. K. N.G. Adar, "Comparison between Real-Time PID and 2-DOF PID Controller for 6-DOF Robot Arm," *International Conference on Computational and Experimental Science and Engineering (ICCESEN 2015),* vol. 130, no. 1, pp. 269-271, 2015.

[29] R. V. Víctor M. Alfaro, Model-Reference Robust Tuning of PID Controllers, Swizerland: Springer, 2016.

[30] K. P. S. R. Vineet Kumar, "On the Model-Based Control of an Electric Oven," in *International Conference on Advances in Control and Optimization of Dynamical Systems (ACODS 2007),* Bangalore , 2007.

[31] G. Deshmukh and C. Kadu, "Design of two degrees of freedom PID controller for temperature control System," in *EEE 2016 International Conference on Automatic Control and Dynamic Optimization Techniques (ICACDOT),* Puna, 2016.

[32] S. N.Nithyarani, "Model Identification of Temperature Process and Tuning with Advanced Control Techniques," *International Journal of Innovative Research and In electrical, Electronics Instrumentation and Control Engineering,* vol. 1, no. 9, pp. 443-447, 2013.

[33] Crydom Campany , [Online]. Available: https://www.digikey.sg/zh/pdf/c/crydom/solid-statements-august-2011. [Accessed 5 April 2021].

[34] [Online].

Available: https://eta.gr/media/documents/SSR_General_information_pdf_cISlPCI.pdf. [Accessed 5 April 2021].

[35] Carlo Gavazi Automation Components, Carlo Gavazi Automation Components, 06 September 2017. [Online].

Available: https://www.gavazzionline.com/pdf/RM1EAAdatasheet.pdf. [Accessed 1 April 2021].

[36] OMRAN Industrial Automation, "OMRAN Industrial Automation," [Online]. Available: https://www.omron-ap.com/service_support/FAQ/FAQ01870/index.asp. [Accessed 30 April 2021].

[37] Professor.M.kaliamoorthy. [Online].

Available: http://www.gvpcew.ac.in/Material%203%20Units/3%20EEE%20PE.pdf. [Accessed 16 April 2021].

[38] Crydom , [Online]. Available: http://www.crydom.com/en/products/catalog/pmp-nova22-proportional-control.pdf. [Accessed 2 4 2021].

[39] J. H.LIENHARD, A HEAT TRANSFER TEXTBOOK, MASSACHUSETTS: PHLOGISTON PRESS, 2019.

[40] Ives Equipment Process Engineering, "The Ives Equipment Process Engineering & Control Blog," IvesEquipment, 5 May 2018. [Online].

Available: https://blog.ivesequipment.com/2018/05/basics-of-thermocouple-junction-design.html. [Accessed 1 January 2021].

[41] J. Wu, "A Basic Guide to Thermocouple Measurements," Texas Instruments, 2018.

[42] OMEGA Engineering, "OMEGA Engineering," OMEGA Engineering, 2003. [Online]. Available: https://www.omega.co.uk/temperature/z/thermocoupleresponsetime.html#nav. [Accessed 23 March 2021].

[43] maximintegrated, "Maximintegrated," Maximintegrated, 7 May 2015. [Online]. Available: https://www.maximintegrated.com/en/products/sensors/MAX31856.html. [Accessed 1 Feburary 2021].

[44] J. K. K. K. P. R. K.. B. A. Yugal K. Singh, "Temperature Control System and its Control using PID Controller," *International Journal of Engineering Research & Technology (IJERT),* vol. 4, no. 02, pp. 78-81, 2016.

[45] K. J. Keesman, System Identification An Introduction, London: Springer, 2011.

[46] O. N. L. K. K. N. Velagić Jasmin, "Incubator system identification and temperature control with PLC & HMI," in *ELMAR*, Bosnia-Herzegovina, 2010.

[47] S. T. ,. M. A. a. F. A.-D. Musatafa Abbas Albadr, "Genetic Algorithm Based on Natural Selection Theory," *Symmetry,* vol. 12, no. 11, pp. 1-31, 2020.

[48] H. A. G. J. J. Suthar, "Two degrees of freedom controller optimization using GAfor shell and tube heat exchanger," in *11 th International Conference on Intelligent Systems and Control (ISCO),* Coimbatore, 2017.

[49] M. N. N. S. Stelmack, "GENETIC ALGORITHMS FOR MIXED DISCRETE/CONTINUOUS OPTIMIZATION MULTIDISCIPLINARY DESIGN," *AIAA/USAF/NASA/ISSMO Symposium on Multidisciplinary Analysis and Optimization,* pp. 1998-4471, 2 September 1998.

[50] R. A. R. Z. S. G. K. K. Mohamed Hussain, "Comparison of PID Controller Tuning Methods with Genetic Algorithm for FOPTD System," *International Journal of Engineering Research and Applications,* vol. 4, no. 2, pp. 308-314, 2014.

[51] S. J. Dodds, Feedback Control, London: Springer, 2015.

[52] D. A. M. K. S. Shaunak Chakrabartty, "Performance Analysis Of Various Anti-Reset Windup Algorithms," *International Journal of Engineering Research and Applications,* vol. 4, no. 5, pp. 13-18, 2014.

[53] M. P. V. Angel, "Practical PID controller implementation for the speed control of a motor generator system," in *IOP Conference Series Materials Science and Engineering*, Bucaramanga, 2018.

[54] D. O. A. P. A. A. Muniru Olajide Okelola, "Performance and Configuration Analysis of Tracking Time Anti-Windup PID Controllers," *Jurnal Ilmiah Teknik Elektro Komputer dan Informatika (JITEKI),* vol. 6, no. 2, pp. 20-29, 2020.

[55] M. H. M. N. K. M. N. T. M. H. F. R. Mohd Hafiz A. Jalil, "Implementation of Anti Windup Scheme on PID Controller for Regulating Temperature of Glycerin Bleaching Process,"

in *IEEE 3rd International Conference on System Engineering and Technology*, Shah Alam, 2013.

APPENDIX

Appendix A: Related to GA Initialization for GA-Model Parameter Estimation

```
%Initialize Genetic Algorithm.
options= optimoptions('ga','PlotFcn',@gaplotbestf);
options.PopulationSize= 30;
options.MaxGenerations= 50;
nvar= 3; % Number of parameters
 %HOT-STEP-UP
 % LB= [0  0  0.01];   % Lower bound of tuning parameters
 % UB= [60  30  0.3];      % Upper bound of tuning parameters
 %COL-STEP-DOWN.
 LB= [0  0   0.01];   % Lower bound of tuning parameters
 UB= [60  30   0.3];    % Upper bound of tuning parameters
  [x,fval]= ga(@EvalObjICM,nvar,[],[],[],[],LB,UB,[],options)
```

Appendix B: Related to Processes Transfer function Model

The Transfer function to an ordinary defferntial equations as

$$Y(s) = \frac{K_s K_h}{(1+T_s s)(1+T_h s)} M(s)$$

$$\frac{Y(s)}{M(s)} = \frac{K_s K_h}{(1+T_s s)(1+T_h s)}$$

$$\frac{Y(s)}{M(s)} = \frac{K_s K_h}{s^2 T_s T_h + s(T_s + T_h) + 1}$$

$$[s^2 T_s T_h + s(T_s + T_h) + 1]Y(s) = M(s) K_s K_h$$

Taking inverse Laplace transform

$$\ddot{y}(t) = \frac{-\dot{y}(t)(T_s + T_h) - y(t) + m(t) K_s K_h}{T_s T_h}$$

$$x_1(t) = y(t)$$

$$\dot{x}_1(t) = x_2(t)$$

$$\ddot{x}_2(t) = \frac{-x_2(t)(T_s + T_h) - x_1(t) + m(t)K_sK_h}{T_sT_h}, \; x = [100; 0]^T$$

Appendix C: Related to GA-Initialization for Controller Parameter Estimation

MATLAB:GA initalization for Optimal TDOF-PID controller tuning

```
options= optimoptions('ga','PlotFcn',@gaplotbestf);
options.PopulationSize= 30;
options.MaxGenerations= 40;
nvar= 6; % Number of parameters
LB= [0  0   0     0   0  0];   % Lower bound of tuning parameters
UB= [35  10  5  1  1  5];    % Upper bound of tuning parameters
[x,fval]= ga(@EvalObjTDOF-PID,nvar,[],[],[],[],LB,UB,[],options)
```

MATLAB:GA initalization for Optimal PID-SP controller tuning

```
options= optimoptions('ga','PlotFcn',@gaplotbestf);
options.PopulationSize= 30;
options.MaxGenerations= 40;
nvar= 3; % Number of parameters
LB= [0  0   0    ];   % Lower bound of tuning parameters
UB= [35  10  5 ];    % Upper bound of tuning parameters
[x,fval]= ga(@EvalObjPIDSP,nvar,[],[],[],[],LB,UB,[],options)
```

MATLAB:GA initalization for Optimal PID-SP controller tuning

```
options= optimoptions('ga','PlotFcn',@gaplotbestf);
options.PopulationSize= 30;
options.MaxGenerations= 40;
nvar= 3; % Number of parameters
LB= [0  0   0 ];   % Lower bound of tuning parameters
UB= [35  10  5 ];    % Upper bound of tuning parameters
[x,fval]= ga(@EvalObjPIDDIS,nvar,[],[],[],[],LB,UB,[],options)
```

Appendix D: Related to Model Approximation

MATLAB: GA initalization for Model Approximation(Reduction)

```
options= optimoptions('ga','PlotFcn',@gaplotbestf);
options.PopulationSize= 30;
options.MaxGenerations= 40;
nvar= 3; % Number of parameters
LB= [0  0   0    ];   % Lower bound of tuning parameters
UB= [3  30  0.1 ];    % Upper bound of tuning parameters
[x,fval]= ga(@EvalObjModelReduc,nvar,[],[],[],[],LB,UB,[],options)
```

MATLAB: Model Reduction Validation

```
load('SOPTD')
t= buf(:,1); y1= buf(:,2);
load('FOPTD')
t2=buf(:,1); y2= buf(:,2);
NRMSE=norm(y1-y2)/norm(y1-mean(y2));
P.FIT=1-NRMSE;
P.Fit=FIT*100
gh=plot(t,y1,'r',t2,y2,'b','linewidth',2)
set(gh(2),'LineWidth',1.5);
set(gca,'YLim',[0  3]);
set(gca,'YTick',[0 1 1.5 2 2.5 3],'YTickLabel',[0 1 1.5 2 2.5 3]);
set(gca,'FontName','Time New Roman','FontSize',12);
%title('Set-Point Tracking')
xlabel('t(sec)');ylabel('y(t)');
```